Tropical Water Quality Hub

National Environmental Science Programme

Final Report

Risk Assessing Dredging Activities in Shallow-Water Mesophotic Reefs

Ross Jones, Rebecca Fisher, David Francis, Wojciech Klonowski, Heidi Luter, Andrew Negri, Mari-Carmen Pineda, Gerard Ricardo, Matt Slivkoff, James Whinney

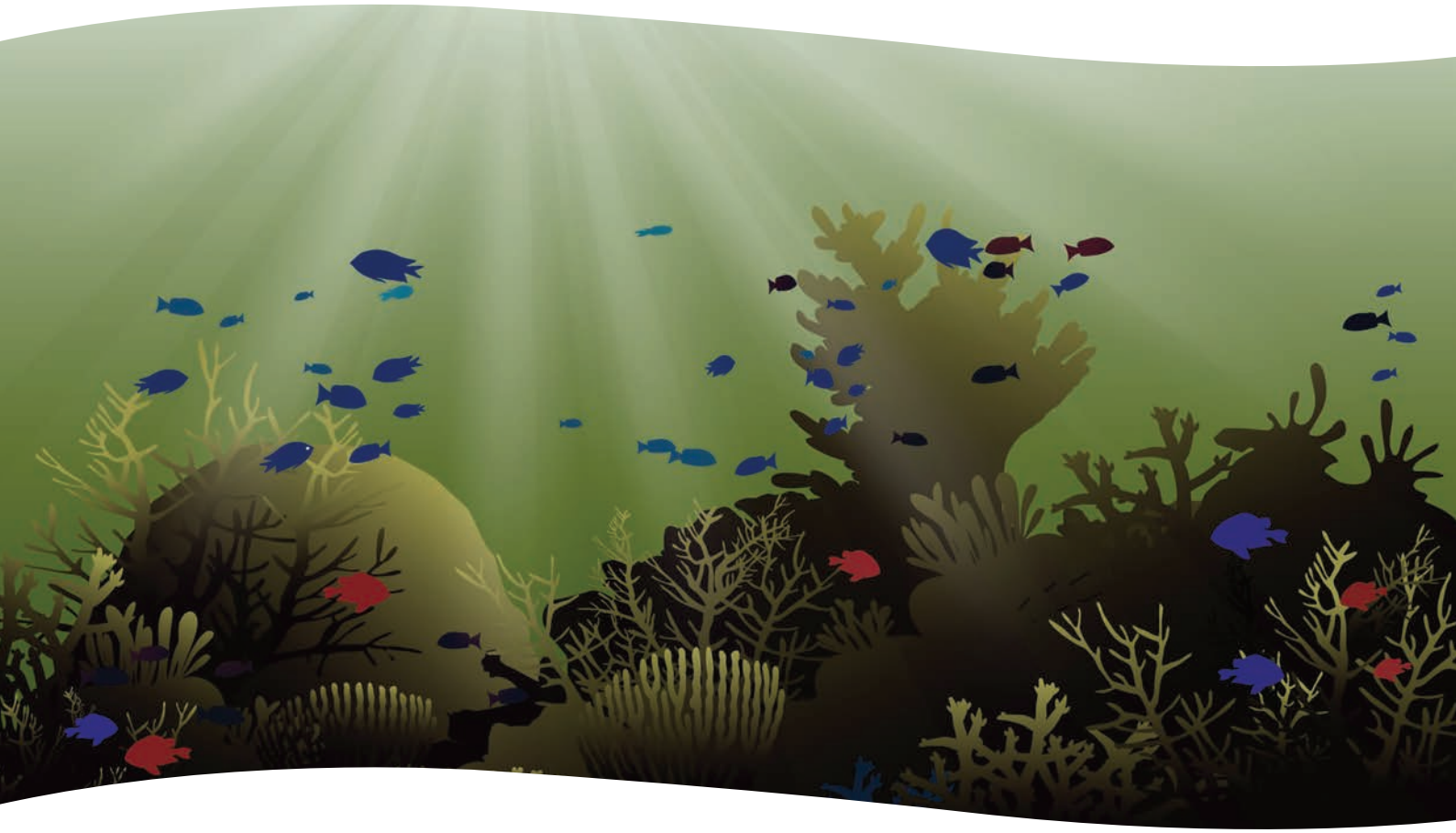

Australian Government

Australian Institute of Marine Science

Risk Assessing Dredging Activities in Shallow-water Mesophotic Reefs

Ross Jones[1], Rebecca Fisher[1], David Francis[2], Wojciech Klonowski[3], Heidi Luter[1], Andrew Negri[1], Mari-Carmen Pineda[1], Gerard Ricardo[1], Matt Slivkoff[3], James Whinney[4]

[1] Australian Institute of Marine Science (Townsville and Perth, Australia)
[2] School of Life and Environmental Sciences, Deakin University (Warrnambool, Australia)
[3] In situ Marine Optics (Perth, Australia)
[4] James Cook University (Townsville, Australia)

Australian Government

National Environmental Science Programme

Supported by the Australian Government's
National Environmental Science Program
Project 2.1.9 Risk assessing dredging activities

National Library of Australia Cataloguing-in-Publication entry:
978-1-925514-47-6

This report should be cited as:

Jones, R., Fisher, R., Francis, D., Klonowski, W., Luter, H., Negri, A., Pineda, MC., Ricardo, G., Slivkoff, M. and Whinney, J. (2020). *Risk Assessing Dredging Activities in Shallow-Water Mesophotic Reefs*. Report to the National Environmental Science Program. Reef and Rainforest Research Centre Limited, Cairns (78 pp).

Published by the Reef and Rainforest Research Centre on behalf of the Australian Government's National Environmental Science Program (NESP) Tropical Water Quality (TWQ) Hub.

The Tropical Water Quality Hub is part of the Australian Government's National Environmental Science Program and is administered by the Reef and Rainforest Research Centre Limited (RRRC). The NESP TWQ Hub addresses water quality and coastal management in the World Heritage listed Great Barrier Reef, its catchments and other tropical waters, through the generation and transfer of world-class research and shared knowledge.

Cover photographs: (Front) Symbolised representation of a shallow-water mesophotic, turbid-zone reef near Townsville in the inshore central Great Barrier Reef (Image courtesy of Ross Jones); (Back) Images of an 85 m long ocean-going trailing arm suction hopper dredge working in Cleveland Bay near Townsville (central, inshore Great Barrier Reef), and scientists on board the Port of Townsville Ltd Pilot boat collecting turbidity and light measurements through sediment plumes generated by maintenance dredging in a shipping channel or through dredge material disposal at the dredge material placement site (Images courtesy of AIMS).

This report is available for download from the NESP Tropical Water Quality Hub website:
http://www.nesptropical.edu.au

CONTENTS

LIST OF TABLES

LIST OF FIGURES

ACRONYMS AND ABBREVIATIONS

AIMS ..... Australian Institute of Marine Science
CHL ..... Chlorophyll
CDOM ..... Chromophoric or coloured dissolved organic matter
DLI ..... Daily Light Integral (sum of per second quantum flux measurements per day)
EC ..... Effect Concentration
EIA ..... Environmental Impact Assessment
ETR ..... Electron Transport Rate
FNU ..... Formazin Nephelometric Units
GAM ..... Generalised Additive Model
GBRMPA ..... Great Barrier Reef Marine Park Authority
GBR ..... Great Barrier Reef
Kd ..... Light attenuation coefficient
LAT ..... Lowest Astronomical Tide
LED ..... Light Emitting Diode
Nm ..... Nanometer
NESP ..... National Environmental Science Program
NTU ..... Nephelometric Turbidity Unit
P ..... Percentile
PAM ..... Pulse-Amplitude-Modulation
PAR ..... Photosynthetically Active Radiation (400–700 nm)
PCO ..... Principal Coordinate Analysis
PCP ..... Peridinin-chlorophyll a-binding protein
PLC ..... Programmable Logic Controller
POTL ..... Port of Townsville Limited
PSD ..... Particle Size Distribution
PUR ..... Photosynthetically Usable Radiation (400–700 nm)
QA/QC ..... Quality Assurance/Quality Control
SeaSim ..... Sea Simulator
SSC ..... Suspended Sediment Concentration
TAG ..... Triacylglycerol
TSHD ..... Trailing Suction Hopper Dredge
WAX ..... Wax ester

ACKNOWLEDGEMENTS

We acknowledge the Port of Townsville Limited (POTL) for access to the long-term water turbidity and light measurements in Cleveland Bay, for information on dredging volumes and locations, for access to the pilot boat and provision of crew for some of the field work, and for enabling and permitting close access to the dredge for sampling. We acknowledge Matt Salmon, Craig Humphrey, Andrea Severati, Paul Boyd and Eduardo Arias at the AIMS SeaSim for assistance with the design of the sediment dosing and lighting systems. We acknowledge Annabel Smith-Moorhouse, Charlotte Harper, Maria Andersen and Zara Marks-Collins for their assistance with aquarium maintenance, sample processing and image analysis.

EXECUTIVE SUMMARY

Dredging to create and maintain navigable shipping channels and allow safe ship access is a necessary component of most ports and coastal infrastructure developments. Dredging activities generate suspended sediment that could impact upon nearby marine communities i.e. it is a potential *hazard*. Well recognised cause-effect pathways include suspended sediment interfering with filtering and feeding mechanisms, increased turbidity (water cloudiness) changing light quantity and quality and increased sediment deposition causing smothering.

How the hazard translates into *risk* was investigated in this study for dredging in inshore coastal areas near reefs in Cleveland Bay (inshore central, Great Barrier Reef), where turbidity regimes and light levels are very different from what is considered a 'typical' reef setting. Data analysed include (1) a time series of benthic light and turbidity levels at five sites supplied by the Port of Townsville Limited, (2) a time series of multispectral irradiance and turbidity on a fringing reef and (3) a study involving 90 vertical turbidity and multispectral light depth profiles collected mostly behind a working trailing suction hopper dredge. This information was used to re-create environmentally realistic exposure scenarios in an advanced aquarium system at the Australian Institute of Marine Science and the physiological responses of corals and sponges examined over an extended, 28 d period.

From the time series data, the 10-minute turbidity and light readings were reduced to daily mean values (producing daily light integrals (DLI) in units of mol quanta m^2 for light) and percentile (P) values from P_0-P_{100} calculated for running mean periods from 1–42 d. This largely encompasses the length of a typical maintenance dredging program. A characteristic feature of the data was that it was highly skewed, indicating water quality was very good for most of the year (hence supporting reefs), but sometimes subjected to multiple short-term periods of poor water quality resulting in a divergence of mean and median values. Overall upper percentiles of turbidity (P_{95} etc) and lower percentiles of light (P_5) were the best descriptors of the data, showing a very clear gradient across the Bay. The water quality time series included six dredging campaigns and at some of the bays dredging may increase the turbidity by 0.6-0.7 times the mean expected values, but these are between two and five times lower than the effects of natural events caused by wind or waves.

The deployment of the multispectral light logger occurred over a brief (7 d) natural turbidity event and also periods of low turbidity, both of which were interspersed with cloudy and cloud-free days. During cloudy and low turbidity days, the benthic light levels were reduced without changing the underwater light spectrum. During turbid days benthic light levels were reduced and the spectrum changed, with relatively greater loss of more photosynthetically usable blue light. A simple ratio of blue (λ455 nm) to green (λ555 nm) wavelengths could identify these different periods of light reduction (i.e. cloud versus turbidity).

The vertical turbidity profiling identified complex 3-dimensional profiles of the plumes showing surface, mid-water and bottom maxima, as well as well mixed homogenous SSC profiles. Overall, the most common profile was as an increase in SSC with depth, with measurements at the surface 3.5 × less than the seabed behind the dredge and 10 × lower at the dredge material placement area. Vertical light profiles in low turbidity 'blue water' outside the Bay showed the well-known exponential decrease in light quantity with depth, the rapid attenuation

of red light in the first few metres, and furthest penetration of green and blue light. In low turbidity water inside the Bay, and beside a fringing reef, there was a similar loss of red light but also much more pronounced attenuation of the blue wavelengths with depth, shifting the spectral profile to green. This pattern is consistent with the attenuation caused by chromophoric (coloured) dissolved organic matter (CDOM). Under elevated SSCs behind the dredge, both the quantity of light and the spectral profile shifted strongly to the green-yellow (550–600 nm) range, with a maximum peak at 575 nm. The spectral shift could be due to absorption by the suspended sediment particles, but it is also likely to be due to the increased scattering of light by the suspended sediments which increases the probability of being absorbed by CDOM. The spectral shift is significant as it means a loss of the quality as well as quantity of light. This spectral shift needed to be replicated as close as practicable in laboratory experiments in order to properly evaluate pressure-response relationships.

Using the wavelength specific light attenuation coefficients for downwelling light under different turbidity levels and using a turbidity to SSC conversion factor from samples collected behind the dredge, an empirical spectral solar irradiance model was constructed for Cleveland Bay. This model was used to produce nomograms for light quantity and colour spectrum at different depths, in different SSCs and in its full form the model could also accommodate different solar zenith angles from the solar declination cycle. The model outputs were used in conjunction with the analysis of the long-term water quality to define likely pressure-fields generated by dredging. The conditions (SSC, light quality and quantity) were then replicated in the AIMS SeaSimulator in a fully automated, computer-controlled dosing system with custom made light emitting diode (LED) lights that could replicate the spectral shifts. Sublethal responses of 3 adult corals (*Acropora millepora*, *Pocillopora verrucose*, *Montipora aequituberculata)* juvenile corals *(A. millepora)* and an encrusting sponge species, *Cliona orientalis* were then examined over a one month exposure period to 5 treatments levels: SSCs ranging from 2.3 to 15.7 mg L^{-1} of Cleveland Bay sediment (with a modal size of 25 µm) and predominantly green-yellow light (peaking at 550 nm) of 5.7–0.06 mol quanta m^{-2} d^{-1}.

All corals and sponges survived the exposures with no whole colony or partial mortality, but clear physiological responses were measured including changes in pigmentation, lipid concentrations, the ratio of structural to storage lipids and density of symbiotic dinoflagellates. All coral species showed changes in lipid ratios at 2.2 mol quanta m^{-2} d^{-1} (and 0.85 mol quanta m^{-2} d^{-1} for the sponge) consistent with mobilizing lipid reserves under sub-optimal light. The branching pocilloporid *Pocillopora verrucosa* was the most sensitive, showing bleaching (the dissociation of symbiosis) at <1 mol quanta m^{-2} d^{-1}(for 30 d), which is a more consequential physiological response. When these physiological responses were mapped back onto the light data around Cleveland Bay the analyses showed corals and sponges occasionally naturally experience light limitation even in shallow (<5 m) depths. This is consistent with known depth distributions and zonation patterns in turbid zone reef communities i.e. that they are shallow-water mesophotic reef systems.

The study included the first empirical measurements of elevated sediment accumulation rates caused by maintenance dredging using newly re-designed deposition sensors. Accumulation rates were highly elevated at a distance of a few hundred metres from a working Trailing Suction Hopper Dredge (TSHD) but there was a strong gradient of decreasing accumulation rates with increasing distance and no effects detectable after a few hundred metres. Given the novelty of the instrumentation, the results are preliminary, but provide evidence to support the

idea that (1) high SSCs produced by dredging in a low energy water column is conducive to rapid settling and enhanced deposition (2) the effects are quite localized.

The light-based monitoring conducted here with the multispectral PAR sensors, supported by the hyperspectral vertical profiling offers many more advantages for inshore water quality monitoring than turbidity measurements. The report concludes with management implications section and suggestions for how to use the results in monitoring and in risk-response reactive management cascades to guide capital and maintenance dredging in inshore coral reef communities.

1.0 INTRODUCTION

Dredging in the marine environment to create and maintain navigable shipping channels and allow safe ship access is a necessary component of most ports and coastal infrastructure developments (Foster et al. 2010). Dredging involves the removal of sediment and/or rock from the seabed (McCook et al. 2015) and the excavation, and often the subsequent disposal at sea in dredge material placements sites, can generate suspended sediment that can impact upon nearby epibenthic marine communities i.e. it is a potential hazard (Rogers 1990, Foster et al. 2010, Erftemeijer et al. 2012, Jones et al. 2016). Well recognised cause-effect pathways include suspended sediment interfering with filtering and feeding mechanisms, increased turbidity (water cloudiness) changing light quantity and quality (for benthic primary producers), and increased sediment deposition causing smothering (Jones et al. 2016).

Predicting the environmental consequences before a dredging program is an important part of the environmental impact assessment (EIA) stage and predicated upon establishing a relationship between these dredging pressures (light reduction, suspended sediment, sediment deposition etc) and biological responses in underlying communities i.e. developing thresholds. In Australia, this information is used in zonation schemes to predict where effects may occur, translating the hazard of dredging to a risk, and typically on a spatial basis (GBRMPA 2012b, EPA 2016). If dredging is permitted then the thresholds are also used in monitoring programs, where they can inform proponents of conditions that are approaching or exceeding levels where mortality can occur and take corrective action if needed according to the zonation plan i.e. to use reactive management (Oliver 1995).

Recently a detailed suite of laboratory experiments has been conducted to address these issues describing how suspended sediments and depositing and deposited sediments affect adult corals and sponges and the early life-history stages of corals from gametes to newly settled corals (Pineda et al. 2015, Ricardo et al. 2015, Pineda et al. 2016a, Pineda et al. 2016b, Ricardo et al. 2016a, Ricardo et al. 2016b, Bessell-Browne et al. 2017b, Bessell-Browne et al. 2017c, Bessell-Browne et al. 2017d, Duckworth et al. 2017, Pineda et al. 2017a, Pineda et al. 2017b, Pineda et al. 2017c, Ricardo et al. 2017, Ricardo et al. 2018). One of the most interesting findings was the significance of the light attenuating properties of the suspended sediments as opposed to the suspended sediment *per se*. Corals form obligate, mutualistic association with photosynthetic endosymbiotic dinoflagellates (family *Symbiodiniaceae* (LaJeunesse et al. 2018) and many sponges host dense and diverse microbial symbionts including photosynthetic symbionts (Wilkinson 1983, 1987, Erwin & Thacker 2008). These symbiont populations are intimately linked to the health, fitness and nutrition of the coral and sponge hosts.

The laboratory-based experiments also provided an indication of the tolerance level to light reduction, and the first steps towards defining thresholds/guideline values for light availability for use in dredging programs near reefs. Light was quantified as a daily light integral (DLI), or the sum of the per second quantum flux measurements over the day. Corals held for extended periods in low light showed a series of physiological changes including photoadaptation involving increasing the pigment concentrations of the algal symbionts. They exhibited changes in lipid levels and ratios of storage to structural lipids. Under very low light levels they eventually lost their symbionts and discoloured (bleached), a well know sublethal stress response of corals (Jones 1997). Overall, most species could tolerate a light reduction to ~2.3

mol quanta m^{-2} d^{-1} (in combination with a SSC of 10 mg L^{-1}) over a 42-d period, although lower growth rates were observed in *Pocillopora damicornis* and *Porites* spp. at that light/SSC combination. The photosynthetic sponges were slightly less sensitive, showing loss of the photosymbionts at lower light levels and albeit over a shorter (28 d) period at DLIs of <~1 mol quanta m^{-2} d^{-1} (Pineda et al. 2016a, Pineda et al. 2017a).

How these light levels relate to conditions that can occur during dredging near reefs (the risk) was addressed for corals using the water quality information during a large-scale capital dredging project in Western Australia (Fisher et al. 2018a). This project yielded an immense amount of water quality data allowing quantitative analyses of temporal and spatial patterns in water quality (Fisher et al. 2015, Jones et al. 2015a). Although clearly measurable changes in suspended sediment and reductions in benthic light levels were detected >20 km away from the dredging, reduction of light levels to levels where effects on corals became possible (~1–2 mol photons m^{-2} d^{-1} only) only occurred <1 km from the dredging (Fisher et al. 2018a, Jones et al. 2019).

Sediment deposition is one of the key cause effect pathways that can result in mortality to corals during dredging program (Bak 1978, Jones et al. 2015b, Jones et al. 2016). It is especially significant during dredging because high suspended sediment concentrations are usually generated in a low energy water column where the hydrodynamics are insufficient to keep the sediments in suspension (Jones et al. 2016). The rapid settling of the sediments can overwhelm the corals' self-cleaning capabilities leading to smothering and sub-lethal and lethal effects (Jones et al. 2019).

Sediment deposition estimates on reefs have traditionally been made with sediment traps, but as has been discussed previously, traps provide at best a 'pseudo-sedimentation rate' and can significantly overestimate deposition rates because of deposition bias and resuspension limitation (Thomas & Ridd 2004, Storlazzi et al. 2011, Browne et al. 2012, Whinney et al. 2017). Sediment deposition sensors based on an optical backscatter technique have been designed (Ridd et al. 2001), and subsequently refined and tested around reefs leading to a better understanding of absolute sediment accumulation rates as per mg cm-2 day-1 under different hydrometeorological conditions (Whinney et al. 2017). Measurements of sediment accumulation rates have not yet been made during active dredging (at least in absolute terms), thus the hazard field associated with sedimentation occurring during dredging has not been characterised.

The laboratory experiments and field observations described above for effects of light and elevated SSCs were conducted with corals collected from an offshore, 'clear water' (low turbidity) environment. However, many capital and maintenance dredging campaigns occur in inshore coastal areas near reefs where turbidity regimes are profoundly different and where light availability may be a much more significant limiting factor even under natural, backgound conditions (Anthony & Connolly 2004, Anthony et al. 2004). The significance of light for the physiology and ecology of corals cannot be overemphasised (Dustan 1982, Wyman et al. 1987, Falkowski et al. 1990, Lesser et al. 2009). Light availability and the exponential decrease in light with depth determines bathymetric zonation patterns, driving changes in species composition and abundance (Goreau & Wells 1967, Sheppard 1982, Veron 2000, Lesser et al. 2009). Light availability has been suggested as the likely critical limiting factor determining

the latitudinal and depth limits of staghorn corals (Muir et al. 2015), although this has been contested (Madin et al. 2016, Muir et al. 2016).

Reefs typically occur in shallow water (30 m) but a focus of recent reef research has been on so called mesophotic coral reef ecosystems which has extended the coral depth distribution from 30 m to 150 m (Lesser et al. 2009). Mesophotic zones have been further defined as an upper and lower mesophotic zone, transitioning at ~60 m (Bongaerts et al. 2010, Slattery et al. 2011, Loya et al. 2016). However, these divisions are defined by depth, generally assuming clear water environments, which are only one end of the range of habitats over which reef formations occur. Morgan et al. (2016) recognised this in their study of the nearshore turbid-zone reef communities of the central Great Barrier Reef (GBR) by describing them as 'shallow water mesophotic reefs', based on a highly compressed zonation pattern and suggestion that this was caused from light limitation from high turbidity.

1.1 Objectives

In this study, a combination of field and laboratory studies were conducted to estimate a set of thresholds for dredging near inshore, coastal, turbid-zone shallow-water mesophotic coral communities based on light and suspended sediment concentrations. We investigate natural spatial and temporal changes in turbidity and underwater light quantity using a 3-year dataset in a turbid-zone reef environment describing what the reefs may naturally experience.

Statistical models were developed to explore the natural drivers of turbidity, and to assess the relative influence of these natural drivers compared to that of dredging. A series of vertically-resolved down-welling planar irradiance light profiles were collected in plumes generated by a working dredge and wavelength specific light attenuation coefficients were developed to mathematically describe the quality and quantity of the underwater light field and how it changes with sun-angle, water depth and suspended sediment concentration. This information formed the basis of an empirical spectral solar irradiance model for shallow-water mesophotic reefs in the inner GBR turbid reef communities that can predict light quality and quantity for a given set of conditions (sun angle, depth, SSCs). The derived spectral solar irradiance model was used to guide laboratory-based exposure studies where the tolerance of adult corals and sponges to environmentally relevant light quality and quantity and suspended sediment concentrations were determined. Experiments were also conducted with recently settled juvenile corals to examine how light quality and quantity affects early post settlement survival. Although the primary focus of the study was on light reduction and elevated SSCs, sediment deposition sensors were also deployed at increasing distances away from a working dredge. These provided some of the first measurement of likely sediment accumulation rates associated with dredging and first order approximation of the areal effects of enhanced sediment accumulation.

2.0 SITE DESCRIPTION

2.1 Cleveland Bay

Fieldwork was conducted in Cleveland Bay and on the reefs around Magnetic Island, in the inner central Great Barrier Reef (GBR), coastal central reef bioregion (GBRMPA 2012a) and the Townsville/Whitsunday management area (Figure 1). The oceanographic and sedimentary setting of Cleveland Bay has been described by Larcombe et al. (1995) and the turbid-zone reef communities have been the subject of many studies associated with understanding sedimentary processes, transport and fate, and the effects of watershed development on reef growth in 'marginal' (cf Perry and Larcombe (2003)) environments (Carter et al. 1993, Larcombe et al. 1995, Lou & Ridd 1996, Larcombe & Woolfe 1999, Orpin et al. 1999, Larcombe et al. 2001, Anthony et al. 2004, Orpin et al. 2004, Browne et al. 2010, Lambrechts et al. 2010, Bainbridge et al. 2012, Browne 2012, Browne et al. 2012, Orpin & Ridd 2012, Perry et al. 2012, Browne et al. 2013, Macdonald et al. 2013, Delandmeter et al. 2015, Whinney et al. 2017).

Briefly, Cleveland Bay is a shallow (reaching 15 m at its seaward edge) northward-facing embayment of around 325 km^2 located off the coastal city of Townsville in Northern Queensland (Figure 1). Tides are dominantly semidiurnal with a strong diurnal inequality and a range up of ~4 m (Lou & Ridd 1996, Browne et al. 2010, 2013). The Bay is landlocked around its southern and eastern sides by the mainland and bordered by Magnetic Island (see below) on its north western margin (Figure 1).

A prominent feature of the Bay is the north easterly sea breeze which develops in the afternoon reaching 15–25 km/h throughout the year. Nevertheless, the summer and winter seasons are quite different. In the winter (May–October) dry season, the Bay is influenced from SE trade winds which produce a northward longshore current and wind-waves which are refracted around Cape Cleveland into the Bay (Patterson 1994, Wolanski 1994, Larcombe et al. 1995, Anthony et al. 2004). In the summer (November–April) wet season, the Bay is primarily affected by monsoonal troughs and cyclones which can occur over relatively short periods bringing high intensity rainfall and resulting in coastal run-off principally through the Ross River and Alligator Creek (Figure 1). Cyclones play a major part in shaping the movement and location of sediments.

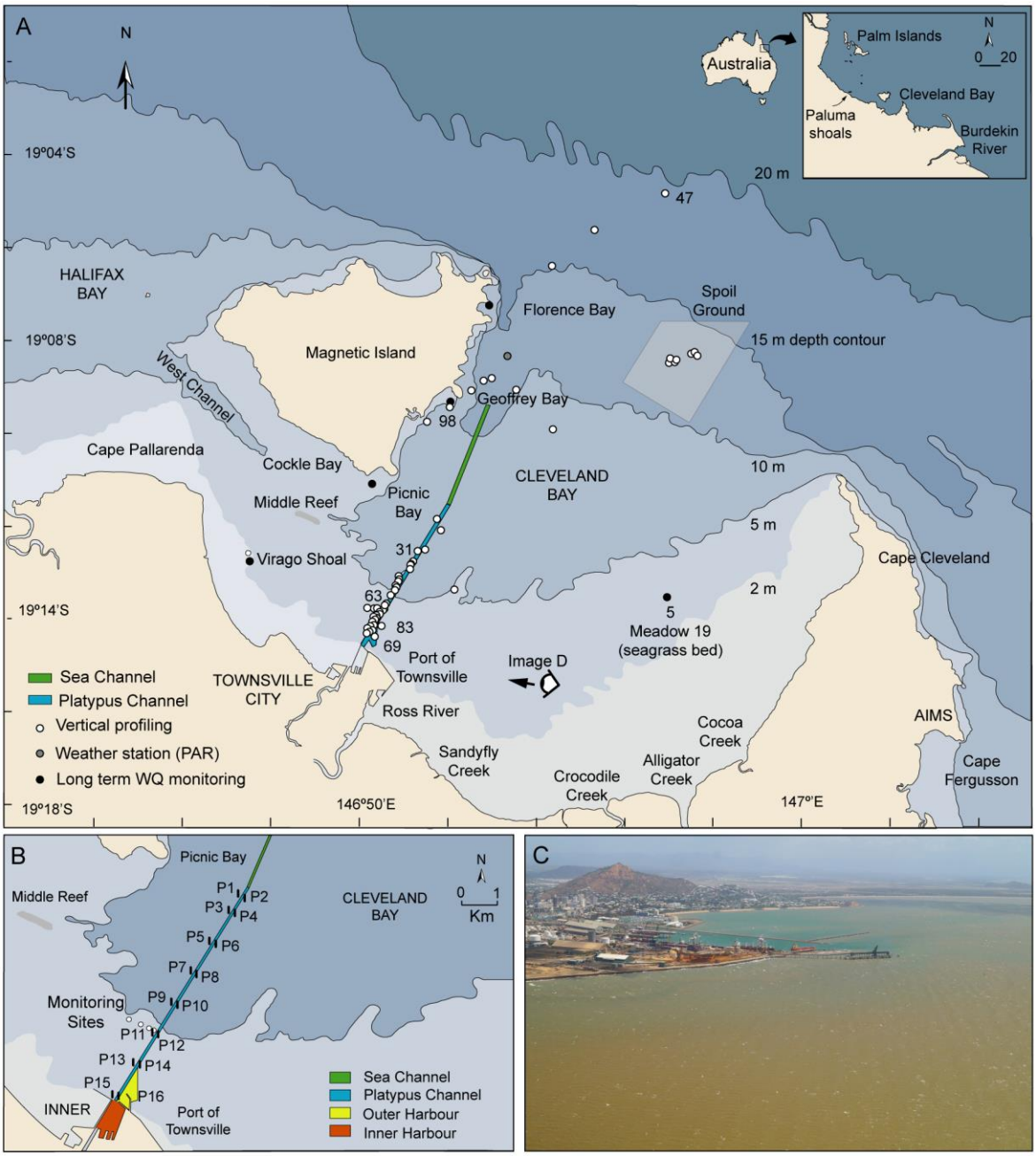

Figure 1: Location map showing Cleveland Bay off the coastal city of Townsville, in the inner central Great Barrier Reef (Australia) displaying (A) the location of the five water quality monitoring sites: (1) Florence Bay (-19.121722°, 146.883111°), (2) Geoffrey Bay (-19.155120°, 146.868340°, (3) Picnic Bay (-19.186560°, 146.838840°), (4) Virago Shoal (-19.213180° 146.792370°), (5) Meadow 19 (-19.226853°,146.949383°), the vertical profile sites (white circles) and the location of the coral collection sites near the Palm Islands (inset Figure), the Cleveland Bay weather station (-19.140556°146.889537°) and the location of the multispectral light logger deployment in Florence Bay (19.121917°, 146.883167°, beside the long term water quality monitoring site). (B) Close up of Platypus channel and the harbour entrance showing the channel markers numbered P1–P16 and the location of the sediment deposition monitoring sites (white circles) located 100 m, 200 m, 400 m and 800 m from the channel. (C) Aerial photograph of Cleveland Bay on 9 Sept 2013 during a natural period of elevated wind speeds (>35–40 kph) which exceed the 95th percentile of winds over 2012–2013 (images courtesy of POTL). The turbidity event is natural, and not caused by dredging activities.

The Bay contains a ~4 m thick layer of muddy sands and sandy muds of mixed siliciclastic–carbonate sediments with a terrigenous component of mainly quartzose, overlying Pleistocene clay (Maxwell & Swinchatt 1970, Belperio & Searle 1988, Carter et al. 1993). It is naturally very turbid (see Figure 1 C and D) and the conclusions from several studies is that locally generated wave induced bottom shear stress is the most significant long-term contributor to bed resuspension and elevated SSCs (Larcombe et al. 1995, Orpin et al. 1999, Anthony et al. 2004, Orpin et al. 2004, Orpin & Ridd 2012). Tidal currents alone are not considered capable of resuspending sediment, although Orpin et al. (1999) suggest they may augment resuspension when occurring with high energy waves. Based on a hydrodynamic analysis of a 22-year data set Orpin et al. (1999) estimated that resuspension of bottom sediment by waves occurs in shallow area (5 m depth) of Cleveland Bay on 220 days per year, or 110 and 40 days per year for depths of 10 m and 15 m (see Table 2 in Orpin et al. (1999)). Cleveland Bay connects to Halifax Bay through the shallow West Channel which separates Magnetic Island from the mainland. The channel has a maximum depth of 4 m and resuspended sediments are transported from the southern sections of the bay northwards through the West Channel as turbid water (Lou & Ridd 1996, Lambrechts et al. 2010) (Figure 1).

2.2 Magnetic Island

Magnetic Island is a granitic continental high island with a surface area of 52 km^2, located 8 km from the mainland and at the western end of the bay (Figure 1). On the SE margin of the island there are a series of bays with well-developed fringing reefs (Florence Bay, Arthur Bay, Geoffrey Bay, Nelly Bay and Picnic Bay) and on the southern section a large detached reef, Cockle Bay (Hopley 1982). Two other reefs involved in this study lie between Magnetic Island and the mainland and include Middle Reef, a linear patch reef system off Cockle Bay, and Virago shoal, a shoal system off Rowes Bay (Figure 1).

The Cleveland Bay reefs are composed of hard and soft corals and algae (Bull 1982, Mapstone et al. 1992, Kaly et al. 1994) overlying accumulations of non-biogenic sediments (Hopley 1982). Some of the fringing reef sites have clear reef flats transitioning to reef slopes which have gentle gradients extending hundreds of metres to 4–8 m below LAT. The coral assemblages have been quite well characterised with species tending to be most numerous (and the assemblage most diverse) on the reef slopes, where coral cover is also higher (Mapstone et al. 1992, Kaly et al. 1994).

The most recent surveys include those of Middle Reef (Browne et al. 2010) and another turbid zone communities the Paluma Shoals Reef Complex (Morgan et al. 2016) (Figure 1) located 50 km north of Townsville in a similar environmental setting. Both studies describe similar depth related preferences and characteristic benthic and geomorphological zones seen on clear water reefs, but compressed or truncated because of the shallow depths and presumably low light availability. Morgan et al. (2016) describe the depth distribution of common coral genera, and coral growth morphotype, with water depth (m below lowest astronomical tide). The *Acropora* spp. were found to occupy a normally-distributed range between 0.5–2.5 m below LAT and together with *Montipora* spp. dominate the shallow water assemblages. Deeper reefal areas are inhabited by massive *Porites* spp. (1.5–4 m LAT) and large stands of foliose *Turbinaria* spp. (1.5–3.5 m LAT, respectively). The sub-massive (hemispherical) colonies (e.g.

Lobophyllia spp., *Galaxea* spp., *Goniopora* spp.) and encrusting Montipora spp. have the deepest depth ranges (> 4–7 m LAT), albeit in very low relative abundances.

2.3 Dredging in Cleveland Bay

Annual or biannual maintenance dredging is needed of two connected shipping channels (Platypus and the Sea Channel) to allow safe passage of cargo ships to the mainland Port of Townsville (Figure 1). Maintenance dredging volumes vary from 250,000–650,000 m^3 of material per year and occurs over about a ~4–5 week period usually commencing in the second half of the year. The majority of the dredging is currently conducted by an 85 m long ocean-going trailing arm suction hopper dredge (TSHD) which has two trailing arm suction heads which are lowered and dragged along the seafloor dredging the seabed either side of the vessel (Figure 2 A–C). The dredge has a central 2,900 m^3 hopper. The current dredge (TSHD Brisbane) is fitted with a number of design features to minimise production of turbid waters (e.g. central column weir anti-turbidity valve and below keel discharge). As such the sediment in the hopper is concentrated and overflow is discharged below keel during maintenance dredging. Turbidity generation is associated with disturbance of the seabed by the drag head and by propeller wash. The second source of turbidity is at the 3.7 $\times$ 3.7 km dredge material placement area located in the bay itself, where sediments and excess water are ultimately disposed (Figure 1) (Figure 2 D).

An analysis of 5 years of data from the dredge logs (June 2012 to August 2017), for maintenance dredging only, shows 1,744 loads of sediment were taken to the dredge material placement area. Of the total loads 46% were from the Platypus Channel, 33% from the Outer Harbour area, 15% was from the Inner Harbour, and 6% was dredged from the Sea Channel adjacent to Magnetic Island (Figure 1 A, B).

In the Platypus and Sea channels filling the hopper (including positioning and lowering and raising the trailing arm and dredging) took ~ 40 mins, and the transit time to or from the dredge material placement area took 48 and 34 mins respectively. Discharging sediments at the placement area took on average 15 minutes involving the dredge moving slowly in an arc whilst a series of valves were opened allowing for gravitational settling of sediments from the hopper through a central weir and the keel, discharging material 5 m below the water line (Figure 2 D).

3.0 METHODOLOGY

3.1 Field studies

3.1.1 Turbidity and light time series

From September 2014 to August 2017, underwater measurements of turbidity and light levels were measured at 10-minute intervals at five sites within Cleveland Bay using submersible instruments mounted to a stainless-steel frame deployed at depth of 3–6 m. Turbidity was measured by optical scatter techniques using a WET Labs ECO-NTU sensor (WET labs, Philomath, Oregon US) giving readings in Nephelometric Turbidity Units (NTU). Underwater light was measured as photosynthetically active radiation (PAR, 400–700 nm) using LI-COR Li-192 underwater quantum sensors (LICOR, Lincoln, Nebraska, US) giving light quanta readings in µmol quanta m^{-2} s^{-1}. Each logger had a cleaning mechanism to maintain the surface of the sensors free of bio-fouling and were retrieved at ~monthly intervals for cleaning and replaced yearly with calibrated sensors (for further information on instrument calibration and QA/QC see GBRMPA (2013)).

To compliment the *in situ* measurements, surface measurements of PAR and wind direction (scalar averaged), wind speed (10 min average prior and maximum wind gust) were obtained from instruments mounted on a channel marker buoy (nominally 10 m above sea level) situated 1.9 km south of Florence Bay (Figure 1, see Cleveland Bay Weather station ((AIMS 2016)). All data was plotted and inspected for data anomalies and in some cases quarantined according to procedures described in Jones et al. (2015a). Due to occasional logger failure and interference by megafauna (turtles) there were some gaps in the data and interpolation was used. Where NTU were available and observed PAR were not, PAR was interpolated from a combination of depth, NTU, surface PAR and month of the year, from a fitted generalised additive model using the gam function from the mgcv package (Wood 2006). GAM models were fitted individually using the available data at each site. Daily light integrals (DLIs) were calculated as the sum of interpolated per second PAR values throughout the day. While predicting PAR from NTU is feasible at the hourly level because of the strong dependence of benthic PAR on surface PAR and turbidity, it is more complex to make such predictions the other way around as it is not possible to predict turbidity at night time based on light levels. For periods where light data were available but NTU was missing, we interpolated mean NTU at the daily level based on a fitted generalised additive model including DLI, mean depth and mean surface PAR. Long term time series of NTU and DLI were used to calculated running daily means across a range of time scales (1 d through to 30 d) and were summarised as quantile and cumulative probability plots.

Dredge log data was supplied by the Port of Townsville Ltd for the period encompassing the long-term monitoring data and included six maintenance dredging campaigns. Dredging pressure was estimated from the total wet weight (tons), summed hourly as well as per day. The bulk of the dredging activity over the period for which logs were supplied occurred along the Platypus channel (Figure 1). We performed a full-subsets generalised additive model (GAM) regression analysis to build an optimal model for predicting NTU across the five sites in Cleveland Bay, fitting all possible combinations of variables up to a maximum of three. We followed the methods described in Fisher et al. (2018b) using a GAM model fitted using the package mgcv (Wood 2006) with a random effect of site specified using the ‘bs=re’ formulation.

The response variable was raw NTU fitted using a tweedie distribution with a log link function, which is suitable for highly skewed continuous data that includes zero. Variables included in the candidate model set were: tidal range (depth.diff, maximum difference in observed daily depth), mean daily wave height (i.1_waves, obtained from Wave Watch 3 and representing large scale ocean waves[1], running daily 7 day mean wind vectors (u, i.7_wind.u; v, i.7_wind.v)[2], Madden-Julian Oscillation (MJO) amplitude and phase[3], the month of the year (for a smooth seasonal trend, month.val), seasons (Season, winter (May–October) or summer (November–April) and the moon phase (illum, obtained using the function lunar.illumination.mean from package lunar (Lazaridis 2014)). Smooth-smooth interactions were allowed, with the correlation among predictors increased to 0.7 to explore a wide range of potential models, and the 'k' argument restricted to 4, to ensure relatively simple mono-tonic relationships. In deriving the optimal environmental model, only data that did not include the dredging periods were used. This was done so that the model could be used to examine the residual fit with respect to dredging status. By accounting for the non-dredging related factors deriving turbidity allows a clearer examination of the evidence for dredging related impacts on turbidity.

Using the best fit predictive model of turbidity, we calculated residual values (observed–fitted), and compared these broadly between dredge and non-dredge periods, as well as the relationship with dredging pressure (calculated as the daily sum of the total wet weight dredged). Using the identified best model for predicting turbidity as a basis, we examined the relative effect size that dredging pressure has on turbidity at each site, compared to the naturally occurring environmental drivers. Effect sizes were calculated from fitted Bayesian models, using the identified best model for predicting turbidity, but using a Bayesian model fit individually to each site using the stan_gamm4 function from the rstanarm (Goodrich et al. 2018) package in R. As a tweedie distribution is not yet available, we instead modelled the response on a natural log transformed scale using a gaussian distribution. Effect sizes were calculated from a regular predicted grid of all the predictors as the difference between the maximum and minimum values obtained for that predictor, when all other predictors were averaged. The effect size of dredging was calculated as the maximum difference across the observed dredge pressure range, during the dredge period only. Effect sizes were standardised against the mean predicted turbidity, to account for the large differences in overall mean turbidity among sites.

3.1.2 Turbidity and light (spectrum) time series

Over a 16 d period (29 May 2017 to 13 June 2017) underwater measurements of PAR, turbidity and depth (m) were also measured at 15 minute intervals (averaging for 10 s) using sensors attached to a seabed mounted stainless steel instrument platform placed on the seabed at 8 m depth at the base of the reef slope in Florence Bay (Figure 1). Instruments included a vertically mounted IMO–MS8 eight wavelength (425, 455, 485, 515, 555, 615, 660 and 695 nm) multispectral irradiance sensor and a horizontally-mounted IMO–NTU turbidity sensor, both connected to an IMO–DL3 data logger with built-in depth and temperature sensors (In Situ Marine Optics, Perth, Western Australia), (Figure 2 G). The MS8 and NTU loggers both

[1] Accessed from http://oos.soest.hawaii.edu/erddap/griddap/NWW3_Global_Best.html),
[2] Accessed from https://apps.aims.gov.au/metadata/view/82422310-5a9d-11dc-8d3c-00008a07204e, .
[3] Accessed from http://www.bom.gov.au/climate/mjo/

have built-in accelerometer sensors (to detect tilt), and both have copper-based wiper mechanisms which regularly (every 15 mins) sweep over the sensors preventing biofouling.

3.1.3 Vertical water quality profiling

Over a 4 d period (12–15 September 2016), and during a period of routine maintenance dredging, 94 light and turbidity vertical profiles were measured through the water column in Cleveland Bay using a USSIMO multispectral radiometer (In Situ Marine Optics, Perth, Australia) and IMO-NTU turbidity sensor (Figure 2 E, F). The USSIMO incorporates a Carl Zeiss UV/VIS miniature monolithic spectrometer module as the internal light recording device providing irradiance measurement values at nanometer spectral spacing (Antoine et al. 217). The instruments were mounted vertically on an aluminium frame, with the radiometer orientated upwards and turbidity sensor downwards (Figure 2 E, F). The frame was designed to sit vertically in the water column using polystyrene floats and designed to be slightly negatively buoyant using lead weights. Sampling involved holding the instrument frame at 0.5 m depth in plumes created by the dredging activities, and simultaneously collecting a water sample using a Niskin™ bottle (General Oceanics, Miami, Florida, US). The instrument frame would then be allowed to drift away from the boat and slowly sink (free-fall) at a rate of 0.5 m/s through the plume recording light and turbidity until it reached the seabed. Profiles were conducted in the shipping channel and swing basin in water depths of up to up to 12 m, in shallower water either side of the channel (depths up to 4–8 m) in the dredge material placement area (n=12 sites, depths up to ~11–13 m) and outside of Cleveland Bay (n=3 sites, depths of (16–21 m) (Figure 2 F). Triplicate water samples were drawn from the Niskin bottle and subsequently filtered onto Whatman 47 mm GF/F filters (nominal pore size 0.7 μm), and 100 mL of distilled water used to rinse the container, filter funnel and filter pads of salts. Filters were then dried overnight in a 65°C oven and weighed with a precision balance (capable of weighing to 0.0001 g) and used to generate the relationship between suspended sediment concentration (SSC) and turbidity NTU.

3.1.4 Sediment deposition measurements

In August 2017, two sediment deposition sensors (Figure 2 J) were deployed on the seabed 100 m (-19.226083° 146.843500°) away from the edge of the Platypus channel near marker beacon P11 at a depth of 5–8 m (Figure 1 B). Single deposition sensors were also placed on a transect line running at right angles from the shipping channel at distance of 200 m (19.225639° 146.842889°), 400 m (-19.224528° 146.841111), and 800 m (-19.222806° 146.837889°) (Figure 1 B). The distances were based on previous observations of maintenance dredging plumes and designed to cover what was perceived, visually, as a gradient from highly to weakly turbid surface water.

The deposition sensor measuring principal, design and calibration and deposition rate calculations have been described in Ridd et al. (2001), Thomas et al. (2003) and most recently in Whinney et al. (2017). Briefly, the instrument uses infrared optical backscatters techniques to estimate the mass of sediment per unit area that deposits on the sensor surface every 10–20 minutes. After 1 h the surface is wiped clean and the process repeated and deposition rates calculated based on laboratory calibration of the instrument in a 3 m settling tube (Whinney et al. 2017). Additional instruments were deployed alongside the sensors including a nephelometer measuring turbidity by means of optical backscatter, a pressure sensor for

estimating wave activity, and a tilt current meter for estimating current speed. For instrument descriptions and calibration details see Macdonald et al. (2013), Marchant et al. (2014), Whinney et al. (2017)

All data went through a quality assurance process involving an algorithm to remove occasional data spikes. This algorithm compares each reading to the average of the readings directly before and after it, and if the reading is greater than twice the average it is replaced by the average. Fouling of sensors was examined by looking for drift in values over the deployment period and from observations of the condition of the sensors at the time of retrieval. Data that have been affected by fouling were removed.

3.1.5 Empirical spectral solar irradiance model

For each vertical profile the irradiance just-below surface incident irradiance Ed (0-, λ) and the light attenuation coefficient Kd (λ) were determined using the Beer-Lambert law. These data were used to calculate the wavelength specific light attenuation coefficients for downwelling irradiance, Kd (λ), using the relationship,

$$\mathrm{E}(\lambda, \mathrm{z}) = \mathrm{E}(\lambda, 0)\ \exp\left(-\mathrm{K\_d}\ (\lambda), \mathrm{z}\right) \qquad \text{Equation 1}$$

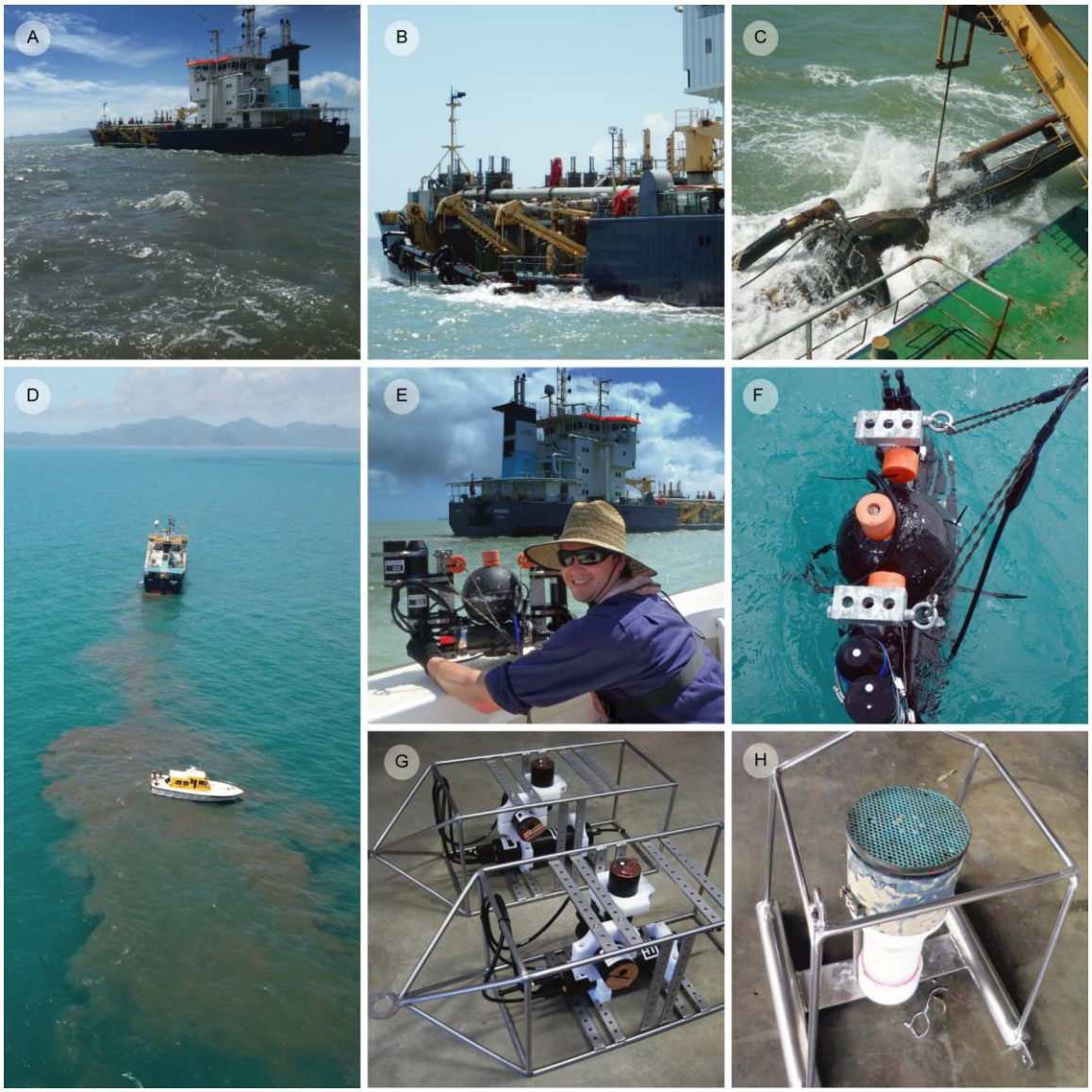

Figure 2: (A, B, C) Images of an 85 m long ocean-going trailing arm suction dredge (TSHD) working in Platypus channel, (D) disposing of sediment at the dredge material placement area (E, F) a USSIMO multispectral radiometer which was placed in plumes generated by dredging (or through dredge material disposal) and allowed to slowly sink, recording underwater irradiance at wavelengths between 400 and 700 nm. The information was used to determine wavelength specific light attenuation coefficients which were incorporated into an empirical spectral solar irradiance model that could predict light quality and quantity at depth knowing the SSC, sun angle (zenith) and water depth. (G) Two upward facing IMO–MS8 eight wavelength multispectral irradiance sensors and sideways facing IMO–NTU turbidity sensors and (H) a sediment deposition sensor.

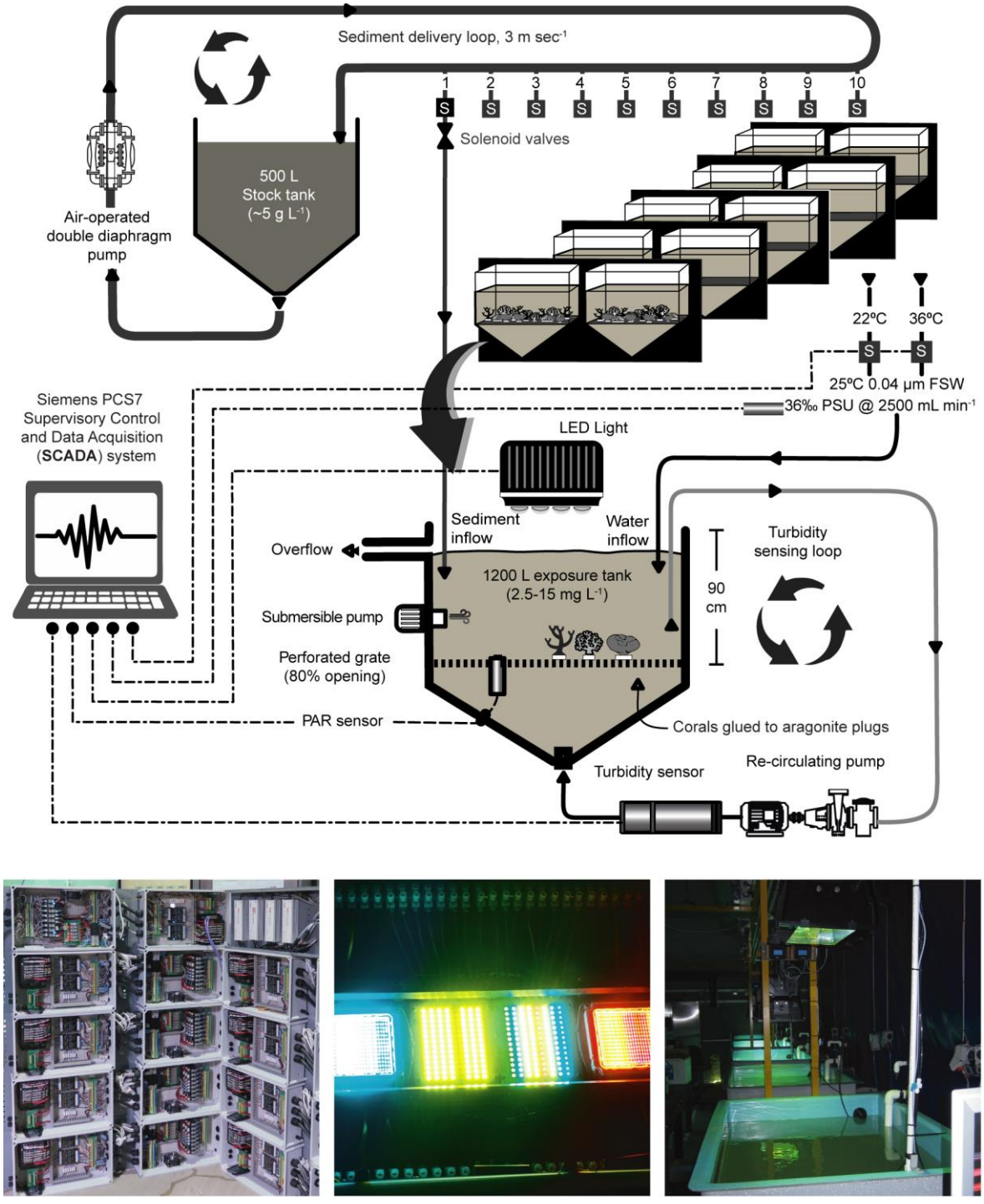

Figure 3: (A) Schematic diagram of the automated, PLC controlled sediment dosing system. At the AIMS SeaSim, corals and sponges were held in 10 × 1,200 L containers receiving a continuous flow of filtered seawater with episodic injections of pulses of suspended sediments from a stock tank via a 'sediment delivery loop'. SSC concentrations were monitored continuously in the 'turbidity sensing loop' for each tank, providing feedback to the PLC system which maintained the SSCs at the desired levels. Light was provided by a custom-made LED light above each tank which was also connected to the PLC and which varied the light intensity and spectrum according to the SSC (see text for further details). Each light was composed of 840 individual LEDs across 28 colours, assembled in four chips with a total power of 1.3 kW. The spectral output of the lights could be adjusted to deliver light of a different spectral composition to match the light quantity and quality corals and sponges would experience *in situ* in a dredging plume or natural resuspension event.

Where: E (λ,z) is the spectral downwelling irradiance at depth z, and E (λ,0) is the spectral downwelling irradiance just below the ocean's surface. The accelerometer in the USSIMO was used to assess if the instrument was vertical and stable and the first 0.2 m of all deployments was discarded prior to calculating K_d.

3.2 Laboratory-based coral and sponge exposure studies

Experiments were conducted using adult corals and sponges examining the effect suspended sediments and changes in light quantity and quality (spectrum), and with recently settled juvenile corals examining the effects of light quantity and quality (spectrum) on growth and survivorship. Both set of experiments were conducted in the same computer controlled experimental set-up as shown in Figure 3.

3.2.1 Experimental setup

All experiments were conducted in 10 × 1,200 L fibreglass tanks with 0.04 µm filtered flow-through seawater (FSW) in an environmentally controlled room within the SeaSim (Figure 3). Water flow into the tanks was standardised to 2,500 mL min^{-1} to ensure approximately three complete turnovers per day, and water temperature was maintained at 25 ± 1.5˚C in all tanks over the course of the experiment. A recirculating Iwaki MX-400 pump (Iwaki Co., Ltd., Japan) at 45 Hz was used to generate upwelling circulation in the tank, as well as supplying the turbidity sensing loop (Figure 3). In addition, an underwater Hydrowizard submersible pump (Panta Rhei, Germany) was set to oscillate from 20% to 35% power in 'wave' mode providing realistic in-tank flow ranging from 4 to 10 cm sec^{-1} as described in (Pineda et al. 2017a). To prevent sediment deposition, one re-suspension event was carried out daily by increasing the in-tank flow rate for one min using the Hydrowizard pump. During the experiments, corals and sponges were placed on a fibre reinforced plastic grating (80% open) at a depth of 90 cm and exposed to 5 different turbidity treatments each with an associated light intensity (Figure 3) for 28 d.

Sediments used in the study were collected from Middle Reef (19°11'39.4" S, 146°48'49.5" E), screened to 2 mm and ground with a rod mill grinder to ~38 µm with a modal size of 25 µm, measured using laser diffraction techniques (Mastersizer 2000, Malvern instruments Ltd, UK). Sediments were thus predominately silt-sized. Total organic content of the sediment was 0.25 ± 0.09 % (w/w) analysed with a Shimadzu TOC-5000 carbon analyser (Shimadzu Corporation, Kyoto, Japan).

To maintain suspended sediment concentrations (SSCs), each tank was equipped with a Turbimax CUS31 nephelometer (Endress and Hauser, Germany) held in the turbidity sensing loop (Figure 3), providing feedback to a programmable logic controller (PLC) system. Nephelometers were calibrated with Formazin and set to measure Formazin Nephelometric Units (FNU), with water samples taken throughout the experiment (n=12) to relate FNU to SSCs (mg L^{-1}). The relationship of FNU to SSC was determined by filtering water samples (250 mL) through pre-weighed 0.4 µm polycarbonate filters, which were then rinsed with deionised water, dried at 60°C for 24 h and re-weighed.

All nephelometers, solenoid valves and lights were connected to the PLC (Figure 3), which recorded FNU levels and controlled the opening of the solenoid valves to inject sediment into the tanks and maintain the SSCs at the desired level. The sediment was pre-blended into a 500 L stock suspension batch, recirculating at high velocity (>3 m s^{-1}) in the loop supplying sediment to all experimental replicates through individual solenoid valves.

A custom-made light fitting based on Light Emitting Diode (LED) technology was fitted above each tank capable of simulating the full solar visible light. Each light was composed of 840 individual LEDs across 28 colours, assembled in four chips with a total power of 1.3 kW (Figure 3). The lighting system was fully integrated with the PLC system and each light was controlled by 19 independent channels. A PAR Quantum sensor (Skye, UK) was positioned on the grid floor next to the corals and sponges and connected to the PLC. This allowed the PLC to control light intensity based on an experimental depth (5 m) and suspended sediment concentration (see below).

The PLC was programmed to manipulate, in real time, the quantity of light and the spectrum of light (quality) according to the turbidity (for a given depth), by adjusting the ratio between the 19 channels for each light. For each tank and for a given SSC, the quantity and quality of light was based on the light profiling field study (Section 4.1.3) and the subsequent empirical spectral solar irradiance model that was developed (see below for more details on choice of the spectral profiles). The PLC also mimicked daylight variation, following a sinusoidal ramping up from sunrise at 06.00 h until noon and ramping down to sunset at 18.00 h.

3.2.2 Adult sponges and corals

Experiments were conducted with two species of branching coral: *Acropora millepora* (Ehrenberg, 1834), *Pocillopora verrucosa* (Ellis & Solander, 1786), a foliose coral species, *Montipora aequituberculata* (Bernard, 1897) and an encrusting sponge species, *Cliona orientalis* (Thiele, 1900). Corals and sponges were collected from approximately 5 m depth from the Palm Island group (Figure 1 inset). Fragments from five colonies of each of the coral species and two individual of *C. orientalis* were collected using a mallet and chisel. Colonies were transported to the National Sea Simulator (SeaSim) at the Australian Institute of Marine Science (AIMS), Townsville, Queensland, where partial colonies were fragmented into smaller clones (~5–10 cm length for corals and ~20–50 cm^2 surface area for sponges) and glued onto circular aragonite discs for support. Fragments were left to acclimate for six weeks in 1,200 L holding tanks with flow-through seawater at 25°C and 36 PSU salinity. Animals were fed daily using enriched *Artemia* spp. (targeted concentration in tanks of 0.5 nauplii mL^{-1}) and a mix of microscopic algae (2,000 cells mL^{-1}). During the acclimation period, specimens were held under a 12-h light:dark cycle of ascending and decreasing light levels and over the course of the day resulting in a daily light integrals (DLI) of ~6 mol photons m^{-2} d^{-1}.

The SSCs treatments were chosen nominally 2.5, 5, 7.5, 10 and 15 mg L^{-1} and each SSC had its own light quantity and quality (see Table 4). Each treatment consisted of two replicate tanks, with a total of 10 replicates for each coral species and 8 replicates for *C. orientalis*. After the 28-d experiment, samples were snap frozen in liquid nitrogen and stored at -80°C for subsequent analyses of zooxanthellae density, and pigments and lipid concentrations.

All species were photographed on 0, 7, 14, 21 and 28 using a high-resolution digital camera (Nikon D810). Changes in colour were assessed using the software, ImageJ (Version 1.52a)

(Schneider et al. 2012) employing the histogram function to acquire mean pixel intensity on a black and white scale as previously described (Bessell-Browne et al. 2017c, Bessell-Browne et al. 2017d).

Coral tissue was removed by air blasting in 30 mL of 0.5 µm filtered seawater. The resulting 'blastate' (tissue slurry) was homogenised for 60 s, the exact volume recorded, and aliquots taken for symbiotic dinoflagellate density (1 mL, fixed in 10% buffered formalin), pigments (1 mL) and lipid (10 mL) analyses. Aliquots for lipids and dinoflagellate density were temporarily stored at -20°C, whereas aliquots for pigments were stored at -80°C until further processing. The surface area of corals was determined using the wax-dip method (Stimson & Kinzie 1991).

To determine symbiotic dinoflagellate density, a volume of 0.4 mm^3 from each aliquot was counted six times using a Neubauer haemocytometer containing 8 µL of homogenised solution. For *C. orientalis*, a previous incubation in 1 M NaOH for one hour allowed for the digestion of the sponge tissue (Zamoum & Furla 2012).

To determine pigment concentrations, algal pellets from the coral blastate were resuspended in 1 mL pre-chilled 95% ethanol and sonicated on ice for 10 s at 40% amplitude, followed by a centrifugation step at 10,000 rpm for 5 min. After recovering the supernatant (~700 µL), the samples were re-extracted with an additional 700 µL ethanol, followed by a 30 min incubation on ice in the dark and 5 min centrifugation at 10,000 rpm. Both extractions were combined and analysed on a Power Wave Microplate Scanning Spectrophotometer (BIO-TEK® Instruments, Inc., Vermont USA) as previously described (Pineda et al. 2016b), and standardise to estimate coral surface area (cm^2) or number of photosymbiont cells per replicate. Pigments from samples incorporating pinacoderm and mesohyl regions from *C. orientalis* were similarly extracted and analysed following procedures described in Pineda et al. (2016) and standardised to sponge wet weight.

For lipid analyses, total lipids and lipid classes were determined by extracting freeze-dried samples following the air-spraying method of Conlan et al. (2017b).

Treatment effects were examined using Gamma mixed models, with tank as a random factor. If appropriate, multiple comparisons were undertaken using the Dunnet's test to identify significant differences from the control (e.g. 5.7 DLI and 2.5 mg L^{-1}). Analyses were carried out in R using the glmer function of the lem4 package (Bates et al. 2015) and the glht function of the multcomp package (Hothorn et al. 2008). Thresholds were derived for the adult corals and sponge for all species and variables which showed a strong consistent change as a function of decreasing light levels. As values for measured variables differed markedly among species, values were first scaled within each species to between 0 and 1. We then used a custom function fit.assy based on the nls package in R to fit seven different non-linear functions to the scaled data, and generated model averaged predicted values based on AICc weight values for each successfully fit model. EC_{50} or EC_{10} values were estimated from the model averaged predicted values based on the lowest to highest predicted scaled value.

3.2.3 Juvenile corals

Before experiments commenced, a light meter connected to a diving pulse amplitude modulating (PAM) fluorometer (Walz) calibrated to a LI-COR (LI-250A) quantum light meter was used to measure light intensities in crevices at Middle Reef (-19.196050, 146.813950) at

3–5 m depth. These values were used to determine the environmentally realistic range of light intensities that recruits are likely to occur *in situ*.

Gravid adult colonies of *A. millepora* were collected from 8 m depth from an inshore reef of the Palm Island group (Falcon Island: -18.765833°, 146.532500°) (Figure 1 B) and transported to the AIMS SeaSim. On the night of spawning, egg-sperm bundles from all colonies were collected, cross fertilised, then washed free of sperm and transferred into 500 L flow-through fiberglass tanks to undergo further embryogenesis and larval development (see (Ricardo et al. 2017) for detailed methodologies).

After 7–9 days the larvae were competent to undergo settlement and were induced to settle on multiple 6-cm diameter PVC discs that had previously been 'conditioned' by incubating them in outdoor aquaria for ~3 months in the presence of *Porolithon onkodes* (a crustose coralline algae (CCA) well known to induce settlement for *Acropora* coral larvae (Heyward & Negri 1999). The discs were 20–40% covered in CCA at the start of the experiment (see (Ricardo et al. 2017) for detailed methodology).

Experiments were conducted using in the PLC-controlled tank system detailed in Section 3.2.1, using 2-replicate 50 L tanks placed in each of 9 large tanks underneath the customised LED lights (where the 1,200 L volume of the tanks acted as a temperature-controlled water-bath). The experiment was designed to examine the effects of changes in light quantity (5 levels) and quality (broad and shifted spectrums that would be associated with suspended sediment concentrations equivalent to 0.5 and 9.1 mg L^{-1}). As with experiments with the adult coral and sponges, the empirical spectral solar irradiance was used to predict the light quantity and quality (spectrum).

Five light intensities were selected to cover the range of environmentally realistic values, but also more extreme combinations were used to improve the model fit and assess the strength of the response. Light intensities were ramped over the course of the day with peak midday PAR levels approximately <1, 10, 30, 100, 300 µmol photons m^{-2} s^{-1}, which equated to DLIs of <0.1, 0.3, 0.9, 3, 9 mol photons m^{-2} d^{-1}. Only one tank was used for the 'near darkness (i.e. <0.1 DLI) light intensity for both spectra, as it was not possible to control the spectral pattern at these very low light levels.

Three discs each with ~10 settled larvae (recruits) were placed in each of the 50 L tanks. The recruits were infected with symbionts of clade C1 which were introduced into the large tanks (to a final concentration of 1–2 $\times$ 10^4 cells L^{-1}) on days 6 and 12 day after settlement. A small proportion of raw water (unfiltered) seawater was mixed with the FSW for heterotrophic feeding (Conlan et al. 2017a), and the total mix pumped into each tank at ~0.75 L min^{-1}. The discs were transferred to new 50 L tanks every 4 d to reduce algal growth and each disc was also lightly wiped with a soft paintbrush to control algae growth. While these measures were used to manage extreme algae growth, they could not entirely remove it. The discs were imaged at settlement and after the 6–week exposure to determine survivorship. Horizontal growth was determined from the images taken after the light exposure.

Changes in the photo-physiology of the corals were measured with pulse amplitude modulating fluorometry (Imaging PAM, Maxi, Walz) using dark-adapted yields and rapid light curves. For all rapid light curves, the relative electron transport rate (rETR) was calculated using (PAR $\times$ ΦPSII) and all rETR data were fit to a standard Marquardt–Levenberg regression algorithm

(Ralph & Gademann 2005)). The parameters α (initial slope), Ek (the minimum saturating irradiance), rETRmax (the maximum relative electron transport rate) and Em (intensities that correspond to the rETRmax) were derived from the model.

4.0 RESULTS AND INTERPRETATION

4.1 Field studies

4.1.1 Turbidity and light time series

Mean daily turbidity levels at the long-term monitoring sites ranged over 2 orders of magnitude from <0.5 to >50 NTU, with the more seaward sites facing the open ocean (Florence and Geoffrey Bay) averaging ~2 NTU, slightly lower than at Picnic Bay (2.2 NTU), and >3 × lower than at the Virago Shoal and Meadow 19 sites (6–7 NTU, Table 1, Figure 4).

Table 1: Site level summary statistics of the 5 water quality monitoring sites (Figure 1) showing (1) the mean daily average values and range (minimum to maximum) of turbidity (NTU), daily light integral (mol quanta m^{-2} d^{-1}) and temperature (°C) divided into year (Y), winter (W, May–October) and summer (S, November–April) over the ~3 year monitoring program, (2) average depth (m) and minimum and maximum (i.e. range) and (3) the minimum and maximum of the 10 minute readings for NTU, light (μmol quanta m^{-2} s^{-1}) and temperature (°C).

		NTU			Daily Light Integral			Temperature (°C)			Depth (m)
		$\bar{x}$	Daily min-max	10 min. min-max	$\bar{x}$[1]	Daily Max[1]	10 min. Max[2]	$\bar{x}$	Daily min-max	10 min. min-max	$\bar{x}$ (min–max) Range (m)
Florence Bay	Y	1.9	0.1–13.0		10.7	26.4		26.7	20.6–31.5		
	S	2.0	0.2–9.9	0.5–29.8	11.3	26.4	1,342	29.1	25.2–31.5	20.0–32.1 (12.1°C)	3.2 (1.2–5.2) Range (4.1)
	W	1.8	0.1–13.0		10.1	22.4		24.2	20.6–27.6		
Geoffrey Bay	Y	1.9	0.6–15.5		10.2	24.1		26.8	20.2–31.8		
	S	1.6	0.6–15.5	0.5–44.5	11.8	24.1	1,253	29.3	25.4–31.8	19.8–32.3 (12.5°C)	4.0 (2.0–6.1) Range (4.1)
	W	2.1	0.6–11.3		8.8	19.4		24.3	20.2–27.8		
Picnic Bay	Y	2.2	0.1–24.1		4.9	14.1		26.8	20.0–32.0		
	S	1.8	0.1–17.9	0.5–46.3	5.7	14.1	654	29.4	25.0–32.0	19.3–32.8 (13.5°C)	3.6 (1.7–5.7) Range (4.1)
	W	2.5	0.6–24.1		4.2	10.6		24.2	20.0–28.1		
Virago Shoal	Y	6.9	0.5–44.9		4.3	19.0		26.9	19.5–32.5		
	S	7.2	1.0–44.9	0.5–97.5	3.9	19.0	917	29.4	24.7–32.5	19.1–33.1 (14°C)	3.9 (2.0–6.1) Range (4.1)
	W	6.5	0.5–41.7		4.7	16.6		24.5	19.5–29.6		
Meadow 19	Y	6.2	0.0–56.8		3.7	19.0		26.6	20.2–32.0		
	S	5.6	0.0–42.5	0.5–127	4.1	19.0	909	29.1	24.9–32.0	19.7–32.5 (12.8°C)	5.8 (3.9–8.0) Range (4.1)
	W	6.8	1.3–56.8		3.3	7.8		24.1	20.2–28.1		

[1] mol quanta m^{-2} d^{-1}
[2] μmol quanta m^{-2} s^{-1}

PAR levels (expressed as a daily light integral) ranged from 0 to >26.4 with average DLIs of 10–11 mol quanta m^{-2} at Florence and Geoffrey Bay which was >2 × more than at Picnic Bay (5 mol quanta m^{-2} d^{-1}) and 2.5× more than at Virago shoal and Cleveland Bay (3–4 mol quanta m^{-2} d^{-1}, Table 1, Figure 4). Average daily mean water temperatures were very similar across the sites, averaging 24C° in the winter and 29°C in the summer months, and 26–27°C over the study period (Table 1). Despite the similarity, the minimum and maximum temperature range (from the 10-minute readings) were very different, with Virago Shoal spanning a 14°C temperature change as opposed to 12°C at Florence Bay (Table 1).

Figure 5 shows exceedance curves for the five sites, displaying the proportion of average daily values (NTU and DLIs) above or below given levels for both winter and summer periods. Across most of the turbidity profile the analysis shows the similarity of the Florence, Geoffrey and Picnic Bay sites, with P_{50} values of 1.4, 1.5 and 1.3 NTU respectively. However, where the sites differ is the occasional periods of high turbidity where at Picnic Bay (during the winter time) the P_{95} value was 9.1 NTU, as opposed to 5.6 and 5.8 NTU at Florence and Geoffrey Bay. This difference resulted in slightly different mean NTUs: 1.9 NTU at Florence and Geoffrey Bay as opposed to 2.2 NTU at Picnic Bay.

Light and seasonality was also examined using the cumulative probability plots, showing that whilst there are clear seasonal differences in light levels, with a median value of ~2 mol quanta m^{-2} d^{-1} more at the offshore sites in summer than winter, similar differences were not seen at the more turbid Virago Shoal and Meadow 19 sites.

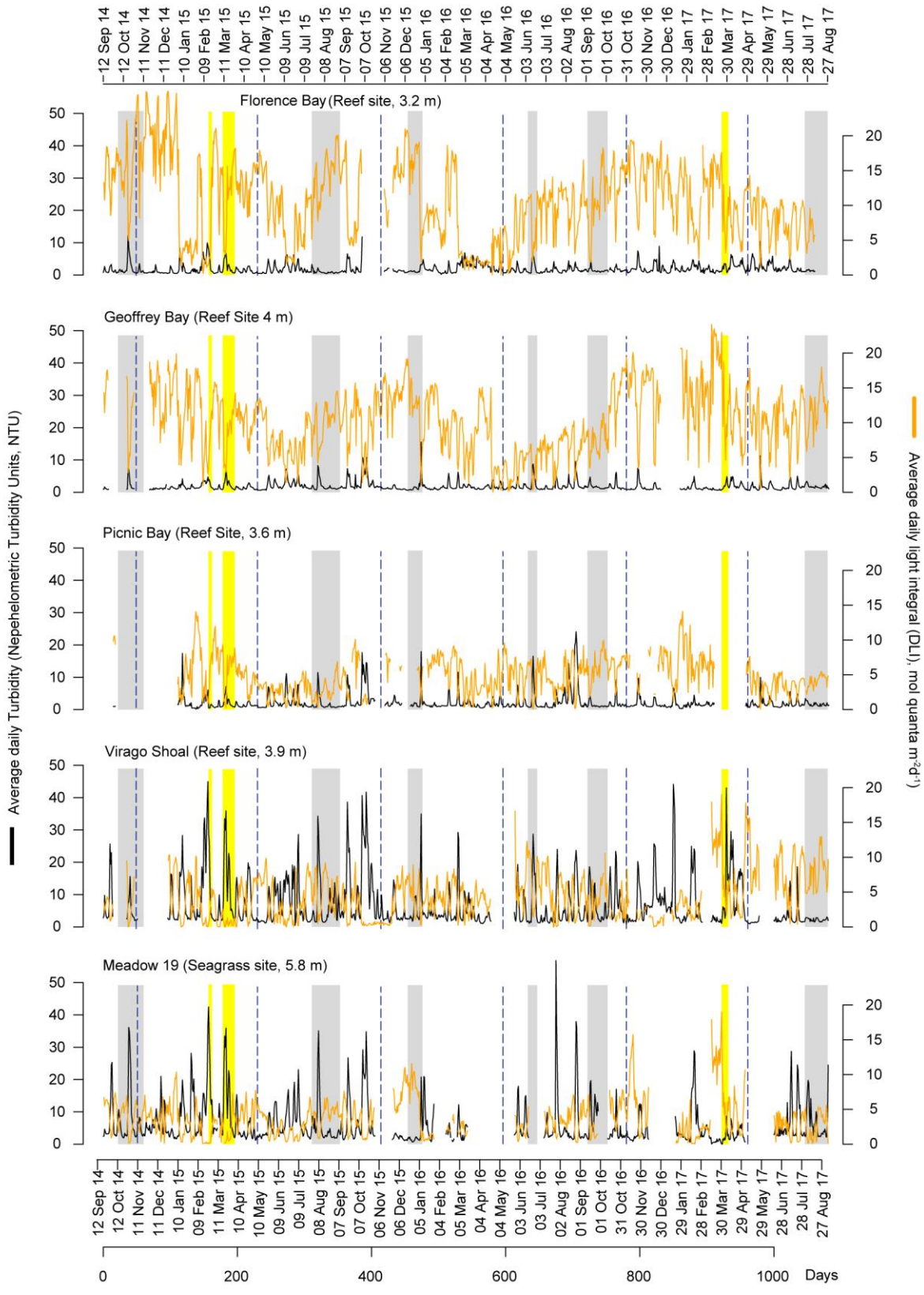

Figure 4: Time series plots showing average daily turbidity (NTU) and daily light integrals (mol quanta m^{-2} d^{-1}) measured at the 5 long-term water quality monitoring sites (Figure 1) at mean depths of 3.2–5.8 m. Grey vertical bars represent periods of annual maintenance dredging in the Sea channel and predominantly the Platypus channel. Yellow boxes indicate cyclone Marcia (16 Feb 2015–21 Feb 2015), Nathan (9 Mar 2015–27 March 2017 and Debbie (22 March 2017–1 April 2017). Blue vertical dashed lines separate seasons.

Table 2: Light (DLIs). Summary statistics for the 5 long-term water quality monitoring sites (see Figure 1 showing the percentile (P) values of the daily light integral (DLI, mol quanta m^2) for the running mean periods of 1, 3, 7, 10, 14, 21, 28 d, 35 and 42 days, divided into summer (November–April) and winter (May–October) periods.

		Summer											Winter										
	d	0	1	5	10	20	50	80	90	95	99	100	0	1	5	10	20	50	80	90	95	99	100
Florence Bay	1	0.0	0.8	1.8	2.3	4.5	12.1	17.0	19.2	20.8	25.9	26.4	0.2	1.7	2.6	4.0	5.4	10.2	14.3	16.1	17.5	20.0	22.4
	3	0.8	1.4	1.8	2.4	4.6	12.3	16.7	18.6	20.6	24.4	26.1	1.2	2.0	3.0	4.6	6.2	10.1	14.0	15.9	17.1	19.2	21.6
	7	1.4	1.7	1.9	2.8	5.4	12.2	16.0	18.8	20.4	23.1	23.8	1.8	2.3	4.3	5.5	6.5	9.8	13.7	15.3	16.1	17.5	18.9
	10	1.4	1.7	2.0	3.2	6.3	12.1	15.9	18.8	20.2	22.3	22.9	2.2	2.4	4.5	5.6	6.8	9.7	13.4	15.3	15.8	17.2	17.6
	14	1.8	1.8	2.0	3.5	7.1	12.4	15.7	18.9	20.2	21.5	22.1	2.3	3.2	4.2	5.9	7.2	9.5	13.2	15.0	15.6	16.8	17.0
	21	1.8	1.9	2.0	3.6	7.5	12.2	15.3	18.9	20.1	20.8	21.4	3.5	3.8	4.5	5.7	7.3	9.2	13.3	14.6	15.4	16.5	16.7
	30	1.9	1.9	2.3	5.4	8.1	12.4	14.9	17.4	20.0	20.3	20.5	3.2	3.8	4.4	5.7	7.3	9.3	12.9	14.0	14.8	16.1	16.3
	35	1.9	1.9	2.6	5.6	8.5	12.4	14.9	17.3	19.8	20.4	20.8	3.0	3.6	4.5	5.9	7.2	9.2	12.7	13.8	14.7	15.8	16.1
	42	1.9	2.0	2.7	5.9	8.8	12.3	14.8	17.1	19.7	20.3	20.5	2.9	3.3	4.3	6.0	7.0	9.1	12.3	13.6	14.2	15.1	15.4
Geoffrey Bay	1	0.0	0.9	3.4	4.6	7.8	12.2	15.8	17.5	18.9	22.7	24.1	0.2	0.5	1.8	3.6	5.4	8.5	12.4	14.3	15.7	17.6	19.4
	3	0.6	1.5	3.9	5.8	8.0	12.1	15.2	17.0	18.4	20.6	23.0	0.7	1.3	2.8	4.1	5.5	8.4	12.1	13.6	14.8	17.4	18.0
	7	1.4	2.4	5.3	6.6	8.4	12.1	14.9	16.5	17.3	20.9	21.9	1.1	1.5	3.4	4.4	5.7	8.4	11.7	12.8	14.1	16.0	17.8
	10	1.9	2.6	5.7	7.3	8.6	12.1	14.7	16.3	17.0	20.4	21.3	1.2	2.1	3.3	4.5	5.6	8.5	11.3	12.5	13.4	15.1	17.3
	14	2.1	3.2	6.1	7.8	9.1	12.3	14.3	16.1	16.7	20.0	20.8	2.0	2.3	3.4	4.5	5.6	8.6	11.2	12.0	12.9	14.1	16.3
	21	3.6	5.3	6.8	8.6	9.6	12.3	14.3	15.4	16.4	18.4	19.2	2.0	2.2	3.0	4.7	5.6	8.6	10.7	11.4	12.0	14.3	15.2
	30	5.5	6.6	7.7	8.8	9.9	12.2	14.4	15.0	16.0	17.0	17.2	2.2	2.3	3.4	4.6	5.6	9.0	10.6	10.9	11.5	12.6	14.0
	35	6.8	7.1	7.9	8.7	10.0	12.2	14.4	15.0	15.7	16.5	16.9	2.3	2.6	3.6	4.6	5.7	9.2	10.5	10.8	11.2	12.2	13.3
	42	7.3	7.4	7.9	8.4	10.0	12.7	14.4	15.0	15.3	16.0	16.3	2.5	2.9	3.7	4.7	5.9	9.1	10.3	10.8	11.1	12.0	12.5
Picnic bay	1	0.2	0.4	1.3	2.1	3.1	5.8	7.9	8.9	10.7	13.3	14.1	0.1	0.3	0.9	1.4	2.3	3.9	6.3	7.3	8.5	9.7	10.6
	3	0.7	1.2	1.8	2.3	3.3	5.7	7.7	8.5	10.6	13.0	13.4	0.3	0.7	1.2	1.7	2.5	3.9	6.0	7.0	7.7	9.2	10.3
	7	1.8	2.2	2.6	2.8	3.4	5.7	7.4	8.2	9.9	12.2	12.7	1.1	1.4	1.7	2.1	2.6	3.9	5.6	6.4	7.3	8.4	8.7
	10	2.2	2.4	2.8	3.0	3.7	5.9	7.3	8.3	9.4	11.4	11.9	1.4	1.5	2.0	2.3	2.7	4.0	5.5	6.1	7.0	7.9	8.4
	14	2.6	2.8	3.0	3.2	3.6	6.1	7.2	8.4	9.3	10.6	10.7	1.5	1.7	2.1	2.4	2.8	4.0	5.3	6.0	6.8	7.7	7.8
	21	2.8	2.9	3.2	3.3	4.0	6.3	7.1	7.9	8.4	9.3	9.4	1.9	1.9	2.2	2.4	2.9	3.9	5.2	5.9	6.4	7.2	7.4
	30	2.8	2.9	3.2	3.4	4.8	6.3	6.9	7.3	7.5	8.1	8.3	2.1	2.2	2.3	2.5	3.0	3.9	5.1	5.6	6.4	6.8	7.0
	35	3.0	3.1	3.2	3.4	5.0	6.4	6.9	7.3	7.5	7.9	8.1	2.2	2.2	2.3	2.6	3.0	3.9	5.1	5.4	6.2	6.7	6.8
	42	3.0	3.1	3.2	3.6	5.1	6.4	7.0	7.3	7.5	7.8	7.9	2.2	2.3	2.4	2.6	3.0	4.0	5.0	5.3	6.2	6.6	6.8
Virago Shoal	1	0.0	0.0	0.2	0.4	1.1	3.3	6.0	7.7	10.3	15.5	19.0	0.0	0.0	0.3	0.5	1.4	4.3	7.9	9.5	10.6	12.9	16.6
	3	0.0	0.1	0.3	0.5	1.2	3.4	5.9	7.0	9.7	14.6	16.4	0.1	0.2	0.4	0.7	1.8	4.3	7.5	8.8	10.5	12.4	15.1
	7	0.2	0.3	0.5	0.6	1.3	3.6	5.2	6.3	8.5	12.7	13.9	0.2	0.3	0.6	1.5	2.3	4.5	7.2	8.5	9.8	12.0	15.4
	10	0.4	0.4	0.5	0.7	1.6	3.8	5.0	6.1	7.2	12.4	13.2	0.3	0.3	0.8	1.7	2.6	4.6	7.2	8.4	9.3	11.9	13.8
	14	0.4	0.4	0.5	0.8	2.0	3.7	4.8	5.9	7.0	12.4	12.8	0.3	0.3	1.2	1.9	2.7	4.7	7.1	8.0	9.0	11.1	11.5
	21	0.5	0.5	0.6	0.8	2.1	3.6	4.8	5.5	6.4	11.7	13.0	0.4	0.4	1.5	2.0	3.2	4.8	6.9	7.8	8.5	10.0	10.6
			0.4	0.7	1.1	2.1	3.7	4.6	5.3	6.1	9.9	10.5	0.4	0.9	1.8	2.2	3.3	4.7	6.8	7.3	7.8	9.0	10.1
	35	0.4	0.4	0.7	1.4	2.1	3.7	4.7	5.1	6.1	9.0	9.9	0.9	1.3	1.9	2.2	3.5	4.7	6.6	7.2	7.7	8.2	9.0
	42	0.4	0.4	0.9	1.4	2.0	3.7	4.6	5.0	6.2	8.4	8.6	1.5	1.8	2.0	2.5	3.5	4.5	6.5	7.1	7.6	8.1	8.1
Meadow 19	1	0.1	0.1	0.2	0.6	1.2	3.2	6.7	8.9	11.3	14.3	19.0	0.1	0.2	0.4	0.7	1.3	3.3	5.1	5.9	6.6	7.3	7.8
	3	0.1	0.1	0.4	0.8	1.4	3.4	6.1	9.0	11.4	13.6	15.5	0.2	0.3	0.6	0.9	1.5	3.2	4.8	5.6	6.1	6.9	7.4
	7	0.1	0.2	0.7	1.0	1.8	3.5	5.6	9.0	11.0	12.7	13.8	0.7	0.8	1.0	1.3	1.8	3.2	4.7	5.1	5.7	6.4	6.6
	10	0.1	0.3	0.8	1.1	1.9	3.6	5.9	9.0	10.5	12.4	13.1	0.7	0.9	1.3	1.6	2.0	3.2	4.5	5.0	5.3	6.0	6.4
	14	0.3	0.5	1.0	1.3	2.1	3.7	6.1	8.8	9.3	12.4	12.8	1.1	1.1	1.4	1.7	2.1	3.2	4.4	4.8	5.0	5.3	5.9
	21	0.9	1.0	1.3	1.5	2.0	3.9	6.7	8.2	9.1	11.5	11.9	1.1	1.2	1.6	1.9	2.2	3.3	4.1	4.7	4.9	5.2	5.3
	30	1.4	1.5	1.6	1.7	2.1	3.8	6.6	7.7	8.4	9.3	9.6	1.4	1.4	1.7	1.9	2.4	3.2	4.1	4.5	4.6	5.2	5.4
	35	1.4	1.4	1.6	1.7	2.4	3.9	6.6	7.7	8.0	8.5	8.5	1.5	1.5	1.6	1.9	2.5	3.1	4.0	4.3	4.5	5.0	5.0
	42	1.4	1.4	1.6	1.9	2.2	3.9	6.4	7.0	7.6	7.9	8.0	1.5	1.6	1.7	2.1	2.5	3.2	4.1	4.3	4.4	4.7	5.2

Table 3: Turbidity (NTUs). Summary statistics for the 5 long-term water quality monitoring sites (see Figure 1) showing the percentile (P) values of the turbidity (NTU) for the running mean periods of 1, 3, 7, 10, 14, 21, 30, 35 and 42 days, divided into summer (November–April) and winter (May–October) periods.

		Summer											Winter										
		0	1	5	10	20	50	80	90	95	99	100	0	1	5	10	20	50	80	90	95	99	100
Florence Bay	1	0.2	0.5	0.6	0.7	0.8	1.5	3.1	4.1	5.0	7.4	9.9	0.1	0.5	0.6	0.7	0.9	1.3	2.3	3.6	4.9	6.6	13.0
	3	0.4	0.5	0.6	0.7	0.9	1.5	3.0	3.9	4.6	6.2	9.0	0.5	0.5	0.7	0.8	0.9	1.4	2.4	3.6	4.6	6.1	9.4
	7	0.5	0.6	0.7	0.8	1.0	1.6	3.1	3.7	4.3	5.8	6.8	0.5	0.6	0.7	0.8	1.1	1.5	2.4	3.2	3.9	4.8	6.3
	10	0.6	0.6	0.8	0.9	1.1	1.6	3.0	3.5	4.0	5.4	6.4	0.6	0.6	0.7	1.0	1.2	1.6	2.5	3.2	3.4	4.5	4.9
	14	0.6	0.7	1.0	1.1	1.2	1.7	2.9	3.4	3.9	5.1	5.7	0.6	0.6	0.8	1.0	1.2	1.7	2.5	2.9	3.2	3.8	3.9
	21	0.8	0.9	1.0	1.0	1.3	1.9	2.6	3.4	3.8	4.2	4.2	0.6	0.7	0.8	1.1	1.3	1.7	2.3	2.8	3.0	3.4	3.5
	30	0.8	0.9	1.0	1.1	1.4	2.0	2.5	3.2	3.4	3.9	4.0	0.7	0.8	1.0	1.2	1.4	1.7	2.4	2.9	3.0	3.2	3.3
	35	0.9	0.9	1.1	1.2	1.4	1.9	2.5	3.0	3.4	3.9	3.9	0.8	0.8	1.0	1.2	1.4	1.7	2.4	2.7	3.0	3.3	3.4
	42	0.9	1.0	1.0	1.3	1.5	1.9	2.5	2.9	3.3	3.8	3.8	0.8	0.9	1.1	1.2	1.4	1.7	2.4	2.8	3.0	3.1	3.2
Geoffrey Bay	1	0.6	0.7	0.8	0.9	0.9	1.3	2.1	2.9	3.7	5.9	15.5	0.6	0.7	0.8	1.0	1.1	1.5	2.5	4.2	5.7	9.5	11.3
	3	0.7	0.7	0.8	0.9	1.0	1.3	2.1	3.0	3.7	5.5	8.0	0.6	0.7	0.9	1.0	1.2	1.6	2.7	3.9	5.6	7.8	10.1
	7	0.7	0.8	0.9	0.9	1.0	1.4	2.2	2.8	3.5	4.3	4.6	0.7	0.7	0.9	1.1	1.2	1.7	2.7	3.5	4.6	7.0	8.4
	10	0.7	0.8	0.9	1.0	1.1	1.4	2.2	2.7	3.2	3.6	3.9	0.7	0.8	1.0	1.2	1.3	1.8	2.6	3.5	4.0	6.2	8.0
	14	0.8	0.8	0.9	1.0	1.1	1.5	2.1	2.6	3.0	3.1	3.4	0.8	0.8	1.1	1.2	1.4	2.0	2.7	3.2	3.5	6.2	6.4
	21	0.8	0.9	1.0	1.1	1.2	1.6	2.1	2.4	2.5	2.7	2.8	0.8	1.0	1.2	1.3	1.5	2.0	2.6	2.9	3.4	5.0	5.1
	30	1.0	1.0	1.1	1.2	1.3	1.6	2.0	2.2	2.3	2.8	4.0	1.2	1.3	1.3	1.4	1.6	1.9	2.5	2.8	3.6	4.2	4.4
	35	1.0	1.0	1.1	1.2	1.4	1.6	1.9	2.2	2.3	3.6	3.7	1.2	1.2	1.4	1.5	1.7	1.9	2.5	2.8	3.3	4.1	4.2
	42	1.0	1.1	1.2	1.3	1.4	1.7	2.0	2.1	2.4	3.3	3.5	1.2	1.2	1.5	1.6	1.7	1.9	2.4	2.7	3.0	3.8	3.9
Picnic bay	1	0.1	0.3	0.6	0.8	0.9	1.3	2.3	3.6	4.5	9.5	17.9	0.6	0.6	0.7	0.8	0.9	1.3	2.8	5.3	9.1	16.7	24.1
	3	0.3	0.4	0.6	0.9	1.0	1.4	2.3	3.3	4.4	8.0	10.5	0.6	0.7	0.7	0.8	1.0	1.4	3.1	5.5	8.5	14.3	21.8
	7	0.4	0.5	0.8	0.9	1.1	1.5	2.5	3.4	4.3	6.0	6.5	0.6	0.7	0.8	0.9	1.1	1.6	3.2	5.2	7.1	12.6	16.8
	10	0.5	0.6	0.8	1.0	1.1	1.6	2.5	3.3	3.7	5.1	5.4	0.7	0.8	0.9	1.0	1.1	1.9	3.1	4.6	6.4	12.0	12.9
	14	0.6	0.7	0.9	1.0	1.2	1.7	2.4	2.9	3.2	4.2	4.7	0.7	0.8	1.0	1.0	1.2	1.9	3.2	4.1	6.8	10.1	11.4
	21	0.8	0.9	1.1	1.2	1.3	1.7	2.4	2.6	2.8	3.3	3.7	0.9	0.9	1.0	1.1	1.5	2.0	3.0	4.4	6.8	8.9	9.1
	30	1.2	1.2	1.3	1.4	1.5	1.7	2.1	2.4	2.4	2.7	2.9	0.9	1.0	1.2	1.4	1.6	2.0	2.9	5.1	5.9	7.3	7.4
	35	1.2	1.3	1.4	1.4	1.5	1.7	2.1	2.2	2.3	2.6	2.6	1.0	1.1	1.3	1.4	1.7	1.9	2.9	4.8	5.8	6.6	6.8
	42	1.3	1.3	1.4	1.5	1.5	1.8	2.1	2.2	2.4	2.4	2.5	1.1	1.2	1.4	1.6	1.7	1.9	2.8	4.7	5.4	5.9	6.0
Virago Shoal	1	1.0	1.1	1.6	1.9	2.2	3.8	10.7	17.0	25.2	36.7	44.9	0.5	1.2	1.4	1.5	1.8	3.2	10.6	16.3	22.8	32.7	41.7
	3	1.1	1.3	1.8	2.1	2.4	4.5	11.4	17.5	21.9	33.2	40.3	1.0	1.3	1.5	1.6	1.9	3.8	10.3	15.3	20.6	30.0	34.1
	7	1.2	1.7	2.1	2.4	2.7	5.3	11.3	16.3	19.5	26.6	31.5	1.2	1.3	1.7	1.8	2.2	5.2	9.8	13.3	16.8	27.3	31.5
	10	1.5	1.8	2.1	2.5	3.1	5.8	11.1	14.7	17.2	24.3	28.9	1.2	1.3	1.8	2.0	2.4	5.5	9.8	12.4	15.3	24.7	30.6
	14	1.8	2.0	2.2	2.7	3.6	6.0	11.5	13.1	15.7	22.3	24.3	1.3	1.4	2.0	2.1	2.6	5.8	9.6	11.3	14.4	23.7	25.2
	21	2.1	2.2	2.6	3.3	4.2	6.8	10.0	12.4	14.7	17.6	17.7	1.5	1.5	2.1	2.3	3.3	6.5	9.0	11.1	12.8	20.1	20.9
	30	2.3	2.7	3.6	4.0	4.6	7.1	9.8	11.9	13.2	14.6	15.8	1.9	2.1	2.5	3.2	4.1	6.1	9.0	10.7	14.8	16.4	16.5
	35	2.7	3.0	4.0	4.2	4.9	6.9	9.9	11.9	12.8	14.3	14.4	2.1	2.1	2.8	3.6	4.5	6.3	9.1	10.2	14.6	16.1	16.6
	42	3.3	3.5	4.0	4.3	5.2	7.2	10.4	11.3	12.5	13.9	14.5	2.1	2.2	3.3	3.5	4.8	6.4	8.7	10.3	13.0	15.8	16.0
Meadow 19	1	0.0	0.5	0.9	1.3	1.7	3.3	7.8	13.3	19.8	32.7	42.5	1.3	1.5	1.9	2.2	2.5	3.8	9.1	16.0	22.9	35.6	56.8
	3	0.2	0.6	1.1	1.4	1.9	3.7	7.9	13.1	17.7	29.5	37.5	1.5	1.6	2.1	2.3	2.7	4.2	9.7	15.6	21.2	30.4	39.1
	7	0.5	0.8	1.2	1.6	2.3	4.1	8.1	12.3	17.4	24.0	26.7	1.9	2.1	2.3	2.6	3.0	5.1	10.5	13.5	17.5	21.7	25.2
	10	0.7	0.9	1.3	1.6	2.5	4.3	8.5	11.6	16.0	22.0	22.2	2.1	2.2	2.5	2.7	3.4	5.7	10.3	13.0	14.9	18.4	22.0
	14	0.8	0.9	1.4	1.8	2.5	4.6	9.1	11.4	15.3	18.5	19.8	2.2	2.5	2.7	3.0	3.8	6.7	9.7	11.4	12.1	16.8	17.0
	21	0.9	1.0	1.5	2.1	2.8	4.8	9.4	11.5	13.9	15.1	15.5	2.6	2.6	2.9	3.4	4.2	7.2	8.9	9.6	10.7	13.0	13.1
	30	1.5	1.6	1.8	2.1	3.2	5.5	9.0	11.5	12.6	14.2	14.8	2.9	3.1	3.2	3.5	5.7	6.9	8.4	9.0	10.2	11.4	12.0
	35	1.6	1.8	1.9	2.2	3.3	6.0	9.0	11.1	12.8	14.4	15.0	2.9	3.0	3.3	3.8	5.5	6.8	8.3	9.2	9.7	11.3	11.4
	42	1.8	1.8	2.2	2.4	3.4	6.0	8.8	11.6	12.3	14.1	14.6	3.0	3.1	3.7	4.1	5.1	6.9	8.5	8.7	9.3	10.2	10.2

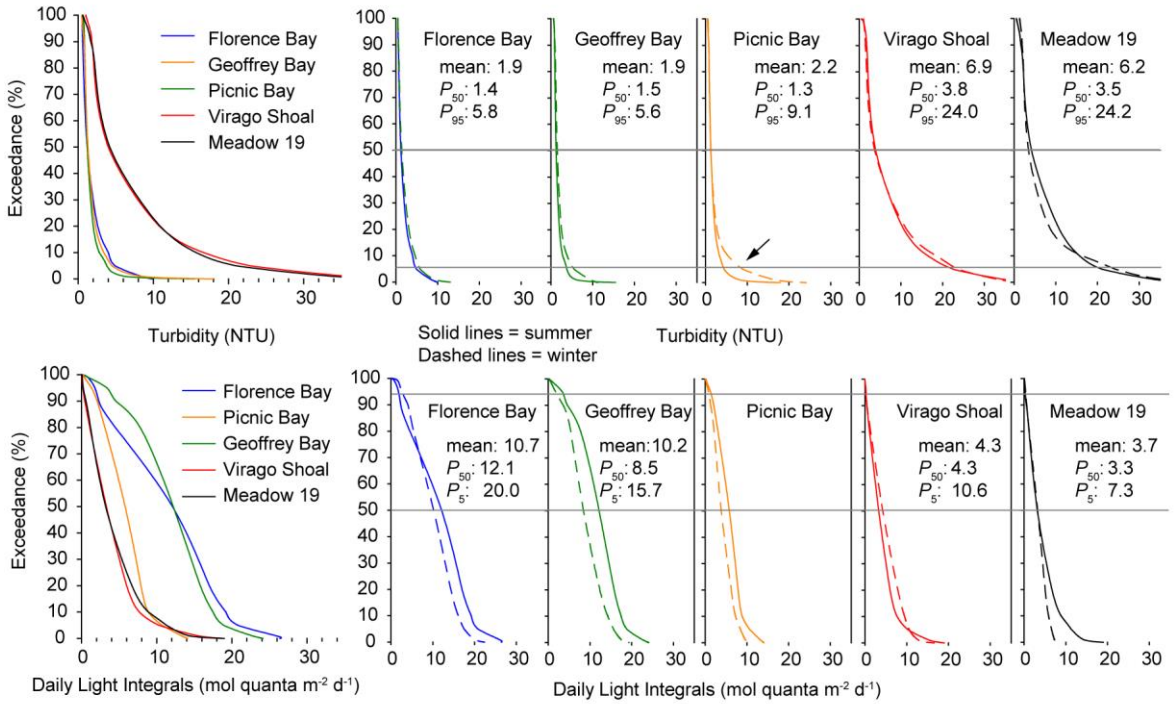

Figure 5: Exceedance plots showing the proportion of average daily turbidity (NTU) or light (DLIs) above or below given levels for the 5 long-term water quality monitoring sites (see Figure 1) across the whole study period, and then for winter and summer. Numbers in the figures refer to the mean, median (P_{50}), and 95th percentile (P_{95}) values for winter periods only.

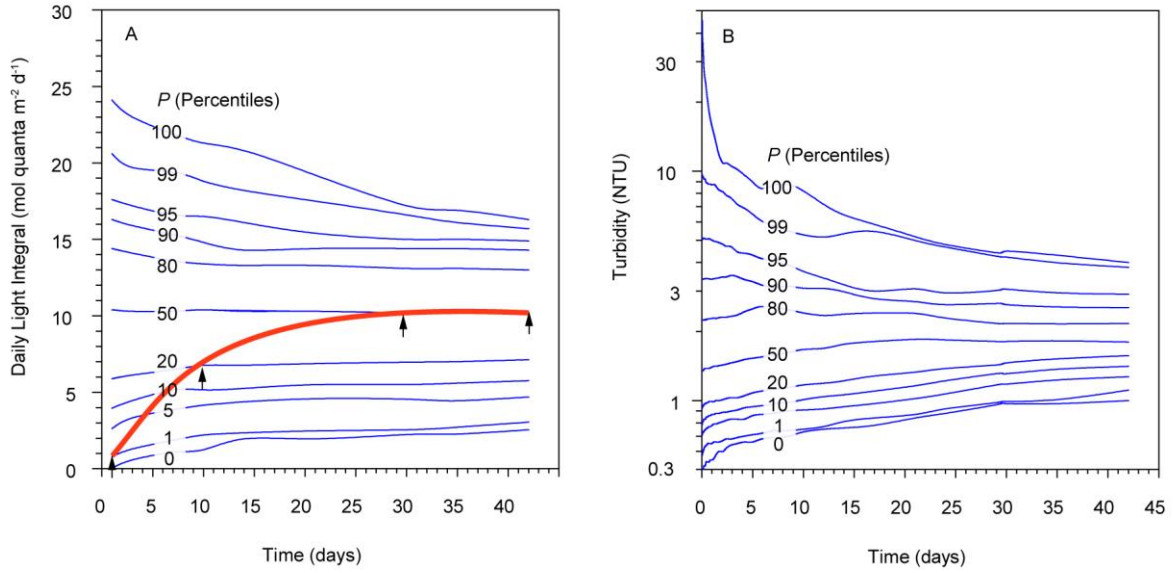

Figure 6: (A. B) Running mean percentiles analysis of the Geoffrey Bay site data showing the P_{100} to P_0 over running mean periods from 1–42 d for light (daily light integrals, mol quanta m^{-2} d^{-1}) or turbidity (NTU) (see Figure 1). The red line is a hypothetical scenario (at Geoffrey Bay), showing the previous 42 days' worth of light monitoring data (see text below for further explanation).

Figure 6 shows a similar analysis to the exceedance curves above but on different running mean periods of 1 to 42 d (i.e. 6 weeks) (see Fisher et al. (2015), Jones et al. (2015a), Jones et al. (2016) for further details). The light and turbidity data from Geoffrey Bay were used to demonstrate the approach. To avoid biased averages, no running mean value was calculated if more than 20% of the data points for any running mean time-period were missing. Once calculated the percentile (*P*) values ($P_{0, 1, 5, 10, 20, 50, 80, 90, 95, 100}$) of the different running mean values were then plotted on the y-axis against the running mean time-period of the x axis, generating a series of curves (Figure 6).

The instruments recorded turbidity every 10 mins and the P_{100} over a 10 min running mean interval at Geoffrey Bay was 44.3 NTU (i.e. the highest NTU recorded at Geoffrey Bay over the three-year study, (see also Table 1). At successively longer running mean intervals (from hours to days to weeks) the upper percentile values $P_{100, 99, 95}$ etc progressively decrease, because water quality will ultimately get better in time (from the worst-case scenario, Figure 6 B). For the lower percentiles ($P_{0, 1, 5)}$ the situation is similar but in the opposite direction: the lowest NTU value was 0.5 NTU (for a 10 minute readings) but as the running mean period increased the NTU values increase as things will ultimately get worse (from a best-case scenario, Figure 6 B). Light was measured at 10-minute intervals, but the analyses was conducted with a daily light integral and the shortest running mean interval was therefore 24 h. For light, the lower percentile values are of most interest (as they represent possible light limitation) and the minimum daily light level measured was 0.04 mol quanta which is functionally equivalent to a day in darkness (see Jones et al. (2015a) for further discussion).

The red line in Figure 6 A is a hypothetical scenario (at Geoffrey Bay), showing the previous 42 days' worth of light monitoring data. In the previous day (day 1 on the x-axis, see arrow), the DLI was very low at 1 mol quanta $m^{-2}\,d^{-1}$, which was at the P_1 of light values recorded (over the 3-year period). This indicates the benthic environment experienced in the last day was close to a worst-case scenario. However, over the previous 10 d (and incorporating the previous day's extremely low light) the benthos has experienced ~6 mol quanta $m^{-2}\,d^{-1}$ (i.e. the P_{20} value, see arrow). Over the previous 30 to 42 days, the light level was equivalent to the median value (P_{50}) and so would be considered normal. Using such a technique, the running means/percentile analyses allows contextualization of any water quality conditions at multiple different time frames against a background that the benthic organisms have naturally experienced (albeit in this case based on the ~3-year monitoring period). Each day a new set of running mean values can be calculated and short-term acute periods (i.e. days) and longer term (i.e. weeks) more chronic disturbances conceptualised, allowing assessment of the amount of 'pressure' being placed on benthic communities. We suggest that this is a useful technique to monitor the effects of dredging on water quality in real time (see Section 0).

The analyses below examine whether there is any evidence of an effect of past maintenance and/or capital dredging activities on the water quality at the five monitoring sites. Analyses exploring the environmental predictors of turbidity indicated overwhelming support (AICc model weight = 1) for a single model involving (perhaps not unexpectedly) a bi-variate smooth between the u and v components for wind summarised as a daily three-day running mean (i.3_wind.u.te.i.3_wind.v), and an additional effect of daily mean wave height (i.1_waves). This is despite a large range of other variables been considered in the model set, including 1, 3 and 7 day running mean wind vectors, MJO amplitude and phase, moon illumination, month of the year and season. This suggests that while there are clear differences in turbidity among

summer and winter, these differences are largely due to the wind and wave conditions differing between the two seasons. Turbidity increased with increasing mean wave height (Figure 7 A) and was further increased when the wind was blowing very strongly from a South-Easterly direction (Figure 7 B). Overall the model explained 44% of the variance (on a log-link scaling, Figure 7 D), including the random site offsets (Figure 7 C).

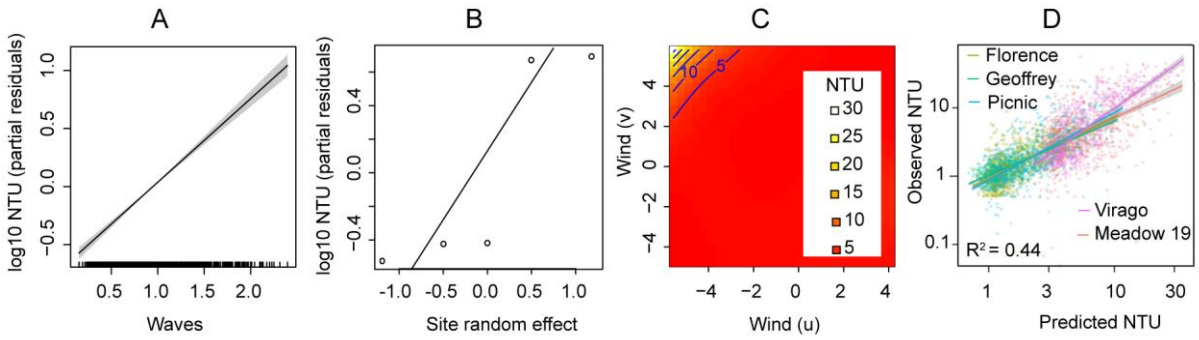

Figure 7: The best fit environmental GAM model for explaining turbidity (NTU) during non-dredge periods across five sites in Cleveland Bay, including partial residual plots for the effect of (A) waves, (B) site offsets (both on a log-link scale), (C) a contour plot of the influence of u, v and wind speed vectors and (D) observed versus predicted NTU.

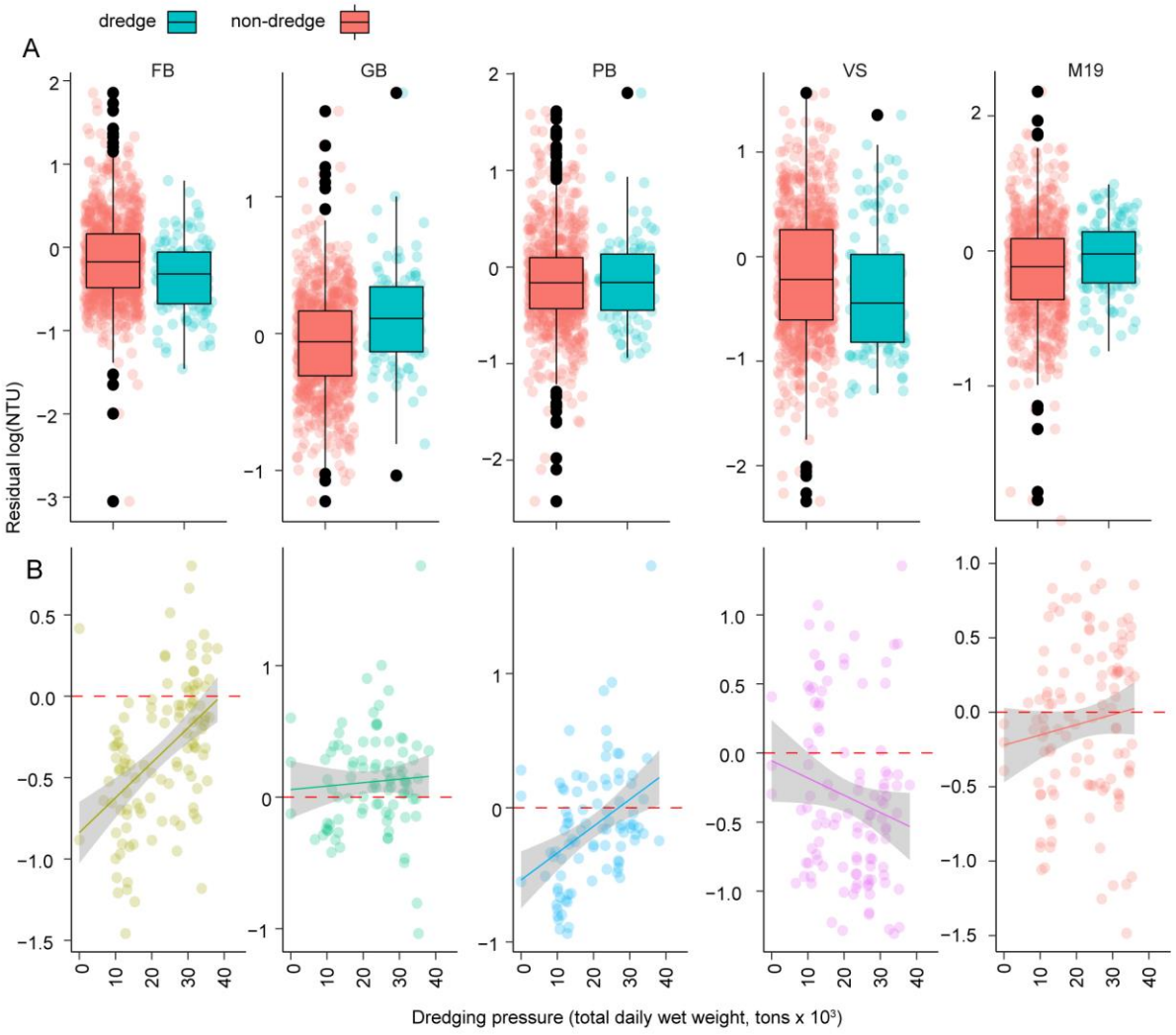

Figure 8: Residual NTU values as a function of dredge period (A, dredge, non-dredge) and dredging pressure (B, total daily dredged wet weight), for five water quality monitoring sites in Cleveland Bay. Residuals were calculated as observe-predicted, with predicted values obtained from the best fit environmental model (Figure 7).

There was considerable variability in residual NTU, with extensive overlap between dredge and non-dredge periods (Figure 8). Florence Bay and Virago Shoal had lower residual NTU values during the dredge periods compared to non-dredge periods whilst Picnic Bay had very similar residual NTU values between dredge and non-dredge periods. Both Meadow 19 and Geoffrey Bay had slightly higher residual NTU values during dredging (Figure 8). There was some evidence that residual NTU did increase with dredging pressure, with reasonably strong relationships at Florence Bay and Picnic Bay, and weak positive relationships at Geoffrey Bay and Meadow 19 (Figure 8). There was a negative relationship between residual NTU and dredging pressure at Virago Shoal (Figure 8).

Bayesian estimates of standardised effect sizes indicated that wind and wave conditions had a much bigger effect on turbidity than the level of dredging pressure (Figure 9). With the exception of Virago Shoals, median posterior probability estimates of the effect of dredging pressure on turbidity were greater than zero, meaning there was some evidence dredging

increases turbidity at these sites (Figure 9). For Meadow 19 and Geoffrey Bay, 95% credible intervals overlapped zero, suggesting limited impacts of dredging on turbidity (Figure 9). For Florence Bay and Picnic Bay 95% credible bounds did not overlap zero, suggesting some positive effect of dredging intensity on water quality (Figure 9).

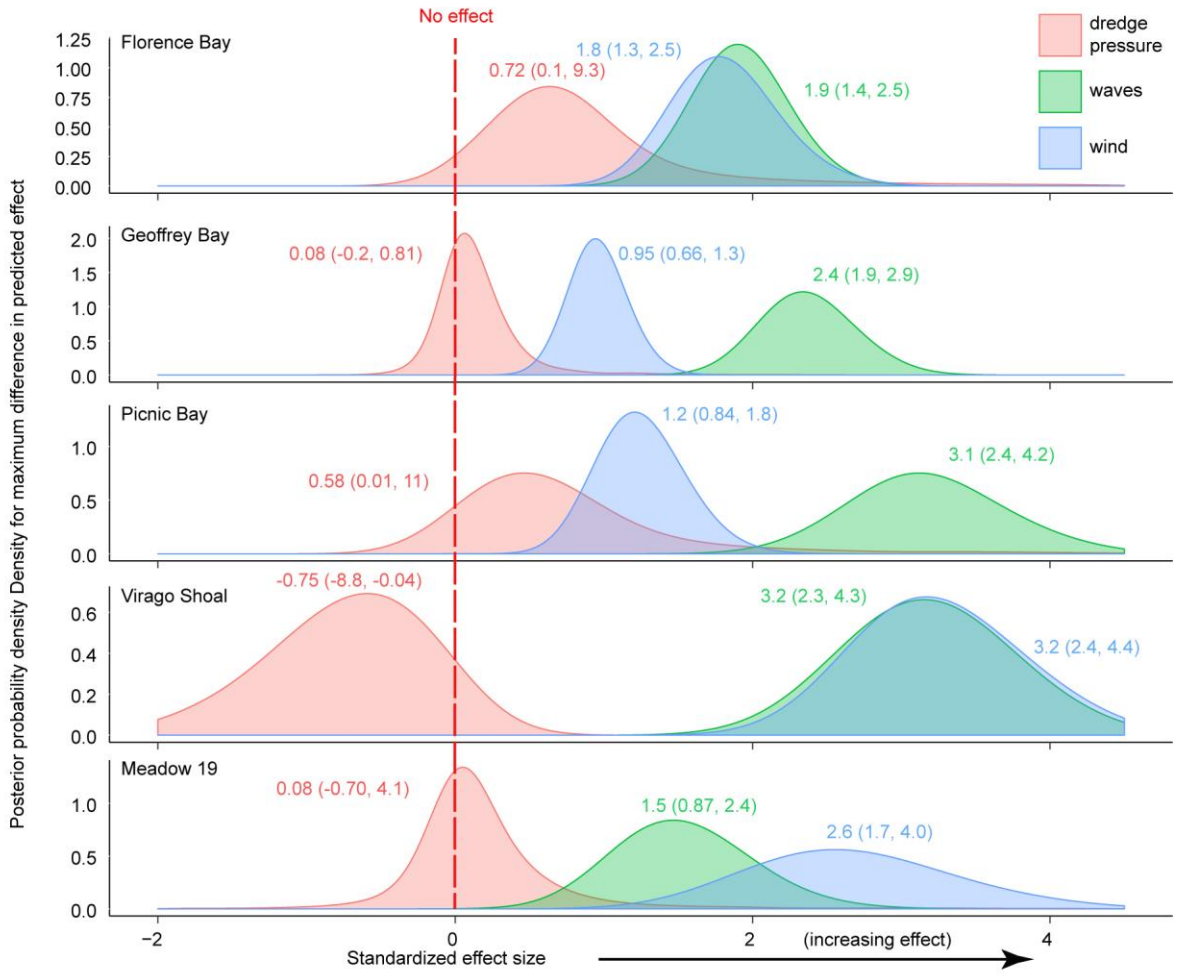

Figure 9: Bayesian estimates of standardised effect of waves, wind and dredging pressure on turbidity (NTU), for the five water quality monitoring sites in Cleveland Bay. Shown are posterior probability density estimates for the maximum difference in predicted values for each predictor, based on averages for the other predictors in the best fit model, standardised by dividing by mean NTU for each site. Coloured values show the median and credible intervals of the posterior probability of the standardized effect (median (0.025, 0.975)). The vertical dashed red line indicates the x-axis location of zero effect. Values to the right indicated higher effect sizes.

Evidence of changes to water quality conditions associated with dredging at Picnic Bay are consistent with the fact that much of the dredging activity occurs along the Platypus channel, and Picnic Bay is the site most likely to be influenced by dredging activities in this area (Figure 1). Similarly, evidence of changes to water quality associated with dredging at Florence Bay may relate to the fact that during maintenance dredging material is placed at the dredge material placement area which is directly to the east (see Figure 1).

Although dredging may have an impact on turbidity at Florence and Picnic Bays, the estimated standardised effects for dredging were only 0.72 and 0.58 times mean site NTU respectively, which are between two and five times lower than the effects of either wind or waves on turbidity at Florence Bay and Picnic Bay (Figure 9). While wind and waves both had stronger effects on turbidity than dredging at all sites, the relative influence of wind and waves varied (Figure 9). At Meadow 19 the effect of wind appears to be higher than that of waves (2.6 versus 1.5 times mean site NTU, Figure 9). At Florence Bay and Virago Shoal the effect of waves and wind were similar, with effects of around 2 (Florence) and 3.2 (Virago) times mean site NTU (Figure 9). At both Geoffrey Bay and Picnic Bay the effect of waves was higher than that of wind, with median wave effects as high as 2.4 and 3.1 times mean NTU respectively (Figure 9).

4.1.2 Turbidity and light (spectrum) time series

Over the 31-d deployment of the spectral light sensor the maximum daily underwater PAR varied over an order of magnitude from <10 µmol quanta m^2 s^{-1} on 1 June to 180 µmol quanta m^2 s^{-1} on 18 June (Figure 10 A). Maximum daily surface light levels varied two-fold, from 750 µmol quanta m^2 s^{-1} during an overcast day on June 11 to ~1500 µmol quanta m^2 s^{-1} during a series of cloud-free days over the month (inferred from the uniform and symmetrical light profiles) (Figure 10 A). In the first week of June a week-long natural turbidity event occurred at Florence Bay caused by a period of increased wind speed (data not shown) (Figure 10 B). Average daily NTUs increased from ~1 NTU at the end of May to ~8 NTU in the first week of June), including a maximum turbidity of 44 NTU at 05:30 h on 1 June (Figure 10 B).

The spectral light profiles over a 2 h period centred on solar noon was calculated for each day of the deployment and then standardised to a mean of zero and standard deviation of 1 (Figure 11 A). The profiles showed considerable variability in the blue wavelength (λ 450–495 nm) over the month as compared to the yellow/green wavelength (λ550 nm) (Figure 10 C). The ratio of blue to yellow/green wavelength and the PUR:PAR ratio (see further below) were plotted over the deployment period and showed pronounced decrease during the turbidity event (Figure 10 C). To further examine this effect, Figure 11 B shows the spectral profile of 8 days during the deployment where there were combinations of either high or low turbidity in combination with high or low surface light caused by the presence or absence of clouds. The high turbidity days showed very distinct spectral profiles irrespective of surface light levels and characterized by preferential loss of more blue light and a shift in the underwater spectrum to longer wavelengths (a red-shift) (Figure 10 B). Although reducing the underwater light levels, cloudy periods had very little effect on the spectral profiles i.e. acted as a neutral density filter.

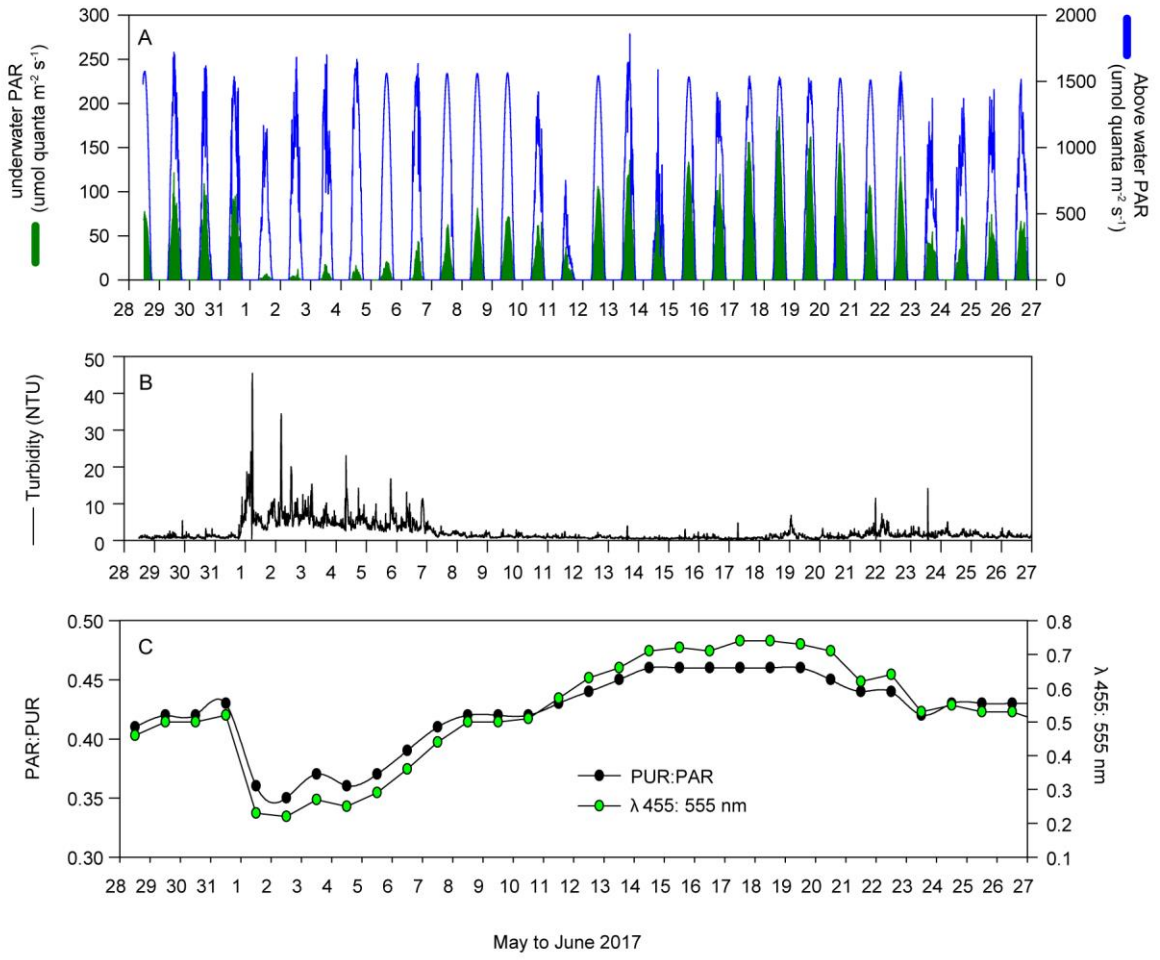

Figure 10: (A) Underwater PAR (primary y-axis, µmol quanta m^2 s^{-1}) at Florence Bay and above water PAR (secondary y-axis, µmol quanta m^2 s^{-1}) at the weather station beside Florence Bay (see Figure 1), (B) Turbidity (NTU) (C) the ratio of PAR/PUR (primary y-axis) and λ455 nm (blue) to 555 (green) wavelength (secondary y-axis). from 28 May to 27 June (2017).

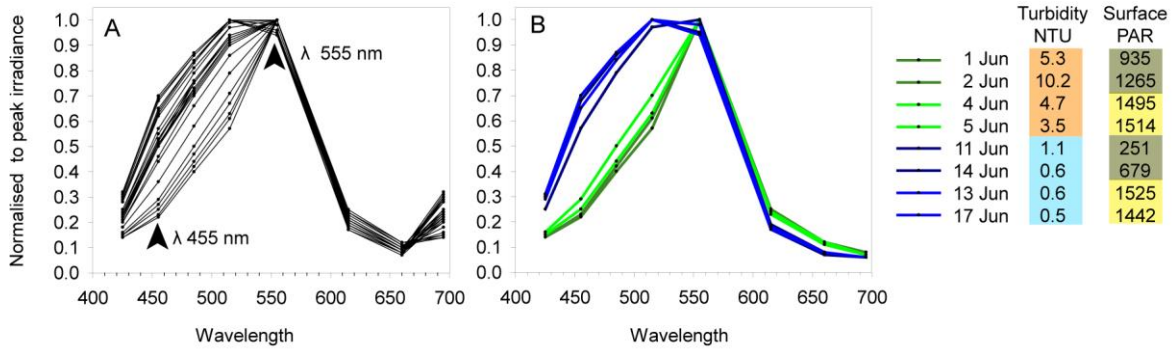

Figure 11: A, B. Normalised irradiance spectra from the multispectral light sensor deployment at 8 m depth at Florence Bay for (A) all days (B) 8 days showing the effects of high and low turbidity with and without cloud cover (see Figure 10).

4.1.3 Vertical water quality profiling

At the start of each water column profile sampling, a water sample was collected by Niskin bottle at ~0.5 m depth and used to generate the relationship between SSC (mg L^{-1}) and NTU. SSCs averaged 23.9 (range 0.04–175.5 mg L^{-1}) and the linear relationship (Figure 12 A) used to determine nephelometrically-derived SSCs from all vertical profiles.

In the shipping channel, the turbidity of the plumes collected immediately behind the dredge showed a range of different vertical profiles, including surface maxima, mid-water maxima and bottom maxima, as well as well mixed homogenous vertical SSC profile. Representative examples of these patterns are shown in Figure 13 A. At the dredge material placement area, the profiles were more consistent with very pronounced turbidity maximum usually >100 mg L^{-1} a few metres from the seabed (Figure 13 B).

For all channel profiles with equivalent depth (n=12 sites) the SSCs were standardised to the maximum value and averaged showing there was an increase in nephelometrically-derived SSCs with depth, with measurements within 1 m of seabed ~3.5× higher than the surface (0.3–0.5m) (Figure 13 C). For the measurements at the dredge material placement area, nephelometrically-derived SSCs within 1 m of the seabed were~10× higher than the surface (0.3–0.5m).

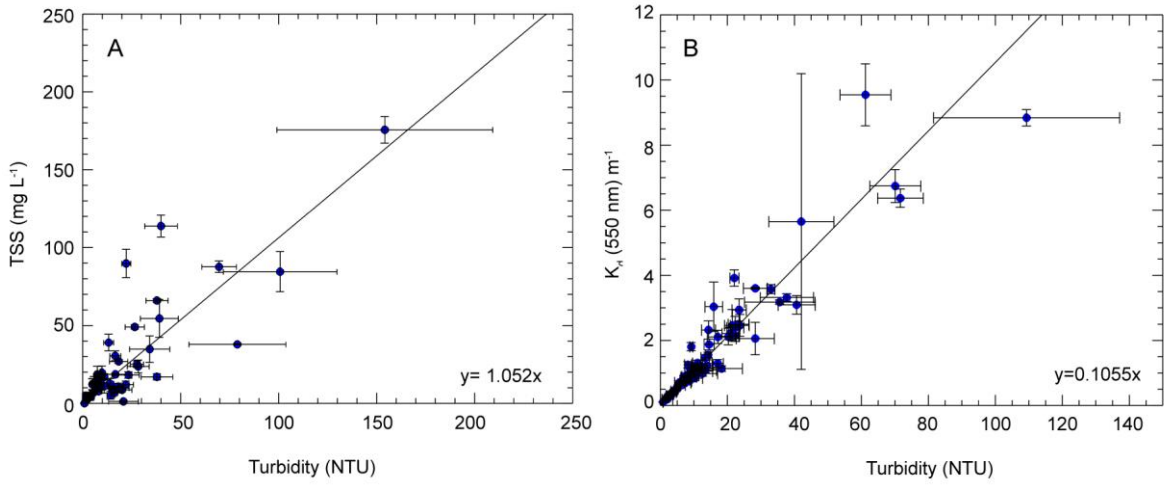

Figure 12: The relationships between (A) TSS (mg L^{-1}) and turbidity (NTU) and (B) K_d (550 nm) (m^{-1}) and turbidity (NTU) from the vertical profiling of the dredge plume.

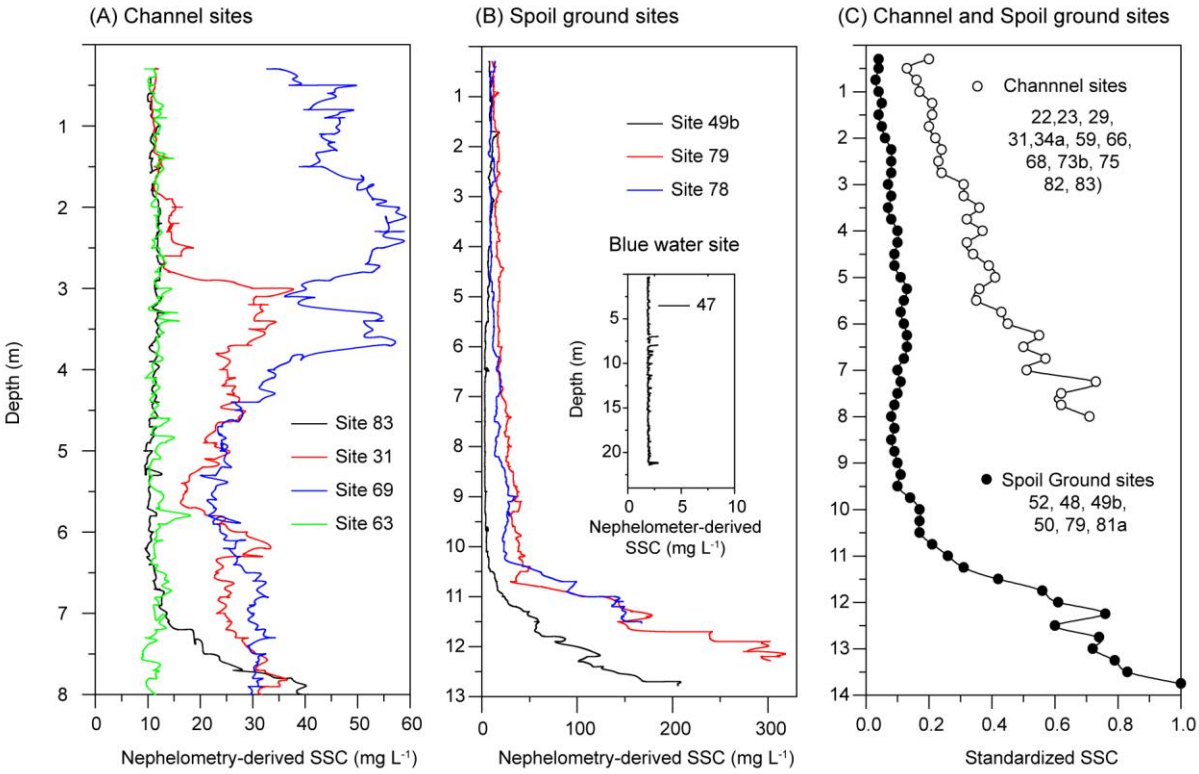

Figure 13: Representative examples of some of the vertical profiles collected from plumes behind the working TSHD showing depth related patterns in nephelometrically-derived SSC (mg L^{-1}) in (A) the channel and (B) the dredge material placement area, (C) Mean standardised profiles of channel and dredge material placement area nephelometrically-derived SSC (mg L^{-1}) profiles with equivalent depths indicating the typical depth-related patterns in SSCs.

Representative examples of vertical light profiles using the USSIMO multispectral radiometer are shown in Figure 14 for the site at the entrance of Cleveland Bay (site 47) and a site just off Geoffrey Bay (site 98) (Figure 1). Both sites had very low turbidity at the time of sampling. In the offshore site the upper 20 cm had a relatively even distribution of blue, green and red wavelengths and there was rapid loss of red light with depth to barely detectable levels by 10 m. Blue light was also attenuated, albeit at a lower rate and at the seabed (20 m) the peak spectrum was between 400–500 nm (blue to green) with maximum light penetration at 475 nm (Figure 14 A). At Geoffrey Bay there was also an even distribution of blue, green and red wavelengths in the upper 20 cm of water and a rapid loss of red light with depth. However, the vertically averaged absorption coefficient K_d was higher for blue wavelengths and at 8 m depth, at the seabed, the peak spectrum was in the 550–600 nm (green-yellow) range with a maximum at 575 nm (Figure 14 B).

Not all wavelength of lights are absorbed equally or are as effective for photosynthesis (see Discussion), and Figure 14 also shows the absorption spectra for symbiotic dinoflagellates (of corals) digitised from Figure 2 B in Hennige et al. (2009). The normalised absorption spectra are an indication of how well the dinoflagellates harvest light of different wavelengths (see Discussion). The data shows that they are most efficient at light harvesting in the blue and red wavelengths and comparatively weak at absorbing in the green and yellow wavelengths.

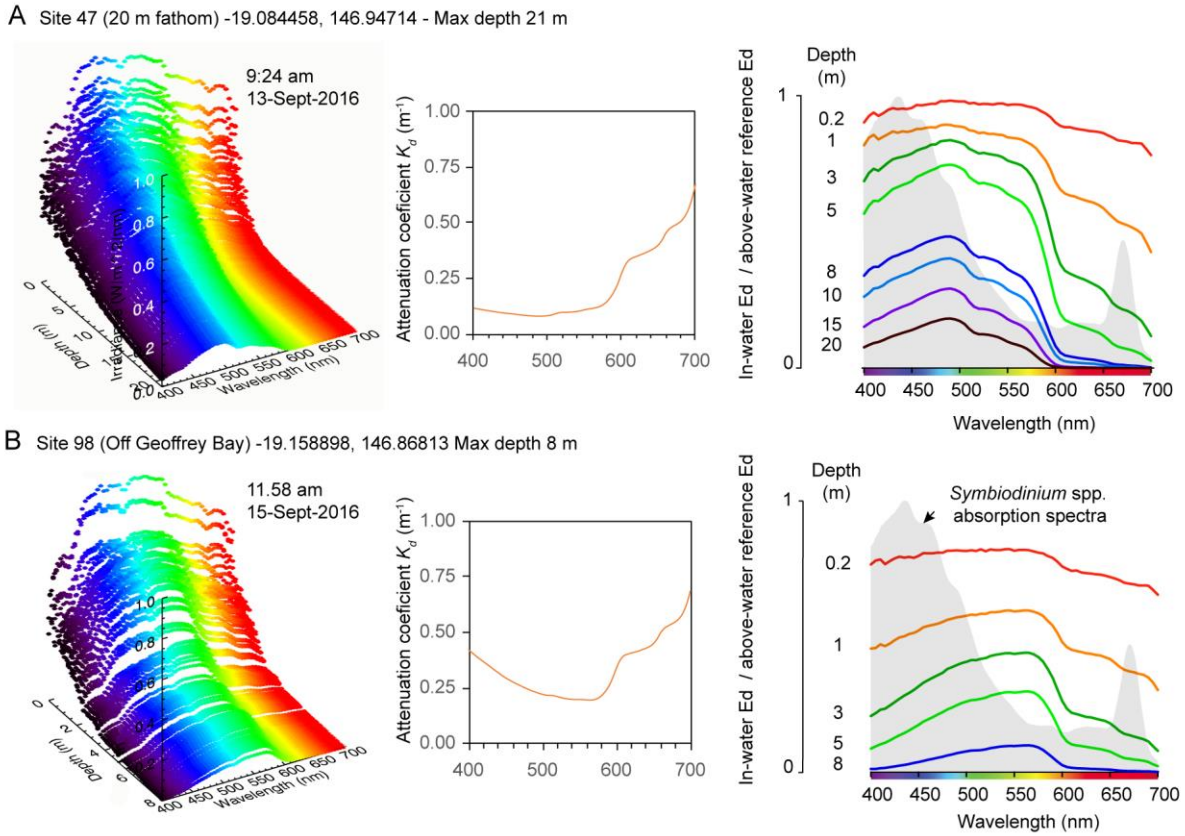

Figure 14: (A) Profile or irradiance (W/m^2/nm) spectra, vertically averaged spectral attenuation coefficients and normalised downwelling irradiance spectra for site 47 (furthest offshore) and (B) site 98 (off Geoffrey Bay) (see Figure 1) in September 2016. Shaded areas represent the absorption spectra for symbiotic dinoflagellates (of corals) digitised from Figure 2 b in Hennige et al. (2009).

Principal coordinate analysis (PCO) was used to visually compare the different sites around Cleveland Bay based on the hyperspectral USSIMO data (at 50 nm increments from 400–700 nm) using data from 3 m depth and all sites where light was detectable at 3 m (~50 sites).

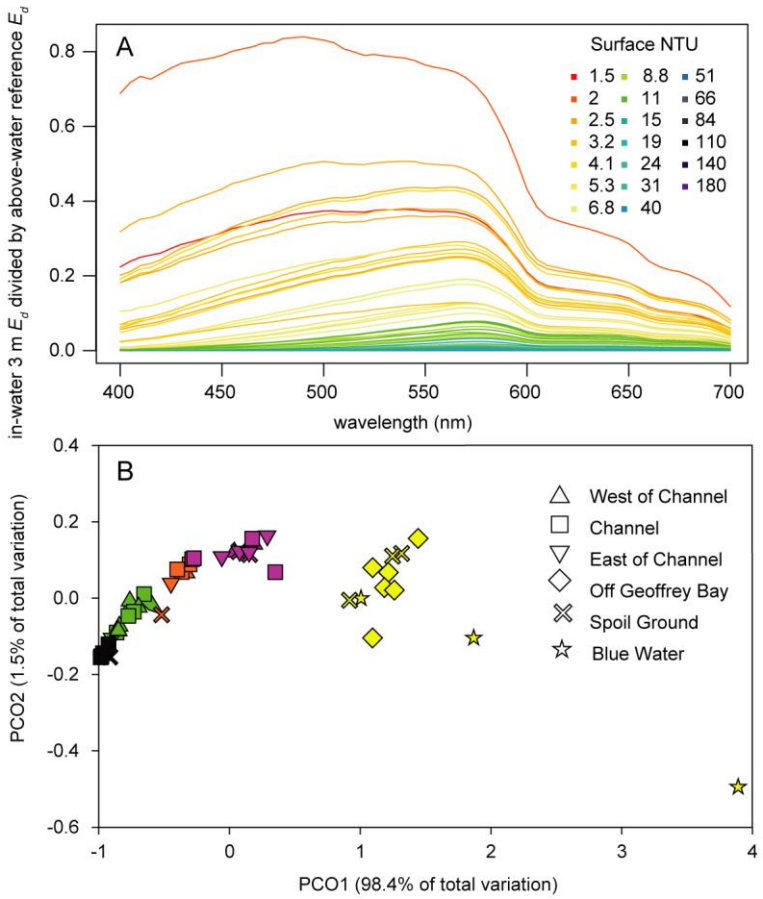

Figure 15: (A) Downwelling irradiance at 3 m depth for 50 vertical light profiles with surface NTU values ranging from 1.5 to 180 NTU. (B) Principal coordinate analysis (PCO) of spectral profiles from 3 m depth for 50 vertical profiles in Cleveland Bay (see text).

Analyses were performed in PRIMER 6 (Plymouth, UK) using Euclidean distances and Spearman Rank correlations to identify wavelengths that contribute most to the differences observed. The colour of the shape corresponds to the sum of the total light, which increases from the lowest values (black; left of the ordination) to the highest values (yellow; right of the ordination). The wavelengths contributing most to the shift of samples to the right of the ordination include 490, 510 and 525 nm, whereas the least correlated wavelengths include 690, 695 and 700 (Figure 15).

Morel (1978) suggested calculating a new parameter, photosynthetically usable radiation (PUR) which is a product of the light availability and absorption efficiency and is a more relevant parameters for expressing light available for photosynthesis. PUR was calculated according to equation 2.

$$PUR = \int_{400\ nm}^{700\ nm} PAR(\lambda)A(\lambda) \qquad \text{Equation 2}$$

where PAR is the incident spectral irradiance and Aλ a weighted probability that a photon will be absorbed at a given wavelength (based on absorption coefficients from Hennige et al. (2009) and as shown in Figure 14).

The ratio of PUR to PAR was calculated for the time series data (Figure 10 E) with the light data from a 3 h period centred on midday. The analyses shows a 25% reduction in the ratio of PUR to PAR during the turbidity peak. Since the analysis was conducted with standardised data (normalised by the peak wavelength at every 15-minute interval) it indicates that in addition to attenuation of light from the high turbidity, the remaining light is potentially less photosynthetically usable (because of the change in spectrum). Since most of these spectral changes are associated with a change from blue to green light an additional, and computationally simpler value was included which is simply the ratio of blue light (455 nm) to green light (555 nm). This value (λ455:555 nm) decreases to ~0.2 during the week-long turbidity event and returning to 0.5 when turbidity levels fell back to 1 NTU. Notably, the λ455:555 nm is 0.25 on day 8 which was a cloud-free day with high turbidity and >0.5 on Day 14 (a cloudy day with low turbidity) (Figure 10 E and Figure 11 B). The implications here are that the ratio could be used as a simple marker or signature of light reductions associated with suspended sediments as opposed to those associated with clouds (see Discussion).

Overall, these analyses suggest that although clouds influence the quantity of underwater light they do not change the spectral quality. Elevated turbidity levels can affect both the quantity and quality of light. The shift in spectral quality is incorporated into the laboratory-based experiments quantifying the effects of turbidity on corals and sponges (see Section 4.2).

4.1.4 Sediment deposition measurements

The TSHD dredge was in Cleveland Bay from 1–27 August 2017 and actively dredging in the Platypus channel for 18 days. The dredge logs record the start and finish of various runs along the channel, the wet and dry volumes and use the channel marker buoys to indicate where the dredging is occurring (i.e. between P7 and P9 etc, Figure 1). In the first half of the month the dredge was working in parts of the channel away from the sensors, but in the middle of the month (16–18 August) the dredge was working up to the marker buoys (finishing the run beside the markers where the sensors were located at P11 and P12, Figure 1 C). From 18–27 August the dredge regularly worked past the sensors, taking 20 hopper loads to the dredge material placement area (Figure 16 A). In addition to turbidity generated from seabed disturbance by the drag heads and the dredge propeller wash, there were 55 transits of large commercial vessels (e.g. cargo and tankers ships) along the Platypus channel (Figure 16 A). These movements also generate turbidity from propeller wash which could have been detected by the sensors in addition to the overall natural wave-induced turbidity from the daily sea breeze.

The deposition sensor deployments occurred over a spring-neap cycle with current speeds <0.15 m/s, and over a relatively calm period with no storms of weather fronts, and with an average windspeed in August 2017 of 16.3 kph which is the 3rd lowest monthly average windspeed over a 78 month period in Cleveland Bay (from July 2012–November 2019)(AIMS 2016) (Figure 16 B, C). Turbidity levels (recorded 200 m from the edge of the channel) were typically low ~5 NTU, but over the second half of the month, which coincided with the dredge working close by (up to 27 August), there were frequent transient increases in turbidity from 5 to >50 NTU which (Figure 16 D).

Sediment accumulation rates were measured each hour and the readings were normalized to 24 h for comparative purposes. For the sites closest to dredging (100 m away from the channel edge) there was a >3 order magnitude variation in the 1 h sediment accumulation from 1 to >2000 mg cm^{-2} d^{-1}, indicating short term periods of intense sediment accumulation (black circles in Figure 16 E). When averaged over the day the accumulation rates ranged from 24–491 mg cm^{-2} d^{-1} and averaged 145 ± 41 mg cm^{-2} d^{-1} ($\bar{x}$ ± 95% confidence intervals)(grey bars in Figure 16 E). Over the second half of the month, when the dredge was working past the sensors, accumulation rates over a 1 h period (normalized to a 24 h period) often exceeded 1000 mg cm^{-2} d^{-1} Figure 16 A) and over a 24 h period averaged 230 mg cm^{-2} d^{-1}(Figure 16 E). Average daily sediment accumulation rate decreased steeply with increasing distance from the channel averaging 52 ± 41 mg cm^{-2} d^{-1} at 200 m and ~40 mg cm^{-2} d^{-1} at the 400 and 800 m sites.

Another way of examining this gradient is by exceedance curves based on daily mean sediment accumulation rate which showed, over the whole August period, the median P_{50} daily value was 120 mg cm^{-2} d^{-1} for the 100 m site which was >2× the value at 200 m (48 mg cm^{-2} d^{-1}) and 3.5–5× the values at 400 and 800 m (22 and 34 mg cm^{-2} d^{-1} respectively) (Figure 17 A). The median and upper and lower quartiles and distance from the channel edge is shown as an inset in Figure 17 A, showing the steep gradient and rapid decrease in sediment accumulation with increasing distance from the channel edge.

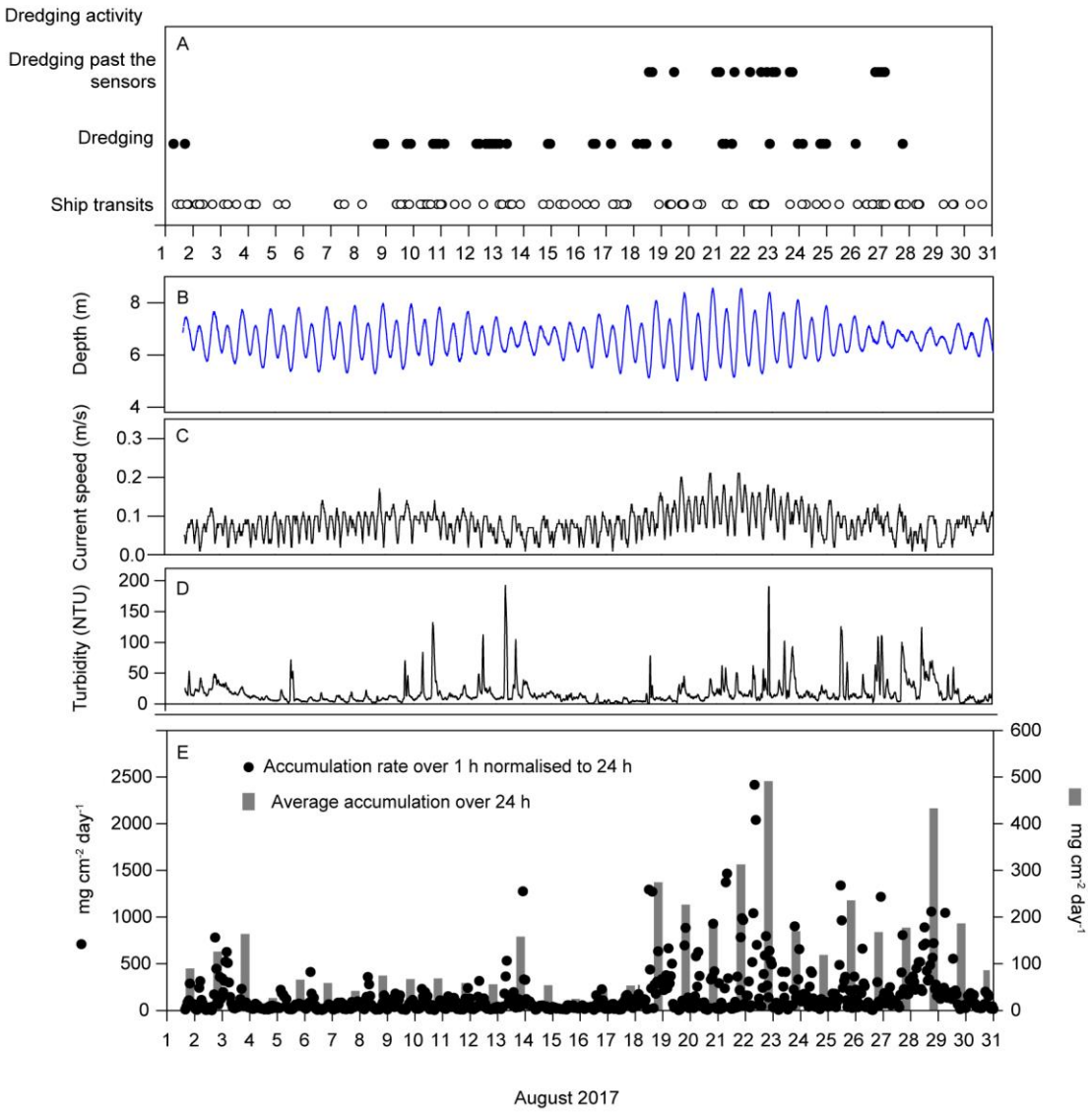

Figure 16: (A) Proximity of dredging activity to the deposition sensor transects showing dredging of the channel past the sensors, or dredging up to the channel markers near the sensors or other areas of Platypus channel away from the sensors (see text), (B–C) Depth (m) and current speed (m/s) at site 4 (800 m away from the channel), (D) A 2 h running mean of turbidity (NTU) at site 2 (20 m away from the channel) and (E) Sediment accumulation rates (mg cm^{-2} d^{-1}) over a 1 h period (normalised to 24 h) (black circles, primary y axis) and average sediment accumulation rates over the day (grey bars) at sites 1–4, 100–800 m away from the channel.

The 1 h values (normalized to 24 h) were also used to generate running means for 6, 12, 24, 48 and 96 h periods and the percentiles calculated (Figure 17 B). As with the similar types of analyses for turbidity and light (Table 2, Table 3, Figure 6) these analyses show what values are close to the worst case scenario for different time periods of sediment accumulation, showing, for example, a P_{95} of 400 mg cm^{-2} d^{-1} over a 1 d (24 h) period 100 m away from the channel edge (Figure 17 B).

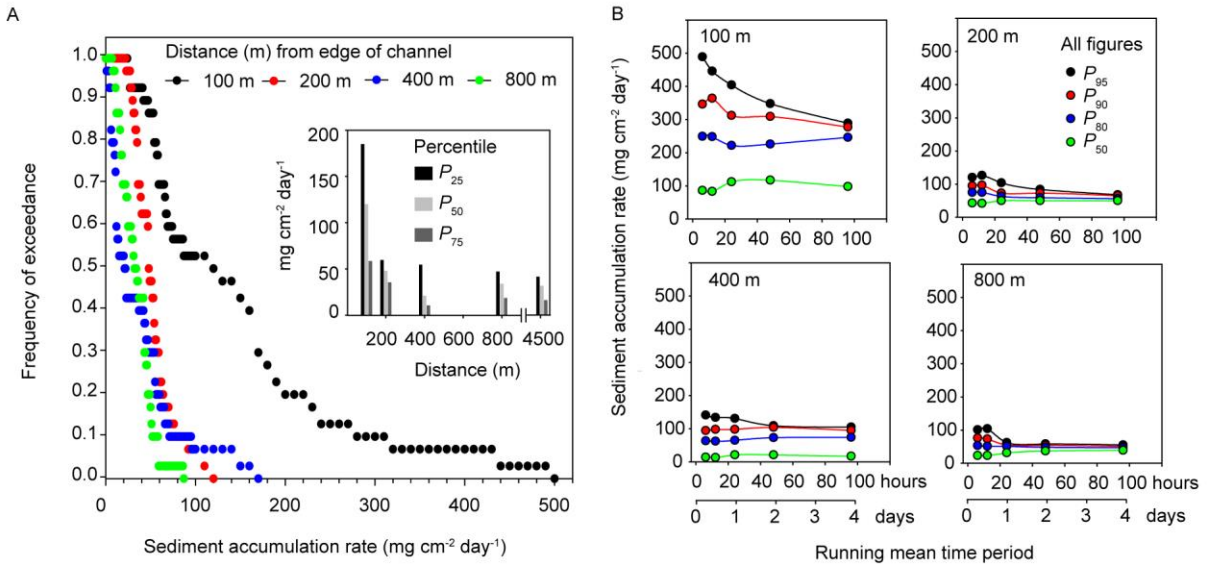

Figure 17: (A) Exceedance plots showing the proportion of average daily sediment accumulation rates (mg cm-2 d-1) above or below given levels for the 1-month deployment of the deposition sensors. Inset figure is the P_{25}, $P5_0$ and P_{75} sediment accumulation value against distance (m) from the channel edge and values for Middle Reef, 4.5 km from the channel from the study of Whinney et al. (2017)(see Discussion). (B) Running mean percentiles analysis of the deposition sensor data showing the P_{95}, P_{90}, P_{80} and P_{50} accumulation rates (mg cm-2 d-1) over running mean periods from 6 h–96 h (0.25–4 d).

4.1.5 Empirical spectral solar irradiance model

Figure 12 shows the relationship between NTU and TSS (mg L^{-1}) and the relationship between vertically averaged K_d (550 nm) (m^{-1}) and turbidity with K_d ranging from <0.1 m^{-1} to ~10 m^{-1} over the turbidity range from 0.5 to 140 NTU (Figure 12). These linear relationships applied to all wavelengths between 400–700 nm, yielded a mass specific spectral attenuation coefficient for SSC. This relationship formed the basis of an empirical spectral solar irradiance model to predict light quality and quantity at different solar zenith angles converting irradiance ($W/m^2/nm$) to energy using the Planck constant and the speed of light, and to μmol quanta m^2s^{-1} using Avogadro's number (Slivkoff 2014)

Figure 18 shows the model predictions of benthic light availability based on the model at depths of 0–10 m and at SSC concentrations from 0.5 to 40 mg L^{-1}. In addition to depth and turbidity, underwater irradiance is dependent on the sun angle from vertical (zenith) which was modelled at solar noon and using a zenith angle of 0° (sun directly overhead). The model does not include cloud cover and the modelled values are therefore the maximum possible levels for a given level of the depth and turbidity. Instantaneous light levels at solar noon at, for example, 5 m depth, varied from 322 µmol quanta m^2 s^{-1} at 2 mg L^{-1} to 0.5 µmol quanta m^2 s^{-1} at 20 mg L^{-1}.

The zenith angle at solar noon also varies seasonally and the inset graph in Figure 18 shows the effects of changing the zenith angle, with the maximum irradiance at solar noon reduced from 322 µmol quanta m^2 s^{-1} at 2 mg L^{-1} on the day of the summer solstice (zenith of 4°), to 230 µmol quanta m^2 s^{-1} on the day of the winter solstice (zenith of 42°).

Figure 19 shows the modelled spectral profiles at 5 m depth at increasing SSCs from 0–15 mg L^{-1} describing the decrease in light levels and the change in the peak wavelength. These spectral profiles were replicated (as close as was logistically possible) in the laboratory-based experiments with corals and sponges to examine the tolerance to reduce light quality and quantity.

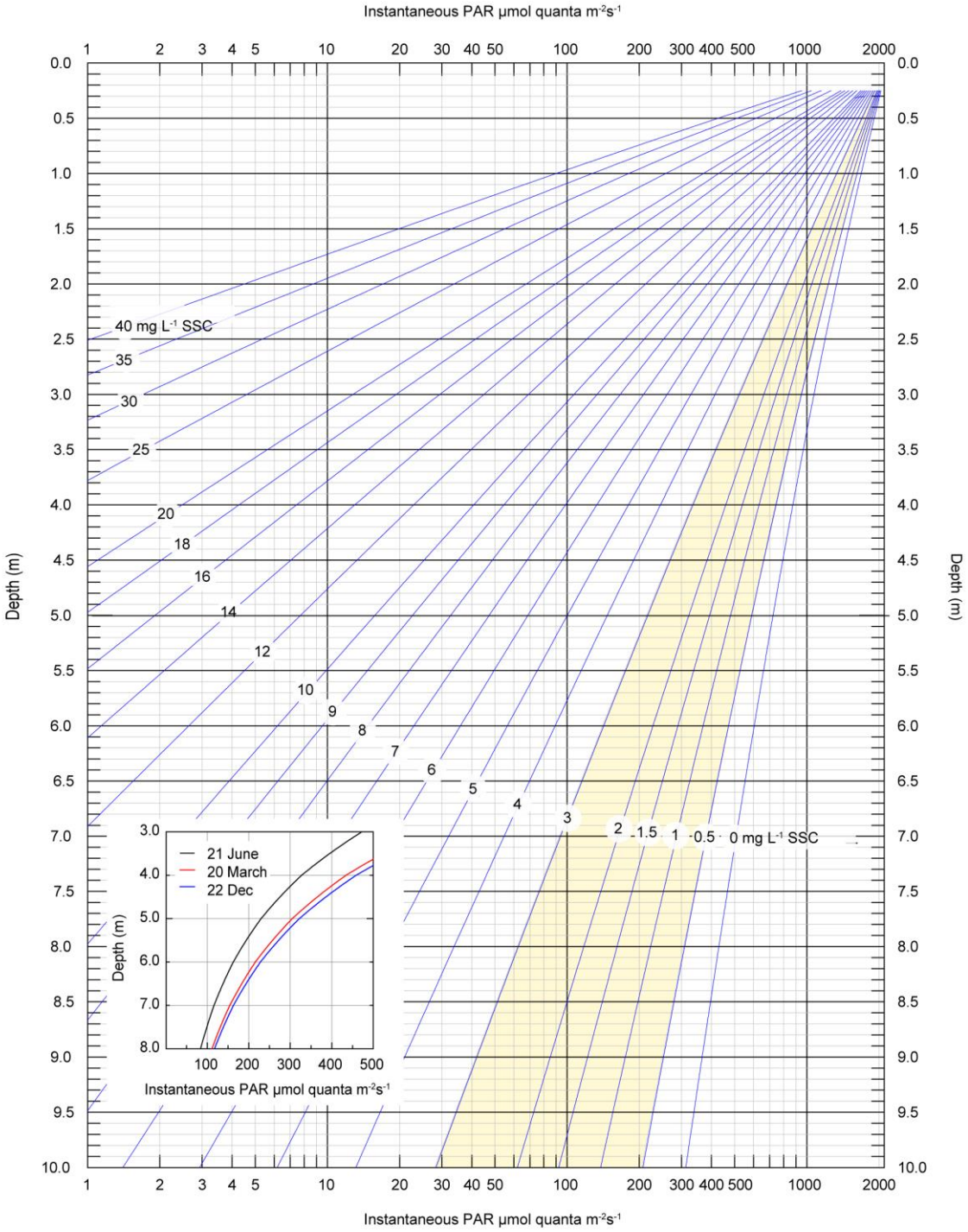

Figure 18: Nomograph showing the modelled estimated maximum instantaneous photosynthetically active radiation (PAR, 400–700 nm) levels in µmol quanta m^{-2} s^{-1} (x-axis, note log scale) from 0.25–10 m water depth (y-axis) under a range of SSCs from 0.5–40 mg L^{-1} and a zenith angle of 0° (i.e. sun directly overhead), based on the Cleveland Bay spectral solar irradiance model. Inset figure shows the effects of changing the zenith angle from 4° (summer solstice), 25° (spring equinox) to 42° (winter solstice).

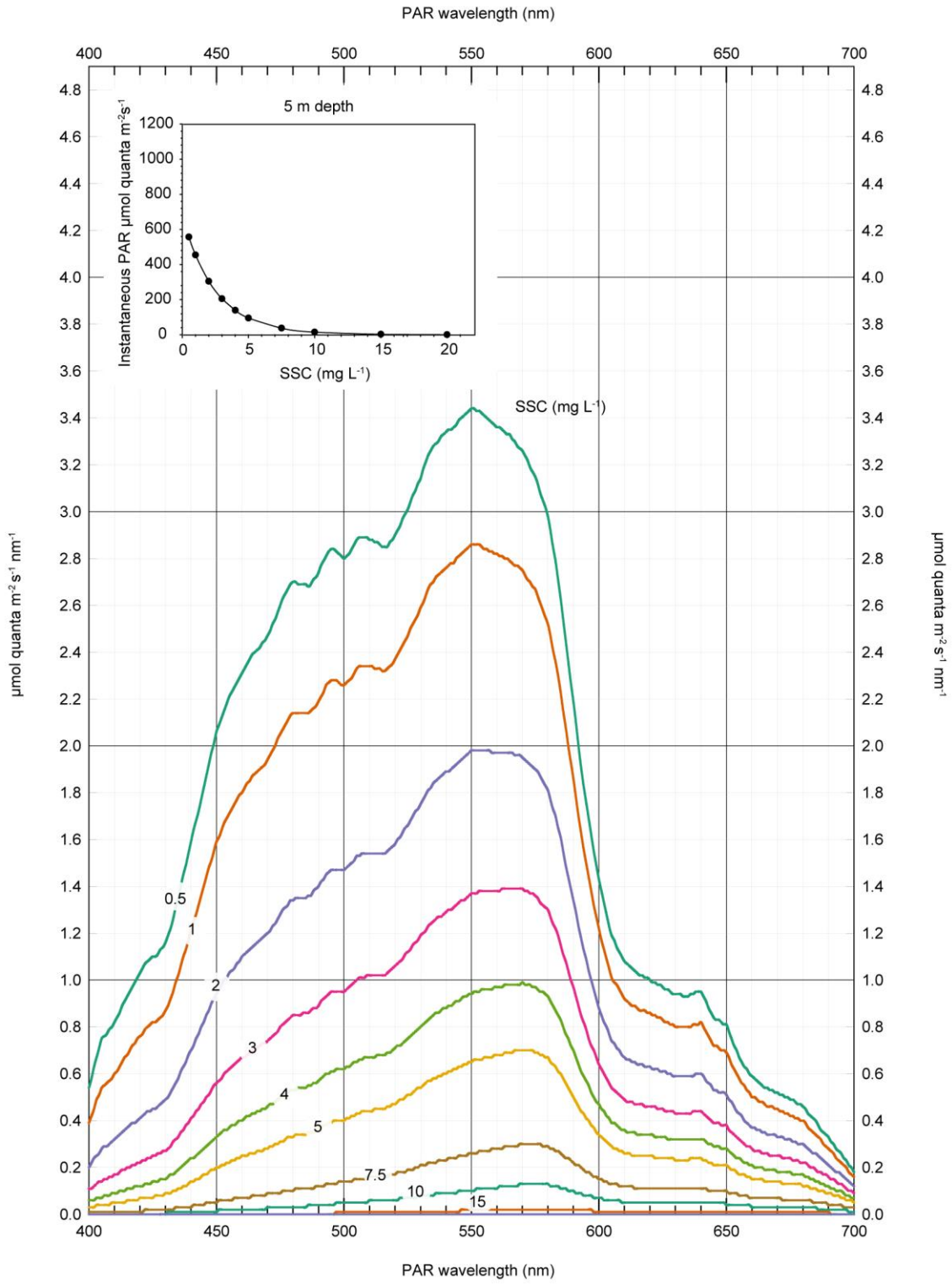

Figure 19: Nomograph showing the modelled spectral profiles over the photosynthetically active radiation (PAR, 400–700 nm) range in µmol quanta m^{-2} s^{-1} nm at 5 m depth under a range of SSCs from 0.5–15 mg L^{-1} at a zenith angle of 0° (i.e. sun directly overhead), and a cloud-free day, based on the Cleveland Bay spectral solar irradiance model.

4.2 Laboratory-based coral and sponge exposure studies

4.2.1 Adult sponges and corals

The SSCs chosen for the laboratory tests were nominally 2.5, 5, 7.5, 10 and 15 mg L^{-1} and corals and sponges were exposed to the concentrations for 28 d. Nominal SSCs are used in the Figures below but measured SSCs (see Table 4) are used in the statistical analyses (see Table 5). The maximum average daily NTUs values at the reef sites ranged from 0.5–41.7 (see Table 1), but over a 30-d running mean period the maximum average value ranged from 3–15.8 NTU the SSCs used in the experiment therefore encompassed close to the worst case SSC values measured *in situ*. For each SSC, the spectral solar irradiance model (see Section 4.1.5 and Figure 18) was used to calculate the likely irradiance levels (at 5 m depth) at solar noon, for a zenith angle of 19° (equivalent to the equinoxes), yielding a 2 order of magnitude span in the maximum irradiance of 2.2–210 µmol quanta m^2 d^{-1} (Figure 20). With the sinusoidal ramping up from 'sunrise' at 06.00 h until the maximum irradiance at noon and ramping down to 'sunset' at 18.00 h this yield DLIs of 0.06–5.7 mol quanta m^{-2} (Table 5). The spectral solar irradiance model was also used to determine the spectral composition at each SSC (see Section 4.1.5 and Figure 20).

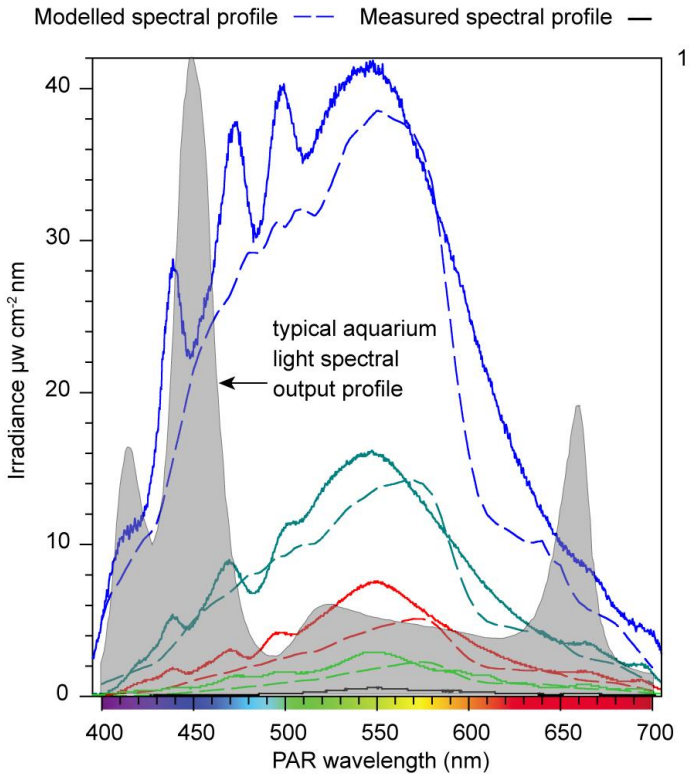

Figure 20: Modelled (dashed lines) and measured (solid lines) irradiance (µW cm^{-2} nm^{-1}) profiles during the laboratory experiments. The spectral profiles were designed to mimic light quantity and spectral quality at 5 m depth (cloud-free days) and a zenith angle of 19° (at solar noon). For comparative purposes also shown is the spectral output of Hydra FiftyTwo HD™ (AquaIllumination Inc.) aquarium light which are designed to have maximum output in the blue and red regions peaking in the major chlorophyll absorption bands.

Table 4: Details of the experimental treatments employed. Values derived from empirical solar irradiance model at a nominal depth of ~5 m. SSC=suspended sediment concentration, PAR=photosynthetically active radiation, DLI=daily light integrals, PUR=photosynthetically usable radiation.

Parameter	units	1	2	3	4	5
SSC nominal	mg L^{-1}	2.5	5	7.5	10	15
Nephelometry-derived SSC	mg L^{-1}	2.3	5.1	8.1	10.5	15.7
PAR max	µmol quanta m^{-2} s^{-1}	210	80	31	13	2.2
PUR max	µmol quanta m^{-2} s^{-1}	85.1	28.3	9.5	3.6	0.5
PAR DLI	mol quanta m^{-2} d^{-1}	5.7	2.17	0.85	0.34	0.06
PUR DLI	mol quanta m^{-2} d^{-1}	2.3	0.77	0.26	0.10	0.01

All corals and sponge species survived the 28 d experiment, with no mortality or even partial mortality observed in any species. *A. millepora* displayed colour changes by the end of the 28 d, with individuals in the lowest light treatment exhibiting the palest tissues (Figure 21 A; Table 5). *P. verrucosa* showed the most marked colour changes, with clear lightening of the tissues observed by day 14 at 0.85, 0.34 and 0.06 mol quanta m^{-2} d^{-1} (Figure 21 A). At the end of the experiment corals were 52% paler in the lowest light treatment than those at 5.7 and 2.2 mol quanta m^{-2} d^{-1}, with a significant difference between 5.7 and 0.06 mol quanta m^{-2} d^{-1} identified (Table 5). While *M. aequituberculata* also displayed colour changes over the course of the experiment, individuals from the 5.7 mol quanta m^{-2} d^{-1} treatment were paler than those at 0.06 mol quanta m^{-2} d^{-1} by the end of the experiment (Figure 21 A). *C. orientalis* from the two lowest SSC treatments showed a slight darkening after day 7 but had lightened by the end of the experimental period, with all five light/SSC treatments lightened by the end of the experiment (Figure 21 A).

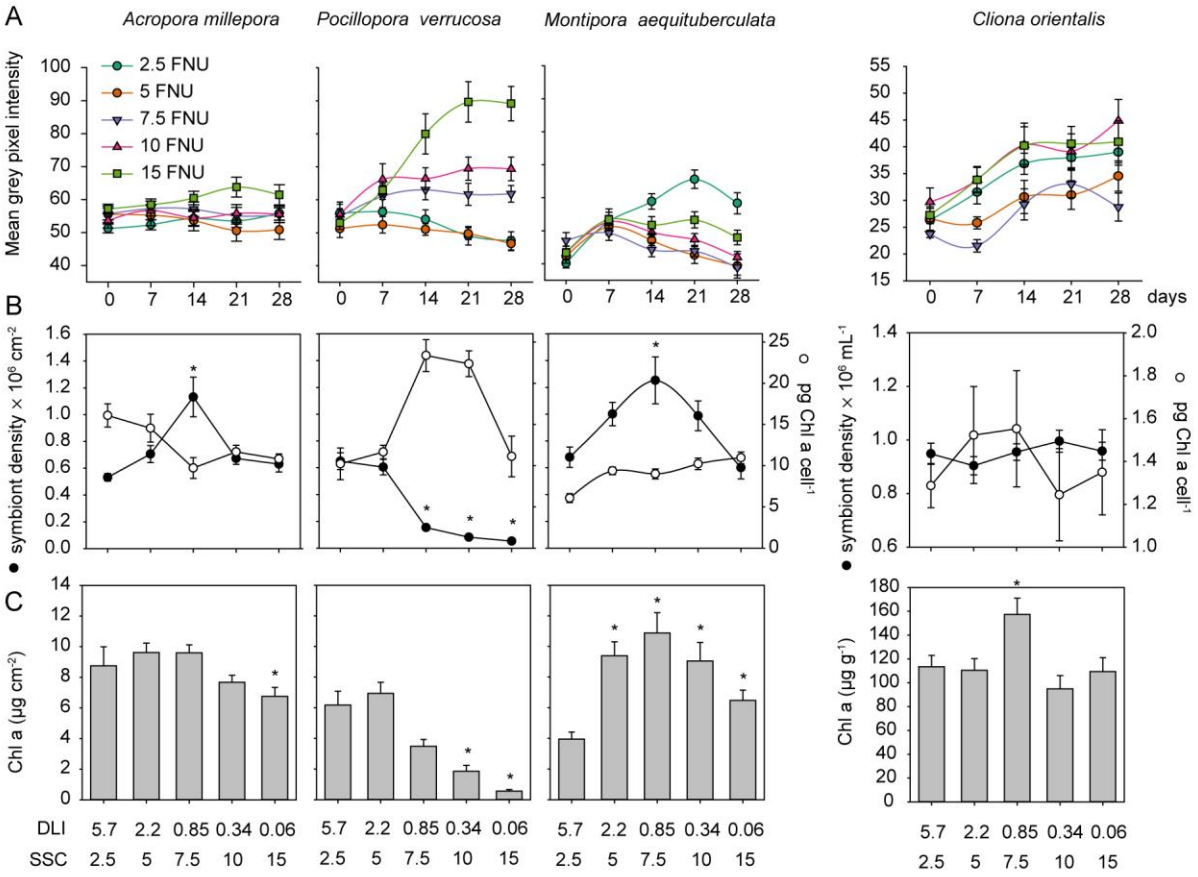

Figure 21: (A) Mean grey pixel intensity for each of the species exposed to five turbidity treatments over the course of the 28-d experiment. The higher the pixel value, the brighter/lighter the coral or sponge. (B) Symbiotic dinoflagellate density (× 10^6) for each of the species (black) and concentration of Chl a in symbiont cells (white). (C) Concentration of total Chl a (µg cm^{-2} for corals and µg g^{-1} for *C. orientalis*). For all panels, note the different units and scale for *C. orientalis*. Error bars represent (1 S.E. and * denotes a significant difference from the control (e.g. 2.5 FNU) according to Dunnett's multiple comparison test.

In addition to colour changes, significant differences in the densities of zooxanthellae were identified between the treatments for all coral species (Figure 21 B). Symbiont densities were highest at 0.85 mol quanta m^{-2} d^{-1} and significantly different from the control for *A. millepora* and *M. aequituberculata* (Table 5). In contrast, *P. verrucosa* symbiont densities decreased rapidly between the highest light treatments and 0.85, 0.34 and 0.06 mol quanta m^{-2} d^{-1} (Figure 21 B; Table 5). While symbiont densities in *P. verrucosa* decreased rapidly at light levels of 0.85 mol quanta m^{-2} d^{-1}, the amount of Chl a per cell shows an opposite pattern with the highest concentrations observed in the 0.85 and 0.34 mol quanta m^{-2} d^{-1} (Figure 21 B). *A. millepora* symbiont Chl a levels were lowest at 0.85 mol quanta m^{-2} d^{-1} (Figure 21 B). Symbiont density in *C. orientalis* was greatest in the two lowest light treatments; however, no significant differences were identified.

Table 5: Summary of the p-values from the Dunnett's multiple comparison test for each of the species and response variables tested. *denotes pairwise test p(MC)-values from PRIMER/PERMANOVA+.

		Colour changes	Zooxanthellae density	Pigment concentration	Total lipids	Lipid ratio	Lipid classes*
Acropora millepora (coral)	2.2	–	–	–	<0.001	<0.001	0.0025
	0.85	–	0.0131	–	<0.001	<0.001	0.0085
	0.34	–	–	–	–	<0.001	0.0244
	0.06	<0.001	–	0.0478	–	0.002	0.0039
Pocillopora verrucosa (coral)	2.2	–	–	–	<0.001	<0.001	0.0039
	0.85	–	<0.001	–	<0.001	<0.001	0.0032
	0.34	–	<0.001	<0.001	<0.001	<0.001	0.0077
	0.06	0.0019	<0.001	<0.001	<0.001	<0.001	0.0013
Montipora aequituberculata (coral)	2.2	–	–	<0.001	–	–	–
	0.85	<0.001	0.0382	<0.001	–	–	–
	0.34	<0.001	–	<0.001	–	–	–
	0.06	0.0095	–	0.0497	–	0.006	–
Cliona orientalis (sponge)	2.2	–	–	–	–	–	–
	0.85	0.0178	–	0.040	–	–	0.0225
	0.34	–	–	–	–	–	0.0150
	0.06	–	–	–	–	–	0.0346

When examining pigment concentrations in the tissues, significant differences were identified between SSC treatments for all species (Figure 21 C). For *A. millepora*, Chl a concentration in the lowest light treatment was significantly lower than the control (e.g. 5.7 mol quanta m^{-2} d^{-1}) (Table 5). Again, the most noticeable differences between treatments were observed for *P. verrucosa*, with significantly lower pigment levels at 0.34 and 0.06 mol quanta m^{-2} d^{-1} compared to 5.7 mol quanta m^{-2} d^{-1} (Figure 21 C; Table 5). Pigment concentrations in *M. aequituberculata* mirrored trends observed in symbiont densities, with Chl a being highest at 0.84 mol quanta m^{-2} d^{-1} (Figure 21 C) and each treatment being significantly different from the control (Table 5). Similarly, Chl a levels were highest and significantly different from the control at 0.84 mol quanta m^{-2} d^{-1} in *C. orientalis* (Figure 21 C).

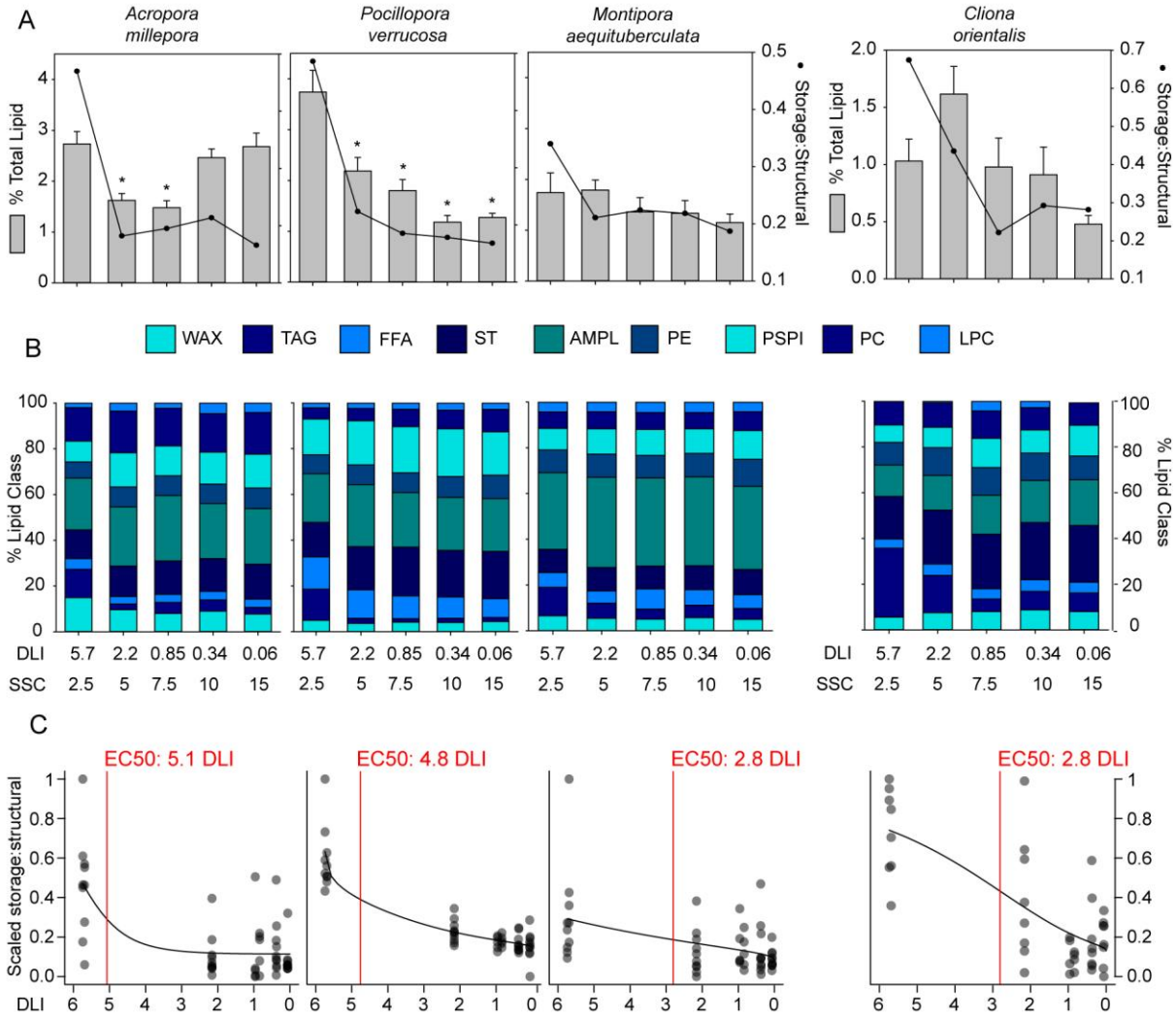

Figure 22: (A) Percent total lipids (bars, primary y-axis) and ratio of storage to structural lipids (lines, secondary y-axis) for each of the species. Note the different scale for *C. orientalis*. Error bars represent (1 S.E and * denotes a significant difference in total lipids from the control (e.g. 2.5 FNU) according to Dunnett's multiple comparison test (B) Lipid classes for each of the species under the five turbidity treatments. WAX=wax ester, TAG=triacylglycerol, FFA=free fatty acid, ST=sterol, AMPL=acetone mobile polar lipid, PE=phosphatidylethanolaimine, PSPI=phosphatidylserine-phosphatidylinositol, PC=phosphatidylcholine, LPC=lyso-phosphatidylcholine (C) Dose response functions for all four species based on rescaled (0-1) ratio of storage to structural lipids. The black solid line shows a model averaged fitted non-linear regression and the vertical red line interpolated EC_{50} threshold values.

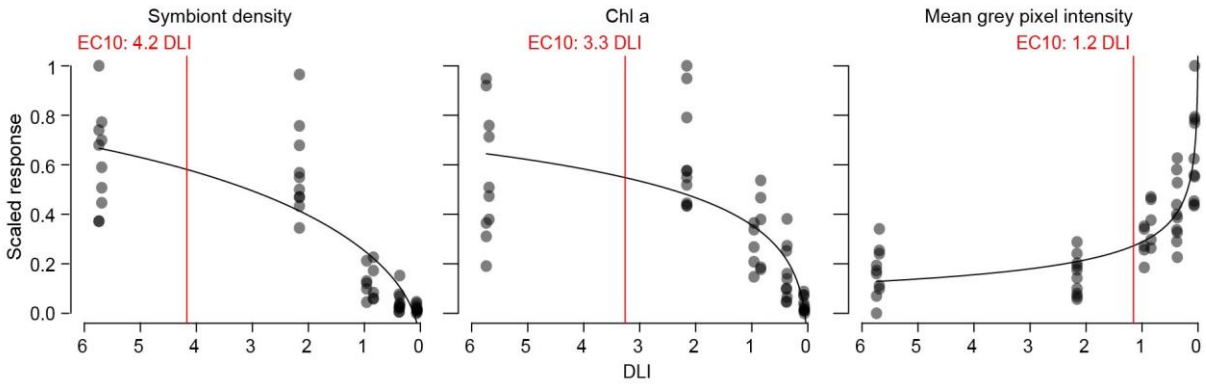

Figure 23: Dose response functions for *Pocillopora verrucosa* based on rescaled symbiont density, total Chl a content and colour, based on the mean grey pixel intensity with higher values indicative of paler tissues. The black solid line shows a model averaged fitted non-linear regression and the vertical red line interpolated EC_{10} threshold values.

The percentage of total lipids varied between species and the five light/SSC treatments (Figure 22 A). For *A. millepora* the amount of total lipids significantly decreased between 5.7 and 2.2 mol quanta m^{-2} d^{-1} (Table 5), but increased again at the two lowest light treatments, whereas little changes were observed between the light/SSC treatments for *M. aequituberculata* (Figure 22 A). However, both species displayed a drop in the ratio of storage to structural lipids at light levels lower than 5.7 mol quanta m^{-2} d^{-1}. Similarly, the ratio of storage to structural lipids steadily declined as light levels decreased for *P. verrucosa*; however, unlike the other species, this decline was mirrored by a significant reduction in the percentage of total lipids (Figure 22 A; Table 5). While *C. orientalis* displayed a similar pattern to the corals with the ratio of storage to structural lipids, the percentage of total lipids increased at 2.2 mol quanta m^{-2} d^{-1} followed by a decrease as light declined (Figure 22 A).

Nine different lipid classes, encompassing both storage and structural lipids, were identified in the corals and *C. orientalis* from the different light/SSC treatments (Figure 22 B). A significant difference in the structure of lipid classes was identified in *A. millepora* and *P. verrucosa* between the control (5.7 mol quanta m^{-2} d^{-1}) and all other treatments (Table 5). This is not surprising given the clear decrease in the ratio of storage to structural lipids from 5.7 to 2.2 mol quanta m^{-2} d^{-1} likely due to the decrease in wax ester (WAX) and triacylglycerol (TAG). Differences between the lipid classes were also observed in *C. orientalis* between the control and 0.85, 0.34 and 0.06 mol quanta m^{-2} d^{-1} (Table 5). As with the corals, there was a decrease in the ratio of storage to structural lipids in *C. orientalis*, with sponges exposed to control light/SSC levels having a higher percentage of triacylglycerol (TAG) than those in the higher SSC treatments (Figure 22 B).

Since all the species in the experiment displayed a consistent response with decreasing light in respect to the ratio of storage to structural lipids, thresholds were derived for the point at which this transition occurs, with EC_{50} values estimated from the model averaged predicted values. The estimated EC_{50}s varied between species but were most similar for *A. millepora* and *P. verrucosa* (Figure 22 C), 5.1 and 4.8 mol quanta m^{-2} d^{-1} respectively. *M. aequituberculata* had the lowest estimated EC_{50} for the corals at 2.8 mol quanta m^{-2} d^{-1}, which was coincidentally shared by *C. orientalis* (Figure 22 C).

In addition to the consistent response of decreasing lipid ratios with light stress, *P. verrusoa* also displayed similar responses in respect to symbiont density, total Chl a concentrations and color/bleaching. Therefore, thresholds were also derived for these response variables. In this case, the estimated EC_{10} values were even lower than the EC_{50} vales observed for the lipid ratio (Figure 23). For instance, the 10% loss of algal symbionts threshold was 4.2 mol quanta m^{-2} d^{-1} and the 10% decrease in total Chl a was 3.3 mol quanta m^{-2} d^{-1}. The bleaching threshold was the most sensitive with a 10% increase in bleaching at 1.2 mol quanta m^{-2} d^{-1}, which is only slight lower than the previously derived threshold for *P. acuta* (Bessell-Browne et al. 2017d).

4.2.2 Juvenile corals

The ecologically relevant range of light intensities that corals recruit in the field is not known because of limitations finding recruits immediately after settlement, and because no technology exists to measure light in minute (< 2mm) crevices. However, field PAR measures in spatially larger ~10 × 10 cm crevices identified as suitable for coral settlement revealed over a magnitude lower light intensity (mean = 15.6 µmol photons m^{-2} s^{-1}) than on horizontal surfaces (mean = 189.3 µmol photons m^{-2} s^{-1}). Therefore, we conservatively consider the likely range of light intensities for early coral recruitment to be <100 PAR (~2.5 DLI). The broad-spectra was slightly right-skewed and had a dominance of wavelengths in the 400–600 nm range (violet, blue and green), whereas the shifted spectra were more normally distributed and had a dominance of wavelengths in the 500–600 nm (green–yellow) range. With some increases in red-light at the higher-light intensities. Visually, the light appeared yellow.

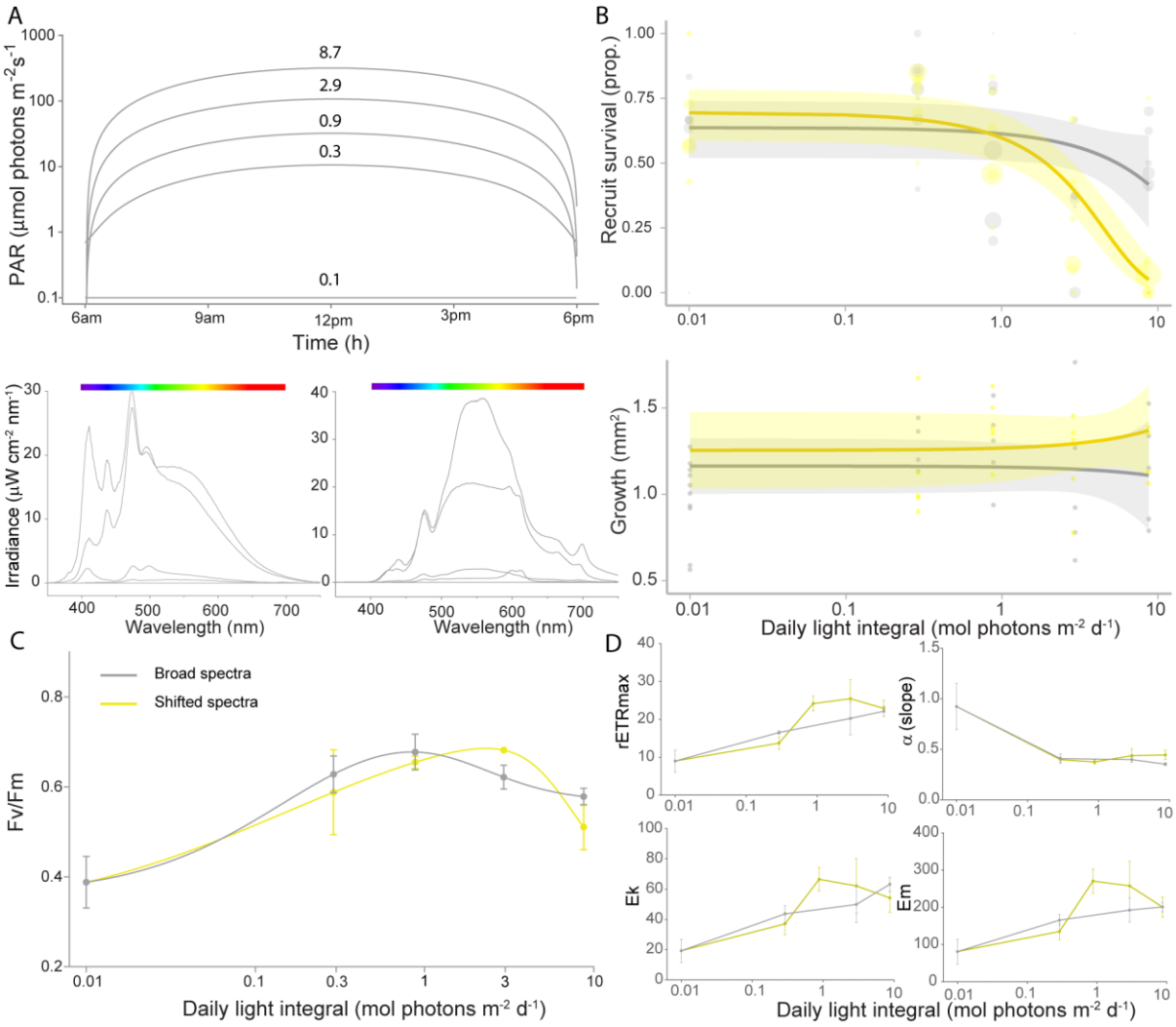

Figure 24: Light intensity and shifted (sediment-simulated) spectra on 6-wk old coral recruits of *A. millepora*. (A) PAR and DLI levels used during the exposure; relative broad-band spectra used to simulate 0.5 mg L^{-1}; and relative shifted spectra used to simulate 9.1 mg L^{-1}. (B) Survivorship and growth of the recruits after light exposure. (C) Dark-adapted yields and (D) rapid light curves parameters rETRmax, α (slope), Ek and Em following light exposure.

Across the range of exposures there was a slight decline in coral recruit survival in the white light (EC_{10} = 2.61, 95% CI: 0–6.24 DLI), and a marked decline under the yellow light at higher light intensities (EC_{10} = 1.23, 95% CI: 0.31–2.15 DLI) (Figure 24 B). However, given the environmental relevant concentrations noted above, and that a chronic SSC at ~9 mg L^{-1} is considered high, the risk posed by the shifted spectra is generally low.

Yellow-green light spectra are considered to have less usable light for algal symbionts; however, this could only in part explain the mortality because many recruits exposed to near-darkness survived for 6 weeks. It is also possible that competitors such as cyanobacteria, turf algae and CCA that may contain pigments that can absorb yellow-green light such as phycocyanin and phycoerythrin, led to the recruits being out-competed. Additionally, increased incident grazing by snails (used in the tanks for algal control) may have impacted recruit survival at the higher light intensities.

Overall, recruits exposed to higher light intensities during the 6-weeks showed more scope for acclimation to these intensities, and recruits grown in the shifted spectra acclimating slightly better at moderate light intensities than those grown in broad spectra (Figure 24 C, D). Down regulation of PSII occurred after 200 µmol photons m^{-2} s^{-1} for the most acclimated recruits (Figure 24 D), indicating recruits may only be able to tolerate half the light intensity than that of adult colonies (Ralph & Gademann 2005) (Figure 24 D). Interestingly, recruits grown in near darkness were still able to uptake symbionts and recorded low but measurable dark-adapted yields (Figure 24 C). Many of these recruits appeared paler but symbionts could be observed within their tentacles.

5.0 DISCUSSION AND CONCLUSIONS

By releasing sediments into the water column dredging and dredging activities such as dredge material placement constitute a risk to benthic communities especially to phototrophic primary producer habitats that rely on light for photosynthesis. The increase in suspended sediment concentrations and changes in light and sediment deposition are a *hazard* of dredging that has been recognised since the 1970s (Dodge & Rimas Vaisnys 1977, Bak 1978). However, few studies have been able to quantify physiological tolerances of corals in a way that allows a description of the *risk* associated with dredging to be quantified.

This study was associated with understanding the effects of dredging on inshore turbid-zone reef communities which are considered to be light limited (Anthony & Connolly 2004, Anthony et al. 2004, Morgan et al. 2016). Given its fundamental importance for all aspects of the physiology and ecology of benthic phototrophs the focus of the study was on underwater light quantity and quality and the effects of water depth, season (sun angle), clouds, and especially the effects of resuspended sediments from dredging and natural events.

5.1 Turbidity patterns and characterisation

The inshore turbid-zone reef communities of the central Great Barrier, encompassing the reefs around Magnetic Island in Cleveland Bay have now been the subject of many studies associated with understanding sedimentary processes, transport and fate, and the effects of watershed development on reef growth in 'marginal' (cf Perry and Larcombe (2003)) environments (Carter et al. 1993, Larcombe et al. 1995, Lou & Ridd 1996, Larcombe & Woolfe 1999, Orpin et al. 1999, Larcombe et al. 2001, Anthony et al. 2004, Orpin et al. 2004, Cooper et al. 2008, Browne et al. 2010, Lambrechts et al. 2010, Bainbridge et al. 2012, Browne 2012, Browne et al. 2012, Orpin & Ridd 2012, Perry et al. 2012, Browne et al. 2013, Macdonald et al. 2013, Delandmeter et al. 2015, Whinney et al. 2017). For the reef sites the water quality data showed a very clear gradient from the nearshore Virago Shoal to the more 'offshore site (Florence) at the entrance to the bay. Overall, mean daily average turbidity in the bays around Magnetic Island levels was $^1/_3$ of the value in the central Cleveland Bay site (Meadow 19), the median (P_{50}) was ½ and the 95th percentile (P_{95}) $^1/_4$ of the value. Turbidity levels measured over this study were not remarkable as compared to previous studies (for example Orpin et al. (2004)) and the main characteristic was the very high variability. This is well known for such water quality datasets in coastal environments (and Cleveland Bay) (Orpin et al. 2004), influenced by a range of factors, such as waves, currents and bed type (Larcombe et al. 1995, Storlazzi et al. 2004, Storlazzi & Jaffe 2008, Verspecht & Pattiaratchi 2010).

The turbidity data were analysed using exceedance curves for determining the proportion of daily mean values (NTU and DLIs) above or below given levels (Larcombe et al. 2001, Macdonald et al. 2013). The analysis was also extended to include different running mean periods to examine temporal exposures (see further below). The turbidity data were highly skewed showing that water quality was very good around Magnetic Island for most of the year (hence supporting reefs), but subject to multiple short-term periods of poor water quality. With such highly skewed data the choice of summary statistics is very important (Gaines & Denny 1993, Zimmermann et al. 2009), as median (P_{50}) as opposed to average values often do not

truly reflect episodic disturbances (discussed in De'ath and Fabricius (2008)). As noted by Macdonald et al. (2013) and Jones et al. (2015a), and as also seen in this study, average values diverged from medians. However, even using average values can be misleading depending on the period of time examined (Jones et al. 2015a). Mean differences of only a few NTUs (which is close to the zero point for many sensors, Macdonald et al. (2013)) can separate sites which have very different patterns in turbidity. For this use of higher, upper percentiles (such as $P_{90, 95, 99}$) is most useful for site characterisations reason (see Fisher et al. (2015) and Jones et al. (2015a) for further discussion). The analyses showed that in effect, during clement conditions, water quality is similar across the Magnetic Island sites; however, when conditions deteriorate, turbidity at Picnic Bay, which is deeper within the Bay, is much worse than at the Florence and Geoffrey Bay sites. For Virago Shoal average NTU values were ~3.5× than the other reefal sites suggesting more chronic low-level higher turbidity through frequent periods of poor water quality.

Exceedance curves and the use of median and upper percentiles are useful for broadly characterizing sites and whether disturbance events are acute as opposed to more chronic. The terms ‘pulse’ and ‘press’ have also been used to describe the contrast (Bender et al. 1984, Glasby & Underwood 1996). However what exceedance curves based on daily values can’t do is describe when disturbances occur which is equally as important from a biological perspective. Sequential days of very poor water quality over an extended period will have different physiological consequences to benthic phototrophs than if the days were evenly distributed and interspersed with normal water quality (allowing time for recovery). For this reason, the percentiles analysis was also conducted on the different running mean periods (1 day to 6 weeks) for turbidity and light. These analyses reflect exactly what benthic phototrophs might actually experience *in situ* and were primarily conducted to justify the exposure condition for the laboratory tests and ensure environmentally realistic experiments were used for the risk assessments (see further below). However, as also discussed below, once constructed from baseline information, any future disturbances can be plotted against the curves and updated daily, allowing conceptualization of and ‘pulse’ and ‘press’ disturbances and an assessment of the amount of ‘pressure’ on benthic communities in the short (days) and long term (weeks). Such a technique is very useful for quantifying the possible effects of dredging on water quality and is a recommended approach for further monitoring.

The water quality time series analysed here included six maintenance and/or capital dredging campaigns. Our analyses suggested that at Florence and Picnic Bays periods of intense dredging pressure may increase turbidity by 0.6-0.7 times the mean expected values. These estimated effect sizes are between two and five times lower than the effects of either wind or waves on turbidity, highlighting that even in the presence of dredging activity, wind and waves are the dominant drivers of turbidity in this system.

Plumes generated by TSHD can have complex 3-dimensional turbidity profiles including surface maxima, mid-water maxima and bottom maxima, as well as well mixed homogenous SSC profiles (cf Figure 13). The most common profile in this study was an increase in SSC with depth with measurements within 1 m of seabed ~3.5× higher than the surface (0.3–0.5 m) and ~10× higher than the surface for the dredge material placement area. Surface measurements of turbidity (via satellite or water sampling) are unlikely to be representative of the seabed turbidity (cf Figure 13 C) and estimates of benthic light availability from NTU to K_d correlations are also unlikely to be yield accurate estimates of benthic light availability.

5.2 Light availability and characterisation

Similar types of statistical analyses were conducted for the underwater light levels using daily light integrals or the sum of the per second quantum flux measurements over the day. DLI values ranged from 0 to 26 mol photons m^2 day^{-1} averaging ~10 mol photons m^2 day^{-1} at the two more seaward reef sites (Florence and Geoffrey Bays) and as low as 3–4 mol photons m^{-2} day^{-1} at the inshore sites.

For the offshore sites there were clear seasonal differences in light availability with winter values 23% lower than summer values. Average above water PAR levels were 20% lower in winter than summer (data not shown). Pronounced seasonal differences were not observed in the turbidity data (despite significant differences in the dominant weather patterns) and the seasonal differences in submarine light field were mostly due to zenith angles and daylength i.e. to the solar declination cycle. The effect of seasonality has implications for future dredging projects, as there have been suggestions to confine dredging to winter months where biological activity is at its lowest (Reine et al. 1998). For corals there have been suggestions to avoid summer periods due to perceptions that corals could be stressed by heat (Benson et al. 1994). Bessell-Browne et al. (2017d) clearly showed that corals may suffer occasional periods of light limitation during winter, but during dredging in winter the additional light attenuation may put corals into extended periods of light limitation. If light is a critical limiting factor i.e. the principle cause-effect pathway (see further below) then dredging during the brighter summer months should not be discounted, and providing water quality conditions remain above levels likely to result in sedimentation or extreme levels of light limitation synergistic impacts between heat stress and dredging should not be expected (Fisher et al. 2019a).

There are surprisingly few published studies of light levels of inshore turbid zone communities of the GBR. Anthony et al. (2004) measured underwater PAR at Cockle Bay (Magnetic Island) using the information to partition the effects of turbidity, clouds, and tides on the underwater light field but did not report empirically derived DLI values. Cooper et al. (2007) also reported summer averaged DLI levels of 24–25 mol quanta m^{-2} d^{-1} at 3 m depth and 12–15 mol quanta m^{-2} d^{-1}at 6 m depth in a 7 day study in the coastal Whitsunday Islands. Jones (2008) reported DLIs ranging from 1.5–11.75 at Nelly Bay (Magnetic Island) over a 3-month, summer period (December to February) period. Cooper et al. (2008) reported DLIs at Magnetic Island ranging from 5–20 mol quanta m^{-2} d^{-1} at 2 m below LAT at Horseshoe Bay. However, all these studies used Odyssey™ photosynthetic irradiance sensors (Dataflow system Pty Ltd, Christchurch New Zealand), and as pointed out by Shaffer and Beaulieu (2012) these sensors were only ever designed as a cost effective alternative for measuring relative rather than absolute light levels. The manufacturer recommended calibration procedure could generate PAR values that are off by a factor of 1.6. Notably the light data at Picnic Bay was collected with an Odyssey™ photosynthetic irradiance sensors as opposed to the LiCOR190SA sensors which were used at all other sites. The underwater light levels at Picnic Bay do appear much lower than at Geoffrey and Florence under similar conditions (of low turbidity) and as predicted by the spectral irradiance model. It is not clear if this discrepancy is due to the light sensor being placed separately from the nephelometer or to calibration issues associated with the Odyssey™ sensor. Nevertheless, the Port of Townsville Limited's dataset (Figure 4) using LiCOR190SA sensors is probably the most comprehensive long-term water quality record to date of light environments within the turbid-zone inshore communities of the central GBR.

In addition to the changes in light quantity, the vertical light profiling with the hyperspectral sensor and the short-term deployment of multispectral sensor provided some new insights into the effects of suspended sediments (from dredging and natural sediment resuspension) on light quality. The studies described the well-known exponential decrease in light quantity and spectrum with depth, but also described the recently reported changes in spectral quality in dredging plumes. Similar spectral changes have now been reported in two other dredging projects in Western Australia, the Cape Lambert B project (Jones et al. 2016) and the Wheatstone project (Fearns et al. 2019). Outside of Cleveland Bay in the blue water at the 20 m contour line (see photograph in Figure 2 F) the profiles showed the well-known rapid attenuation of red light by water itself in the first few metres, and furthest penetration of green and blue light (Kirk 1994, Maritorena & Guillocheau 1996). Within Cleveland Bay, in addition to the loss of red light, there was much more attenuation of the blue wavelengths with depth. This pattern of increased attenuation with a shortening of wavelength to the blue and ultraviolet wavelengths is similar to the absorption spectrum caused by the decay of plant and animal matter which has previously been called gelbstoff, gilvin, yellow substance, dissolved colloidal organic matter, humic substances or more recently 'chromophoric (or 'coloured') dissolved organic matter' (CDOM) (Hansell & Carlson 2014). Under elevated SSCs both the quantity of light and spectral profile changed dramatically with a very pronounced shift in the spectrum to green-yellow light. The spectral shift could be due to absorption by the suspended sediment particles (Kirk 1980), but it is also likely to be due to the increased scattering of light by the suspended sediments which increases the probability of absorption by CDOM (Kirk 1985). Irrespective of the cause, the net effect of loss or red and blue light with increasing SSCs was a shift in colour spectrum to green light (550–600 nm) which is outside the spectral region of the major photopigments. This implies not only a loss of light quantity but also light quality.

In symbiotic dinoflagellate species (family *Symbiodiniaceae*) the major light harvesting pigments are chlorophylls *a* and c_2 and a carotenoid peridinin that bind to two major antennae proteins (Prézelin & Haxo 1976) (Song et al. 1976). The absorption peaks for *Symbiodinium* spp. are in in the blue (440–480 nm range) due to chlorophyll *a*, chlorophyll c_2 and carotenoids and at 662 nm due to chlorophyll *a* (Halldal 1968, Prézelin et al. 1976, Dustan 1982, Kuhl et al. 1995, Levy et al. 2003, Hennige et al. 2009, Szabó et al. 2014, Wangpraseurt et al. 2014). The peridinin-chlorophyll a-binding protein (PCP) is unique to dinoflagellates (Larkum 1996) and peridinin can have a photoprotective role (quenching the Chl *a* triplet state preventing singlet oxygen formation) as well as a light-harvesting role. The absorption spectrum of *Symbiodinium* PCP is a broad band between 400–550 nm and a peak at 476 nm. Although PCP extends the absorption profile into the blue green wavelength, absorption at 550–600 nm is still weak for *Symbiodinium* and this coincides with the peak wavelength of light transmission under elevated SSCs. Kinzie et al. (1984) showed corals grown under blue or white light showed increased growth and had higher algal densities than corals grown in green or red light. Mass et al. (2010) showed corals from different depths were chromatically adapted to the different light spectra.

PAR sensors typically have uniform sensitivity across the PAR waveband giving equal weight to light of different wavelengths, and daily light integrals calculated using PAR can therefore be misleading. Morel (1978) suggested calculating photosynthetically usable radiation (PUR) which adjusts PAR values for the proportion of the light that is usable. In the absence of action spectra (which describes photosynthetic rate at different wavelength for corals) PUR calculations in this study were based on absorption coefficients of isolated algal symbionts

from *in vivo* cultures of multiple different *Symbiodiniaceae* clades (described in Hennige et al. (2009)). Absorption spectra and action spectra are usually quite similar (Kirk 1994) but the use of isolated algae is also a simplification. In the intact symbiosis (*in symbio*), the dinoflagellates receive a very different light climate from that of the surrounding water or surface tissue (Kuhl et al. 1995, Wangpraseurt et al. 2012). The dinoflagellates are located intracellularly in the polyp tentacles, coenosarc, and in oral and aboral layers each of which differ in proximity from the underlying white aragonite skeleton. The microscale light habitat is complex with scattering of light leading to an enhancement of scalar irradiance (Kuhl et al. 1995, Enrıquez et al. 2005). Using microsensors, Wangpraseurt et al. (2012) described pronounced vertical light gradients in the tissues and Lichtenberg et al. (2016) described differences in spectral composition of scalar irradiance from the tissue surface towards the skeleton (see also (Wangpraseurt et al. 2012). The host tissues may also contain optically active green fluorescent proteins (FP) which may convert non-photosynthetic shorter wavelength light to blue-green increasing light availability (Schlichter et al. 1986, Dove et al. 2001, Lichtenberg et al. 2016).

It is presently difficult to evaluate the full significance of the spectral changes that occur under dredging plumes. The short-term deployment of the multispectral light sensor showed clear spectral changes that were caused by natural resuspension (not maintenance dredging) (cf Figure 11), and so changes in light quality is something that phototrophs in nearshore turbid communities are naturally exposed to. However, where the spectral changes are most significant is in laboratory-based studies that relate changes in coral and sponge health to light availability (see Section 4.2). Commercially available aquarium lighting systems (such as those used in the AIMS SeaSim) have been specifically designed to excite the major chlorophyll absorption bands (see shaded area of Figure 20) and the light profile is effectively opposite to the spectral profile that occurs in the inshore CDOM- and sediment-influenced turbid zone reef environments. For this reason, the LED light system (Figure 3) was designed and used in the exposure studies described below.

Given the fundamental importance of light for all aspects of the physiology and ecology of benthic phototrophs – and despite concerns about the effects of increased turbidity on reefs from coastal runoff dating back to the 1980s and 1990s (Brodie et al. 2012) – it is unusual that benthic light has been so under-investigated in the inshore GBR (see also Yentsch et al. (2002)). Water quality monitoring has focussed on assessing nutrients and turbidity with nephelometers even though the parameter of primary interest (to photoautotrophs) is light and the main cause-effect pathways is light reduction. Recently, Bessell-Browne et al. (2017c) manipulated light levels in experiments on the effects of elevated SSCs on corals, and demonstrated highly elevated suspended sediments had no effect as along as light levels were sufficient i.e. it was the light attenuating properties that was the principal cause effect pathway.

There has been an increasing realization that much of the sediments from rivers entering the GBR remain close to the river mouth and only a portion of fine material reaches coral reefs and seagrass beds (Bartley et al. 2014, Bainbridge et al. 2018). Plumes transition from brown to green with increasing distance from river mouths (Orpin & Ridd 2012) as sediments settle out of suspension allowing more light for phytoplankton biomass to increase from the elevated nutrient concentrations (Devlin et al. 2001). Increased phytoplankton abundance will in turn have ecologically relevant effects on benthic light quantity (and quality by removing blue and green wavelength) but would not be identified by seabed mounted nephelometers (Orpin & Ridd 2012). Similarly, stratified low salinity buoyant surface plumes with elevated SSCs would

affect benthic light but again would not be detected by seabed mounted benthic nephelometers.

Affordable underwater multi spectral sensors for routine light monitoring have only just become available and their use offers considerable opportunities to further quantify, understand and then assess the risk of sediment and nutrient run-off in the inner GBR. As shown in Figure 10, cloud cover reduced the total PAR but acted as a neutral density filter without any marked effects on the underwater spectrum compared to cloud-free days. The elevated SSCs associated with the 7-d turbidity event reduced the PAR but also by changing the spectrum, reduced the ratio of PUR to PAR as well. Analyses of spectral signatures (cf Figure 15) and calculation of the ratio of PUR:PAR, or even more simple approaches such as the ratio of blue (455 nm) to green (555 nm) light (cf Figure 10 E), can provide information on what is causing light reduction in monitoring programs (i.e. sediments, plankton and interannual variations in cloud cover etc). This diagnostic capacity seems important for long term water quality monitoring programs and partitioning changes in photic depth to proximal causal factors (natural and anthropogenic).

Another advantage of transitioning from nephelometer-based turbidity monitoring to PAR and PUR-based light monitoring is that light can be much more accurately quantified and in absolute terms. Turbidity measurements are cross referenced to formazin standards and need to be translated to suspended sediment concentrations using very site-specific conversion factors to be able to relate the information to exposure studies of biological effects. The conversion factors can vary according to sediment particle size distributions, shape and colour and particle composition (Kirk 1994, Davies-Colley & Smith 2001). PSDs in the water column are also likely to differ significantly during cyclones, storms, swell related resuspension and anthropogenic activities such as dredging and dredging activities (propeller wash and dredge material placement). The conversion factors are also likely to change in time during dredging projects (and following terrestrial runoff events – see Fabricius et al. (2013)) due to the build-up of finer more easily resuspendable material which is different from the original seabed composition (Jones et al. 2016). Storlazzi et al. (2015) also showed fine darker sediments attenuated more light than coarser lighter sediments (see also Duckworth et al. (2017) and so NTU to SSC conversion factors need also to consider surrounding sediment types (mineralogy) and will likely vary from nearshore (siliciclastic dominated) to more offshore (carbonate dominated) sediment types (Conner & De Visser 1992, Davies-Colley & Smith 2001). Fearns et al. (2018) further describe some of the limitations associated with using nephelometers especially when used as a proxy estimate of SSCs. Risk and Edinger (2011) discuss these issues further, concluding that the subjectivity and inherent errors associated with nephelometers offset their quick and easy advantage, and they should not be used in reef research — and presumably also for setting water quality guidelines.

Turbidity measurements cannot also be used to accurately estimate underwater PAR because of the three-dimensional structure of the plumes (see Anthony and Larcombe (2000)). The vertical profiling of turbidity behind the dredge showed surface, mid-water and bottom maxima all of which would affect scattering and light propagation through the water column in different ways. The seabed turbidity (0.5 m off the bottom) was 3–10× higher than the surface measurements. Transitioning to PAR based water quality monitoring using seabed mounted instruments that can spectrally profile, allowing calculation of PAR and PUR quantities and turbidity related light reduction will overcome most of the issues discussed previously.

5.3 Sediment accumulation

The measurements of sediment accumulation by the deposition sensors beside the Platypus Channel are the first empirical estimates of their kind during dredging. Sediment deposition fields and sediment accumulation rates have been estimated previously during a large capital dredging project, but in relative and not absolute terms (Jones et al. 2019). The sensors estimated average accumulation rates of 230 mg cm^{-2} d^{-1} 100 m away from the channel where the dredge was working. Short periods of very high sediment accumulation (>1000 mg cm^{-2} d^{-1}) over a 1-hour period were recorded, but over a 24 h period the worst daily average value was 590 mg cm^{-2} d^{-1}. There was a very strong gradient of decreasing sediment deposition rates with increasing distance away from the channel.

Since the deposition sensors have only recently been designed and deployed there is little information to compare these results with. The only study so far has been at Middle Reef in Cleveland Bay (4.4 km away from Platypus Channel) where during a period of high but gradually decreasing turbidity at the end of a storm recorded similar sediment accumulation profiles to those sites 400 m and 800 m away from the channel during dredging (cf inset Figure in Figure 17A) (Whinney et al. 2017). With the caveat that these are early, preliminary studies, and need to be repeated and verified, the data supports the notion that the high levels of SSCs caused by dredging in low energy water columns creates conditions conducive to enhanced levels of sediment deposition. With an additional caveat that these results are highly specific to the nature of the dredge and dredging, and local currents, tides and sea state at the time, as a first order approximation the results suggest an area of enhanced deposition in the order of a couple of hundred metres away from the edge of the Platypus Channel during maintenance dredging.

In a detailed study of a large (7.6 Mm^3) 1.5-year capital dredging project on a reef in WA (Fisher et al. 2015, Jones et al. 2015a, Bessell-Browne et al. 2017a, Fisher et al. 2018a) the distances over which the various pressure parameters and biological responses occurred were examined. The distance at which 90% of the effect of the dredging from maximum to minimum had dissipated (termed an effect distance or ED_{10}) was 20 km for suspended sediment concentrations and light attenuation. For sediment deposition measured by sensors it was 14 km, and 4.6 km for measurable changes in seabed clay and silt content. For biological response such as mucous sheet production (Bessell-Browne et al. 2017a) and smothering of corals, the ED_{10} was closer still at 3 km and 3.3 km respectively (Jones et al. 2019). Collectively these studies provide empirical data to suggest the turbid plumes caused by dredging can be detected the furthest away from the source, and that enhanced sediment deposition rates associated with dredging occurs much closer and biological effects such as smothering of corals by sediment occurs even closer still.

Not all species of corals are susceptible to smothering and in a recent study of the sedimentation during a dredging project, tolerance appeared very related to coral morphology and inclination of the corals' surfaces (Jones et al. 2019). The ability to avoid smothering – defined as the build-up of patches or pools of sediment that cannot be moved by self-cleaning – was related to colonies having uninterrupted downhill pathways for settled sediment to be transported across the colony surface to the edges (Jones et al. 2019). Encrusting and foliose forms, where sediments accumulated in hollows, were very susceptible to deposition. Smothering was never observed on branching species, even under very high levels of

sedimentation, or on smooth hemispherical colonies (although was sometimes observed on hemispherical growth forms where surface undulations or bumps which allowed sediments to pool). If remaining in place and not removed by currents, sediment smothering resulted in tissue bleaching and partial mortality (lesion formation), but when sediments were eventually removed, bleached areas regained pigmentation over weeks and there was regrowth/reparation of lesions over weeks and months (Jones et al. 2019).

5.4 Laboratory-based coral and sponge exposure studies

All corals and sponge species survived the 28-d experiment, with no mortality or even partial mortality observed in any species under light levels which ranged from 5.7–0.06 mol quanta m^{-2} d^{-1}. These light levels (in combination with elevated SSCs) exceeded the lowest light levels measured at the reef sites during the long-term water quality monitoring study (range 0.4 to 5.5 mol quanta m^{-2} d^{-1})(see Table 2 and Table 3). However, there were a range of sub-lethal effects in some species associated with lipid and colour changes.

Lipids are an important energy reserve in corals, with previous studies reporting levels ranging between 11–40% of the total dry weight (Harland et al. 1993, Yamashiro et al. 1999, Grottoli et al. 2004, Imbs 2013), with levels often varying between species, seasons, depths and light (Oku et al. 2002, Saunders et al. 2005, Imbs 2013). Due to their ubiquitous nature, lipids are often used as a proxy for coral health in response to environmental stress (Anthony et al. 2009, Lesser 2012). Lesser (2012) points out that using mass-specific lipid content as a marker for energy reserves is potentially misleading if the other biological constituents (e.g. proteins and carbohydrates) are not also considered. With that said, lipids have almost twice the caloric content in comparison to proteins and carbohydrates and in almost all species studied, lipids are preferentially catabolised over proteins and carbohydrates. However, if proteins and carbohydrates are not examined, using the proportion of storage to structural lipids can provide more valuable information (Lesser 2012). In addition, using the ratios of storage to structural lipids removes the need to standardise to surface area or dry weight making studies more comparable between different species and morphologies (Saunders et al. 2005).

One of the most consistent responses exhibited by all species in the current study was the decrease in the ratio of storage to structural lipids from the highest light and to the lowest SSC treatment (e.g. <5.7 mol quanta m^{-2} d^{-1} and >2.5 mg L^{-1}). This can be directly attributed to a decrease in the storage lipids, wax ester (WAX) and triacylglycerol (TAG), both of which constitute important energy reserves in corals (Imbs 2013, Lin et al. 2013) and can account for 40–73% of the total lipids (Harland et al. 1993, Yamashiro et al. 1999, Oku et al. 2002). Like the corals in the present study, an immediate reduction of TAG was identified after experimental and natural bleaching in *Porites compressa* and *Montipora verrucosa* (Grottoli et al. 2004, Rodrigues et al. 2008), as well as in less nutritional feeding regimes in *Acropora millepora* (Conlan et al. 2018). Although individual lipid classes were not analysed, the ratio of storage to structural lipids also decreased in the coral *Acropora nobilis* at a shallow turbid site and deep low light site (Saunders et al. 2005). This indicates that light may be an important factor for lipid ratios as previously shown for total lipid composition, with a 30% reduction in light from the field to the experimental system during a three week acclimation period contributing to a 30-50% drop in lipid content (Anthony & Connolly 2007). Interestingly, in the

same experiment the combination of low temperature, high light and high sediments resulted in a 50% increase in total lipids indicating these conditions are nutritionally favourable (Anthony & Connolly 2007). Given the current experiment did not combine a high sediment treatment with a high light treatment, it makes sense that no increases were observed.

Of all the species examined in this study, the branching pocilloporid coral *P. verrucosa* displayed the most noticeable changes as light decreased (and SSCs increased) in all response variables measured. Most notably, the drop in the ratio of storage to structural lipids and total lipids, was mirrored by a decrease in the number of algal symbionts. Zooxanthellae can utilise excess carbon from the coral host to synthesise fatty acids which are transferred back to the host in the form of storage lipids (Patton et al. 1977). Therefore, changes in the density of algal symbionts can have a direct impact on lipid storage content. In fact, a positive correlation between symbiont density and lipid content was identified in *Acropora tenuis,* with higher symbiont densities and lipid content identified in corals from poorer water quality sites, close to river mouths (Rocker et al. 2017). While *A. millepora* from the current study showed a similar trend of higher total lipids at the highest SSCs, their symbiont density displayed an inverse relationship to that of *A. tenuis* in the field, being lowest at the highest two SSCs. The increased lipid content might be related to an increase in photosynthesis to compensate for the lower algal density, with pg of Chl a increasing after 7.5 mg L^{-1}.

While the ratio of storage to structural lipids decreased for *C. orientalis* in the present study (again driven by a decrease in WAX and TAG), no significant differences were observed in percent total lipids as light decreased and SSCs increased. Similarly, previous work examining the effects of elevated SSCs on sponges revealed no significant difference in the percentage of total lipids in *C. orientalis* between 0, 30 and 100 mg L^{-1} (Pineda et al. 2017c).

Several studies have examined the effects of extreme light reduction on corals and these have mostly been associated with investigating the role of the symbiotic dinoflagellates in the nutrition and physiology of the symbiosis. Yonge and Nicholls (1931) showed that extrusion of symbiotic algae and subsequent discolouration (bleaching) in several tropical reef flat corals held in darkness for several weeks. Franzisket (1970) showed bleaching in four species of hermatypic corals held in darkness, with colonies bleaching in 10–20 days and with the most sensitive species, *Pocillopora elegans*, dying after 30 days. Titlyanov et al. (2001) and Hoegh-Guldberg and Smith (1989) showed bleaching in <10 d for *Stylophora pistillata* and DeSalvo et al. (2012) reported a similar time-course, with colonies of *Acropora palmata* and *Montastraea faveolata* paling and eventually bleaching after between 3 and 5 days in darkness. Most recently Jones et al. (2016) showed clear discolouration of the *Pocillopora acuta* and *A. millepora* held in darkness for 30 d consistent with the dissociation of the symbiosis (bleaching). In a recent study of the effects of light reduction (and elevated SSCs) on 4 species of corals collected from a high light environment, bleaching (as loss of alga symbionts) decrease in lipid levels and changes in structural to storage lipid ratios was observed with the sensitivity *P. damicornis> A. millepora>*, massive *Porites* spp. and *Turbinaria mesenterina* (Jones et al. unpublished). A common theme in these studies is the greater sensitivity of the branching pocilloporid colonies – *P. acuta*, *P. elegans*. *P. damicornis*, *P. verrucosa* and *S. pistillata* – to light limitation and usefulness of bleaching of this family as an early warning indicator during dredging programs.

For the juvenile corals, there was no obvious impact of light on mortality and growth across the whole light intensity range and the 6-week exposure period. These results are somewhat surprising and recruits in the first few weeks must be relying on lipid stores and heterotrophic feeding while algal symbionts reach sufficient densities to provide energy from autotrophy. Another interesting result was the ability of recruits grown in near darkness to uptake symbionts. These recruits appeared paler but algal symbionts could be observed within their tentacles. This *prima facie* evidence suggests that recruits are not more sensitive than the adults to light reduction from first settlement up to 6 weeks old.

5.5 Risk assessing dredging activities

Figure 25 shows the daily light integrals from the POTL long-term water quality monitoring program in Cleveland Bay for the 5 sites, four of which (Florence Bay, Geoffrey Bay, Picnic Bay and Virago Shoal) have reefs. Plotted through the data is a 30-d running mean DLI which has been colour coded to indicate period where the running mean is the range 5-3, 3-2, 2-1 mol quanta m^{-2} d^{-1} and <1 mol quanta m^{-2} d^{-1}. At Florence and Geoffrey Bay there are occasional periods where the 30-d running mean DLI value falls below 5 and 3 mol quanta m^{-2} d^{-1}, and at Florence Bay even below the 2 mol quanta m^{-2} d^{-1} level albeit for <5% of the time (March to April 2016). At Picnic Bay the running mean dips more frequently below the 3 and 2 mol quanta m^{-2} d^{-1} level and such an overall pattern is inconsistent with the turbidity information. Because of the different type of sensor used (see above) we have not interpreted this further. At Virago Shoal there are frequent periods where the running mean value drops below the 3 and 2 mol quanta m^{-2} d^{-1} levels and even the 1 mol quanta m^{-2} d^{-1} level in both winter and summer.

These analyses in conjunction with the laboratory-based studies indicate that the corals at Florence and Geoffrey Bay are likely to be occasionally suffering light limitations where storage lipids are being mobilised (changing lipid ratios). Further into Cleveland Bay, at Virago Shoal, this is likely to be happening much more frequently. Very few species exist at Virago Shoal (G. Ricardo pers. obs) and the reef is quite depauperate. The light recordings in Figure 25 were conducted at 3–4 m depth which corresponded to where the majority of the corals were located but even 1–2 metres deeper the frequency at which corals would drop into energy deficits would increase, as would the length of time based on the spectral solar irradiance model (see Figure 18). In between low light periods corals could have the opportunity to recover energy deficits and although not yet experimentally proven, the rapid replenishment of energy reserves in clement (high light) periods could be mechanisms by which turbid-zone coral water communities could survive episodic caliginous period. Other mechanisms include photoadaptation to low light (Anthony & Hoegh-Guldberg 2003), and heterotrophic feeding (Anthony & Fabricius 2000) but there are limits to the buffering which is why zonation patterns are highly compressed and truncated in these shallow-water mesophotic communities.

In summary, the results of this study, and in combination with other laboratory-based studies (Bessell-Browne et al. 2017c, Bessell-Browne et al. 2017d) and studies from of other dredging projects (Fisher et al. 2015, Jones et al. 2015a, Jones et al. 2016, Fisher et al. 2018a, Jones et al. 2019), suggest seabed light availability is the most suitable parameter to monitor and assess risks when dredging close to turbid-zone coral communities. The pressure-response

relationships and statistical summaries of Figure 21, Figure 22, Figure 23, Table 5, provide information that can be used with (a) plume trajectory modeling before dredging (GBRMPA 2012b) or (b) *in situ* monitoring programs during dredging, and can also be incorporated into risk-response reactive management cascades (see Chin and Marshall (2003)) to guide dredging operations once underway. A significant benefit of using light-based monitoring is that natural low light periods from turbidity events or cloud cover are accounted for when determining the cumulative stress, reducing the possibility of a type 2 error (failure to detect).

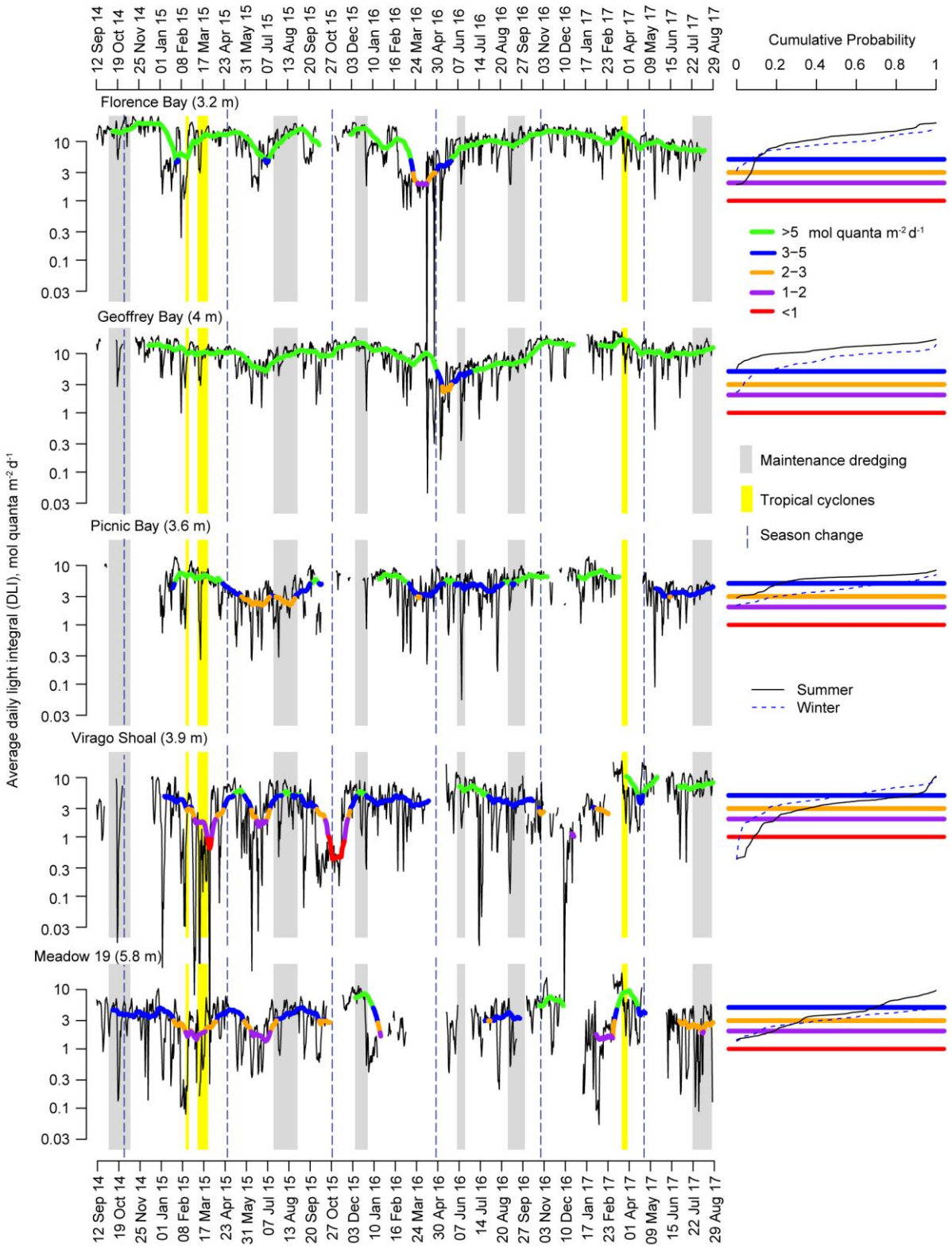

Figure 25: Time series plots showing daily light integrals (mol quanta m^{-2} d^{-1}) measured at the 5 long-term water quality monitoring sites (Figure 1) at mean depths of 3.2–5.8 m. Grey vertical bars represent periods of annual maintenance dredging in the Sea channel and predominantly the Platypus channel. Yellow boxes indicate cyclone Marcia (16 Feb 2015–21 Feb 2015), Nathan (9 Mar 2015–27 March 2017 and Debbie 22 March 2017–1 April 2017). Coloured lines represent the 30 d running mean and different colours represents area when the running mean is below certain DLIs.

Elevated levels of sediment deposition that leads to smothering of corals is another significant cause-effect pathway for certain coral morphologies. The present evidence suggests that smothering effects occur much closer to the source of turbidity generation than the longer-range movement associated with plumes. Continued use of the modified sediment deposition sensors employed in this study is recommended for future dredging and can further define the risk and areal extent of the risk associated with sediment smothering. An alternative approach is to use turbidity as a proxy for deposition and Fisher et al. (2019b) describe a series of turbidity ‘profiles’ over different running mean periods that describe where biological effects to a shallow water reefs are ‘possible’ and ‘probable’; the caveats and limitations associated with this approach are also described.

6.0 MANAGEMENT IMPLICATIONS

1) The study supports the idea that light is a key parameter in inshore turbid-zone coral reef communities around Cleveland Bay with species abundance and zonation patterns compressed to only a few metres. The coral communities occasionally experience periods of light limitation and it is a key pressure-parameter that should be monitored during dredging programs close to these environments.

2) Turbidity (water clarity) is not an absolute measure (it is a relative index of side scattering compared to an arbitrary standard, formazin) and in the past has been used as a proxy for suspended sediment concentrations and even light availability. Conversion of turbidity to SSCs is very dependent on particle size distribution and to a lesser extent the mineralogical characteristics of the sediment and conversion factors will vary in time and space. The subjectivity and inherent errors associated with nephelometers are such that they should not be favoured over light measurements. If nephelometry is used to provide proxy estimates of SSCs (for example to support modelling studies) then NTU to SSC calibrations need to be conducted across the range of likely SSCs, performed regularly and preferably with sediments collected from sediment traps rather than surficial seabed samples.

3) Plumes generated by a TSHD can have complex 3-dimensional turbidity profiles including surface maxima, mid-water maxima and bottom maxima, as well as well mixed homogenous SSC profiles (cf Figure 13). The most common profile in this study was an increase in SSC with depth with measurements within 1 m of seabed ~3.5× higher than the surface (0.3–0.5 m) behind the dredge and ~10× higher than the surface for the measurements at the dredge material placement area. Surface measurements of turbidity (via satellite or water sampling) are unlikely to be representative of the seabed turbidity (cf Figure 13 C) and estimates of benthic light availability from NTU to K_d correlations are also unlikely to yield accurate estimates of benthic light availability.

4) Elevated suspended sediment concentrations (from natural turbidity events (cf Figure 1 C**,** D) and dredging activity (cf Figure 2 E) have profound effects on light quantity (cf Figure 18). In addition, in inshore coastal areas elevated SSCs can also affect the underwater light spectrum (cf Figure 11, Figure 14, Figure 19), creating green-yellow light which is less photosynthetically useful. Spectral changes are likely to vary between different geographical locations depending on CDOM content, river influence and sediment characteristics. Some caution is needed in extrapolating information from past laboratory based physiological studies (or other locations) that have not addressed the light quality issue.

5) Affordable multispectral submersible PAR sensors are now commercially available that can provide information to assess changes in light quality as well as quantity (cf Figure 2 G, Figure 10, Figure 11). Use of seabed mounted multispectral PAR sensors, analyses of spectral profiles and calculations of PUR and PAR (or even more simply the ratio of red to blue light) can allow partitioning of light reduction associated with clouds and suspended sediments. Use of seabed mounted multispectral PAR sensors is recommended for future studies around dredging and also for long-term, wider scale studies of water quality of the inshore GBR to understand and assess the potential effects of terrestrial run off.

6) In interpreting water quality data especially for turbidity, the choice of summary statistics is important as median values (as opposed to mean values) may obscure turbidity events that are ecologically relevant, and even mean values can be difficult to interpret if used over long time periods. Use of upper percentiles (P_{95} etc) are recommended for site characterization (cf Table 1, Table 2, Table 3).

7) Given the variability in turbidity and light data (from tidal changes, clouds etc) sampling frequencies of 10–15 minutes intervals is suitable but summarizing the data to daily mean values is also appropriate. Light based monitoring needs reliable surface measurements in close proximity (kms) to the underwater monitoring sites.

8) Expressing turbidity and light data during dredging as percentiles of baseline levels of multiple different running mean time periods (1 d to many weeks) allows contextualization of the 'pressure' being placed on benthic communities (cf Figure 6). We suggest that this is a very useful technique to monitor the effects of dredging and to use with reactive management thresholds.

9) For the offshore sites near the entrance of Cleveland Bay there were clear seasonal differences in light availability, with winter values 23% lower than summer value and this was due to solar declination (cf Table 1, Table 2, Table 3, Figure 4, Figure 5). Lower winter light levels need to be considered when planning dredging campaigns (see Discussion).

10) Reefs naturally experience periods of low light from combinations of high turbidity (from dredging or natural storms) and also cloud cover (Figure 10). This needs to be accommodated for in monitoring programs and thresholds for dredging should be based on absolute light levels – and not light levels relevant to baseline, background levels. This issue is discussed at length in (Fisher et al. 2019b). Ecophysiological and energy balance models of how corals in turbid zone communities cope with periods of low light incorporate the idea of corals rapidly regaining energy balances during clement conditions. This could be incorporated into monitoring programs using different running mean time intervals (Fisher et al. 2019b).

11) The water quality time series analysed here included six maintenance and/or capital dredging campaigns. The analyses suggested that at Florence and Picnic Bays periods of intense dredging pressure may increase turbidity by 0.6-0.7 times the mean expected values. These estimated effect sizes are between two and five times lower than the effects of either wind or waves on turbidity, highlighting that even in the presence of dredging activity, wind and waves are the dominant drivers of turbidity in this system.

12) The study included the first empirical measurements of elevated sediment accumulation rates caused by maintenance dredging using newly re-designed deposition sensors. Over a 24 h period, accumulation rates were highly elevated (i.e. hundreds of mg cm^{-2} d^{-1}) at a distance of a few hundred metres from a working TSHD. However there was strong gradient of decreasing accumulation rates with increasing distance from the channel to a few tens of mg cm^{-2} d^{-1} at >200 m distance (Figure 17, Figure 16).

13) As discussed in Whinney et al. (2017), periods of elevated turbidity and high suspended sediment concentrations are not always associated with high levels of deposition in the short term, as it also depends on local hydrodynamics (current speed, wave orbital

velocities, tidal cycles etc). Given the novelty of the instrumentation, the results are preliminary, but provide evidence to support the idea that high SSCs produced by dredging in a low energy water column is conducive to rapid settling and enhanced deposition. The upper percentiles of the running mean periods (6 h to 4 d) for the 100 m location (Figure 17 B) provide a first order approximation of the levels of sediment deposition possible during maintenance dredging activities in Platypus channel with a medium sized TSHD.

14) The experiments described in Figure 21, Figure 22, Figure 23 were conducted over a range of environmentally relevant SSCs (Figure 4), using locally (to Cleveland Bay) collected sediments and appropriate particle size distributions, and local coral and sponge species. During the experiments the light quantity was adjusted to replicate the underwater light levels (at 5 m) for a given SSC (cf Figure 18) and the light spectra (cf Figure 19) were also adjusted using custom made lights (cf Figure 3) to replicate spectral changes that occur in inshore environments (based on empirical data from free-fall, hyperspectral light profiling study). The ensuing pressure-response relationships and statistical summaries (Figure 21, Figure 22, Figure 23, Table 5) provide information that can be used with (a) plume trajectory modelling before dredging (GBRMPA 2012b) or (b) *in situ* monitoring programs during dredging, and can also be incorporated into risk-response reactive management cascades (see Chin and Marshall, 2003) to guide dredging operations once underway.

15) Multiple studies have now shown that branching pocilloporid corals (genus *Pocillopora* and *Stylophora*) are very sensitive to light reduction (cf Figure 21, Figure 22, Figure 23) and could be used as an early warning (bioindicator) of low light effects during monitoring programs in inshore turbid-reef zones.

16) Corals normally keep their surfaces sediment-free, and simple assessments of the percentage of the surface covered by sediment (% smothered) could also be used as early warning bioindicator and is a very practical and rapid survey technique for monitoring that could be conducted by roving diver techniques or even diver-less assessments using remotely operated vehicles (Jones et al. 2019).

REFERENCES

AIMS (2016) Australian Institute of Marine Science (AIMS). (2009). Northern Australia Automated Marine Weather and Oceanographic Stations, Sites: [Cleveland Bay]. https://doi.org/10.25845/5c09bf93f315d. accessed 18 Nov 2019

Anthony K, Connolly S (2004) Environmental limits to growth: physiological niche boundaries of corals along turbidity–light gradients. Oecologia 141:373-384

Anthony K, Fabricius K (2000) Shifting roles of heterotrophy and autotrophy in coral energetics under varying turbidity. J Exp Mar Biol Ecol 252:221-253

Anthony K, Hoegh-Guldberg O (2003) Kinetics of photoacclimation in corals. Oecologia 134:23-31

Anthony K, Hoogenboom M, Maynard J, Grottoli A, Middlebrook R (2009) Energetics approach to predicting mortality risk from environmental stress: a case study of coral bleaching. Funct Ecol 23:539-550

Anthony K, Larcombe P (2000) Coral reefs in turbid waters: sediment-induced stresses in corals and likely mechanisms of adaptation. Proceedings of the 9th International Coral Reef Symposium Bali, Indonesia 1:239-244

Anthony K, Ridd P, Orpin A, Larcombe P, Lough J (2004) Temporal variation of light availability in coastal benthic habitats: Effects of clouds, turbidity, and tides. Limnol Oceanogr 49:2201-2211

Anthony KRN, Connolly SR (2007) Bleaching, energetics, and coral mortality risk: Effects of temperature, light, and sediment regime. Limnol Oceanogr 52:716-726

Antoine D, Schroeder T, Slivkoff M, Klonowski W, Doblin W, Lovell J, David Boadle D, Brett Baker B, Elizabeth Botha E, Robinson C, King E, Fearns P, Hardman-Mountford N, Johnson R, Cherukuru N, Dekker A, Malthus T, Mitchell R, Thompson P, Van Ruth P (217) The IMOS Radiometery Task Team. Final Report. http://imos.org.au/facilities/task-teams/radiometry/. Integrated Marine Observing System (IMOS), Tasmania (Hobart), Australia, 100 pp.

Bainbridge Z, Lewis S, Bartley R, Fabricius K, Collier C, Waterhouse J, Garzon-Garcia A, Robson B, Burton J, Wenger A (2018) Fine sediment and particulate organic matter: A review and case study on ridge-to-reef transport, transformations, fates, and impacts on marine ecosystems. Mar Pollut Bull 135:1205-1220

Bainbridge ZT, Wolanski E, Alvarez-Romero JG, Lewis SE, Brodie JE (2012) Fine sediment and nutrient dynamics related to particle size and floc formation in a Burdekin River flood plume, Australia. Mar Pollut Bull 65:236-248

Bak RPM (1978) Lethal and sublethal effects of dredging on reef coral. Mar Pollut Bull 9:14-16

Bartley R, Bainbridge ZT, Lewis SE, Kroon FJ, Wilkinson SN, Brodie JE, Silburn DM (2014) Relating sediment impacts on coral reefs to watershed sources, processes and management: A review. Sci Total Environ 468:1138-1153

Bates D, Mächler M, Bolker B, Walker S (2015) Fitting Linear Mixed-Effects Models Using lme4. 2015 67:48

Belperio A, Searle D (1988) Terrigenous and carbonate sedimentation in the Great Barrier Reef province. Dev Sedimentol, Book 42. Elsevier, 143-174

Bender EA, Case TJ, Gilpin ME (1984) Perturbation experiments in community ecology: theory and practice. Ecology 65:1-13

Benson L, Goldsworthy P, Butler I, Oliver JJ (1994) Townsville Port Authority capital dredging works 1993: Environmental monitoring program.

Bessell-Browne P, Fisher R, Duckworth A, Jones R (2017a) Mucous sheet production in Porites: an effective bioindicator of sediment related pressures. Ecol Indicators 77:276-285

Bessell-Browne P, Negri A, Fisher R, Clode P, Jones R (2017b) Cumulative impacts: thermally bleached corals have reduced capacity to clear deposited sediment Sci Rep 2017

Bessell-Browne P, Negri AP, Fisher R, Clode PL, Duckworth A, Jones R (2017c) Impacts of turbidity on corals: The relative importance of light limitation and suspended sediments. Mar Pollut Bull 117:161-170

Bessell-Browne P, Negri AP, Fisher R, Clode PL, Jones R (2017d) Impacts of light limitation on corals and crustose coralline algae. Sci Rep 7:11553

Bongaerts P, Ridgway T, Sampayo EM, Hoegh-Guldberg O (2010) Assessing the 'deep reef refugia' hypothesis: focus on Caribbean reefs. Coral Reefs 29:309-327

Brodie J, Kroon F, Schaffelke B, Wolanski E, Lewis S, Devlin M, Bohnet I, Bainbridge Z, Waterhouse J, Davis A (2012) Terrestrial pollutant runoff to the Great Barrier Reef: an update of issues, priorities and management responses. Mar Pollut Bull 65:81-100

Browne NK (2012) Spatial and temporal variations in coral growth on an inshore turbid reef subjected to multiple disturbances. Mar Environ Res 77:71-83

Browne NK, Smithers SG, Perry CT (2010) Geomorphology and community structure of Middle Reef, central Great Barrier Reef, Australia: an inner-shelf turbid zone reef subject to episodic mortality events. Coral Reefs 29:683-689

Browne NK, Smithers SG, Perry CT (2013) Spatial and temporal variations in turbidity on two inshore turbid reefs on the Great Barrier Reef, Australia. Coral Reefs 32:195-210

Browne NK, Smithers SG, Perry CT, Ridd PV (2012) A field-based technique for measuring sediment flux on coral reefs: application to turbid reefs on the Great Barrier Reef. J Coast Res 284:1247-1262

Bull G (1982) Scleractinian coral communities of two inshore high island fringing reefs at Magnetic Island, North Queensland. Marine Ecology Progress Series Oldendorf 7:267-277

Carter R, Johnson D, Hooper K (1993) Episodic post-glacial sea-level rise and the sedimentary evolution of a tropical continental embayment (Cleveland Bay, Great Barrier Reef shelf, Australia). Aust J Earth Sci 40:229-255

Chin A, Marshall P (2003) Reactive monitoring at Nelly Bay Harbour using environmental monitoring to manage marine construction activities. In: Monitoring Coral Reef Marine Protected Areas. Australian Institute of Marine Science and the IUCN Marine Program.:34-35

Conlan JA, Bay LK, Severati A, Humphrey C, Francis DS (2018) Comparing the capacity of five different dietary treatments to optimise growth and nutritional composition in two scleractinian corals. PLoS ONE 13:e0207956

Conlan JA, Humphrey CA, Severati A, Francis DS (2017a) Influence of different feeding regimes on the survival, growth, and biochemical composition of Acropora coral recruits. PLoS ONE 12:e0188568

Conlan JA, Rocker MM, Francis DS (2017b) A comparison of two common sample preparation techniques for lipid and fatty acid analysis in three different coral morphotypes reveals quantitative and qualitative differences. PeerJ 5:e3645

Conner CS, De Visser AM (1992) A laboratory investigation of particle size effects on an optical backscatterance sensor. Mar Geol 108:151-159

Cooper TF, Ridd PV, Ulstrup KE, Humphrey C, Slivkoff M, Fabricius KE (2008) Temporal dynamics in coral bioindicators for water quality on coastal coral reefs of the Great Barrier Reef. Mar Freshw Res 59:703-716

Cooper TF, Uthicke S, Humphrey C, Fabricius KE (2007) Gradients in water column nutrients, sediment parameters, irradiance and coral reef development in the Whitsunday Region, central Great Barrier Reef. Estuar Coast Shelf Sci 74:458-470

Davies-Colley R, Smith D (2001) Turbidity, suspended sediment and water quality: a review. J Am Water Works Assoc 37:1085-1101

De'ath G, Fabricius K (2008) Water quality of the Great Barrier Reef: distributions, effects on reef biota and trigger values for the protection of ecosystem health. Great Barrier Reef Marine Park Authority

Delandmeter P, Lewis S, Lambrechts J, Deleersnijder E, Legat V, Wolanski E (2015) The transport and fate of riverine fine sediment exported to a semi-open system. Estuar Coast Shelf Sci 167:336-346

DeSalvo M, Estrada A, Sunagawa S, Medina M (2012) Transcriptomic responses to darkness stress point to common coral bleaching mechanisms. Coral Reefs 31:215-228

Devlin M, Waterhouse J, Taylor J, Brodie J (2001) Flood plumes in the Great Barrier Reef: spatial and temporal patterns in composition and distribution. Great Barrier Reef Marine Park Authority

Dodge RE, Rimas Vaisnys JR (1977) Coral populations and growth patterns: responses to sedimentation and turbidity associated with dredging. J Mar Res 35:715-730

Dove SG, Hoegh-Guldberg O, Ranganathan S (2001) Major colour patterns of reef-building corals are due to a family of GFP-like proteins. Coral Reefs 19:197-204

Duckworth A, Giofre N, Jones R (2017) Coral morphology and sedimentation. Mar Pollut Bull 125:289–300

Dustan P (1982) Depth-dependent photoadaption by zooxanthellae of the reef coral *Montastrea annularis*. Mar Biol 68:253-264

Enrıquez S, Méndez ER, Iglesias-Prieto R (2005) Multiple scattering on coral skeletons enhances light absorption by symbiotic algae. Limnol Oceanogr 50:1025-1032

EPA (2016) Technical Guidance - Environment Impact Assessment of Marine Dredging Proposals. Environmental Protection Authority, EPA, Western Australia, 26 pp

Erftemeijer PL, Riegl B, Hoeksema BW, Todd PA (2012) Environmental impacts of dredging and other sediment disturbances on corals: a review. Mar Pollut Bull 64:1737-1765

Erwin P, Thacker R (2008) Phototrophic nutrition and symbiont diversity of two Caribbean sponge–cyanobacteria symbioses Mar Ecol Prog Ser 362:139–147

Fabricius KE, De'ath G, Humphrey C, Zagorskis I, Schaffelke B (2013) Intra-annual variation in turbidity in response to terrestrial runoff on near-shore coral reefs of the Great Barrier Reef. Estuar Coast Shelf Sci 116:57-65

Falkowski P, Jokiel P, Kinzie R (1990) Irradiance and corals. In: Z D (ed)Ecosystems of the world, Book 25: Coral reefs. Elsevier, , Amsterdam, pp 89–107, 89-107

Fearns P, Dorji P, Broomhall M, Chedzey H, Symonds G, Mortimer N, Branson P, Contardo S, Shimizu K, Sun C (2019) Plume Characterisation – Field Studies. Report of Theme 3 – Project 3.2.1, prepared for the Dredging Science Node, Western Australian

Marine Science Institution, Perth, Western Australia, 300 pp. Available at: https://www.wamsi.org.au/dredging-science-node/dsn-reports.

Fearns P, Dorji P, M B, Branson P, Mortimer N (2018) Plume Characterization – Laboratory Studies. Report of Theme 3 - Project 322, prepared for the Dredging Science Node, Western Australian Marine Science Institution, Perth, Western Australia 57 pp Available at: https://wwwwamsiorgau/dredging-science-node/dsn-reports

Fisher R, Bessell-Browne P, Jones R (2019a) Synergistic and antagonistic impacts of suspended sediments and thermal stress on corals. Nature Communications 10:2346

Fisher R, Jones R, Bessell-Browne P (2019b) Effects of dredging and dredging related activities on water quality: Impacts on coral mortality and threshold development. Report of Theme 4 Project 4.9 prepared for the Dredging Science Node, Western Australian Marine Science Institution. Perth, Western Australia. 128 pp. Available at: https://www.wamsi.org.au/dredging-science-node/dsn-reports

Fisher R, Stark C, Ridd P, Jones R (2015) Spatial patterns in water quality changes during dredging in tropical environments. PLoS ONE 10:e0143309

Fisher R, Walshe T, Bessell-Browne P, Jones R (2018a) Accounting for environmental uncertainty in the management of dredging impacts using probabilistic dose-response relationships and thresholds. J Appl Ecol:1-11

Fisher R, Wilson S, Sin T, Lee A, Langlois T (2018b) A simple function for full-subsets multiple regression in ecology with R. Ecol Evol 8:6104-6113

Foster T, Corcoran E, Erftemeijer P, Fletcher C, Peirs K, Dolmans C, Smith A, Yamamoto H, Jury M (2010) Dredging and port construction around coral reefs. PIANC Environmental Commission, Report No 108

Franzisket L (1970) The atrophy of hermatypic reef corals maintained in darkness and their subsequent regeneration in light. Internationale Revue der gesamten Hydrobiologie und Hydrographie 55:1-12

Gaines S, Denny M (1993) The Largest, Smallest, Highest, Lowest, Longest, and Shortest: Extremes in Ecology. Ecology 74:1677-1692

GBRMPA (2012a) Protecting the reef bioregions in the Great Barrier Reef Marine Park and World Heritage Area. Retrieved 10 May 2019.

GBRMPA (2012b) The use of hydrodynamic numerical modelling for dredging projects in the Great Barrier Reef Marine Park, Great Barrier Reef Marine Park Authority, Townsville. GBRMPA External Guideline. Townsville (Queensland, Australia), 8 pp.

GBRMPA (2013) Reef rescue marine monitoring program quality assurance and quality control manual 2011/12. Great Barrier Reef Marine Park Authority, Townsville, Queensland, 111 pp.

Glasby TM, Underwood AJ (1996) Sampling to differentiate between pulse and press perturbations. Environ Monit Assess 42:241-252

Goodrich B, Gabry J, Ali I, Brilleman S (2018) rstanarm: Bayesian applied regression modeling via Stan. R package version 2.17.4. http://mc-stan.org/.

Goreau TF, Wells J (1967) The shallow-water Scleractinia of Jamaica: revised list of species and their vertical distribution range. Bull Mar Sci 17:442-453

Grottoli AG, Rodrigues LJ, Juarez C (2004) Lipids and stable carbon isotopes in two species of Hawaiian corals, *Porites compressa* and *Montipora verrucosa*, following a bleaching event. Mar Biol 145:621-631

Halldal P (1968) Photosynthetic capacities and photosynthetic action spectra of endozoic algae of the massive coral *Favia*. The Biological Bulletin 134:411-424

Hansell DA, Carlson CA (2014) Biogeochemistry of marine dissolved organic matter. Academic Press

Harland AD, Navarro JC, Spencer Davies P, Fixter LM (1993) Lipids of some Caribbean and Red Sea corals: total lipid, wax esters, triglycerides and fatty acids. Mar Biol 117:113-117

Hennige SJ, Suggett DJ, Warner ME, McDougall KE, Smith DJ (2009) Photobiology of *Symbiodinium* revisited: bio-physical and bio-optical signatures. Coral Reefs 28:179-195

Heyward A, Negri A (1999) Natural inducers for coral larval metamorphosis. Coral Reefs 18:273-279

Hoegh-Guldberg O, Smith GJ (1989) The effects of sudden changes in light, temperature and salinity on the population density and export of zooxanthellae from the reef corals *Seriatopora hysterix* and *Styllophora pistillata*. Mar Ecol Prog Ser 129:279-303

Hopley D (1982) The Geomorphology of the Great Barrier Reef. Wiley New York

Hothorn T, Bretz F, Westfall P (2008) Simultaneous Inference in General Parametric Models. Biom J 50:346-363

Imbs AB (2013) Fatty acids and other lipids of corals: Composition, distribution, and biosynthesis. Russ J Mar Biol 39:153-168

Jones R, Bessell-Browne P, Fisher R, Klonowski W, Slivkoff M (2016) Assessing the impacts of sediments from dredging on corals. Mar Pollut Bull 102:9-29

Jones R, Fisher R, Bessell-Browne P (2019) Sediment deposition and coral smothering. PLoS ONE 14:e0216248

Jones R, Fisher R, Stark C, Ridd P (2015a) Temporal patterns in water quality from dredging in tropical environments. PLoS ONE 10(10): e0137112

Jones R, Ricardo G, AP N (2015b) Effects of sediments on the reproductive cycle of corals. Mar Pollut Bull 100:13-33

Jones RJ (1997) Zooxanthellae loss as a bioassay for assessing stress in corals. Mar Ecol Prog Ser 149:163-171

Jones RJ (2008) Coral bleaching, bleaching-induced mortality, and the adaptive significance of the bleaching response. Mar Biol 154:65-80

Kaly UL, Mapstone BD, Ayling AM, Choat JH (1994) Coral Communities. In: Benson L, Goldsworthy P, Butler I, Oliver J (eds)Townsville Port Authority Capital Dredging Works 1993: Environmental monitoring program. Townsville Port Authority, Townsville, Queensland Australia, 55-87

Kinzie RA, III, Jokiel PL, York R (1984) Effects of light of altered spectral composition on coral zooxanthellae associations and on zooxanthellae in vitro. Mar Biol 78:239-248

Kirk J (1980) Spectral adsorption properties of natural watres: contribtion of the soluble and particulate fractions to light absorption in some inland watres of south-eastern Australia. Mar Freshw Res 31:287-296

Kirk J (1994) Light and photosynthesis in aquatic ecosystems. Third Edition. Cambridge University Press, New York,

Kirk JT (1985) Effects of suspensoids (turbidity) on penetration of solar radiation in aquatic ecosystems. Perspectives in Southern Hemisphere Limnology. Springer, 195-208

Kuhl M, Cohen Y, Dalsgaard T, Jorgensen BB, Revsbech NP (1995) Microenvironment and photosynthesis of zooxanthellae in scleractinian corals studied with microsensors for O_2, pH and light. Mar Ecol Prog Ser 117:159-172

LaJeunesse TC, Parkinson JE, Gabrielson PW, Jeong HJ, Reimer JD, Voolstra CR, Santos SR (2018) Systematic revision of Symbiodiniaceae highlights the antiquity and diversity of coral endosymbionts. Curr Biol 28:2570-2580. e2576

Lambrechts J, Humphrey C, McKinna L, Gourge O, Fabricius KE, Mehta AJ, Lewis S, Wolanski E (2010) Importance of wave-induced bed liquefaction in the fine sediment budget of Cleveland Bay, Great Barrier Reef. Estuar Coast Shelf Sci 89:154-162

Larcombe P, Costen A, Woolfe KJ (2001) The hydrodynamic and sedimentary setting of nearshore coral reefs, central Great Barrier Reef shelf, Australia: Paluma Shoals, a case study. Sedimentology 48:811-835

Larcombe P, Ridd P, Prytz A, Wilson B (1995) Factors controlling suspended sediment on inner-shelf coral reefs, Townsville, Australia. Coral Reefs 14:163-171

Larcombe P, Woolfe K (1999) Increased sediment supply to the Great Barrier Reef will not increase sediment accumulation at most coral reefs. Coral Reefs 18:163-169

Larkum T (1996) How dinoflagellates make light work with peridinin. Trends Plant Sci 1:252

Lazaridis E (2014) Lunar: Lunar Phase & Distance, Seasons and Other Environmental Factors (Version 0.1-04). . Available from http://statistics.lazaridis.eu)

Lesser MP (2012) Using energetic budgets to assess the effects of environmental stress on corals: are we measuring the right things? Coral Reefs 32:25-33

Lesser MP, Slattery M, Leichter JJ (2009) Ecology of mesophotic coral reefs. J Exp Mar Biol Ecol 1:1-8

Levy O, Dubinsky Z, Achituv Y (2003) Photobehavior of stony corals: responses to light spectra and intensity. J Exp Biol 206:4041-4049

Lichtenberg M, Larkum AWD, Kühl M (2016) Photosynthetic acclimation of *Symbiodinium* in hospite depends on vertical position in the tissue of the Scleractinian coral *Montastrea curta*. Front Microbiol 7

Lin C, Wang L-H, Meng P-J, Chen C-S, Tsai S (2013) Lipid content and composition of oocytes from five coral species: potential implications for future cryopreservation efforts. PLoS ONE 8:e57823

Lou J, Ridd PV (1996) Wave-current bottom shear stresses and sediment resuspension in Cleveland Bay, Australia. Coastal Engineering 29:169-186

Loya Y, Eyal G, Treibitz T, Lesser MP, Appeldoorn R (2016) Theme section on mesophotic coral ecosystems: advances in knowledge and future perspectives. Coral Reefs 35:1-9

Macdonald R, Ridd P, Whinney J, Larcombe P, Neil D (2013) Towards environmental management of water turbidity within open coastal waters of the Great Barrier Reef. Mar Pollut Bull 74:82-94

Madin J, Allen A, Baird A, Pandolfi J, Sommer B (2016) Scope for latitudinal extension of reef corals is species specific. Frontiers of Biogeography 8

Mapstone BD, Choat J, Cumming R, Oxley W (1992) The fringing reefs of Magnetic Island: benthic biota and sedimentation-a baseline study: a report to the Great Barrier Reef Marine Park Authority. Research report No.13. Great Barrier Reef Marine Park Authority, Townsville, Australia

Marchant R, Stevens T, Choukroun S, Coombes G, Santarossa M, Whinney J, Ridd P (2014) A Buoyant Tethered Sphere for Marine Current Estimation. IEEE Journal of Oceanic Engineering 39:2-9

Maritorena S, Guillocheau N (1996) Optical properties of water and spectral light absorption by living and non-living particles and by yellow substances in coral reef waters of French Polynesia. Mar Ecol Prog Ser 131:245-255

Mass T, Kline DI, Roopin M, Veal CJ, Cohen S, Iluz D, Levy O (2010) The spectral quality of light is a key driver of photosynthesis and photoadaptation in *Stylophora pistillata* colonies from different depths in the Red Sea. J Exp Biol 213:4084-4091

Maxwell W, Swinchatt J (1970) Great Barrier Reef: regional variation in a terrigenous-carbonate province. Geol Soc Am Bull 81:691-724

McCook L, Schaffelke B, Apte A, Brinkman R, Brodie J, Erftemeijer P, Eyre B, Hoogerwerf F, Irvine I, Jones R, King B, Marsh H, Masini R, Morton R, Pitcher R, Rasheed M, Sheaves M, Symonds A, M.St.J W (2015) Synthesis of current knowledge of the biophysical impacts of dredging and disposal on the Great Barrier Reef: report of an independent panel of experts. Great Barrier Reef Marine Park Authority, Townsville, Australia

Morel A (1978) Available, usable, and stored radiant energy in relation to marine photosynthesis. Deep Sea Research 25:673-688

Morgan KM, Perry CT, Smithers SG, Johnson JA, Daniell JJ (2016) Evidence of extensive reef development and high coral cover in nearshore environments: implications for understanding coral adaptation in turbid settings. Sci Rep 6:29616

Muir PR, Wallace CC, Done T, Aguire D (2016) Response to letter regarding “Limited scope for latitudinal extension of reef corals”. Frontiers of Biogeography, 8(4). .

Muir PR, Wallace CC, Done T, Aguirre JD (2015) Limited scope for latitudinal extension of reef corals. Science 348:1135-1138

Oku H, Yamashiro H, Onaga K, Iwasaki H, Takara K (2002) Lipid distribution in branching coral *Montipora digitata*. Fish Sci 68:517-522

Oliver J (1995) Is the 'Limits of Acceptable Change' concept useful for environmental managers? A case study from the Great Barrier Reef Marine Park. In: Grigg GC, Hale PT, Lunney D (eds)Conservation Through Sustainable Use of Wildlife. Centre for Conservation Biology. The University of Queensland., Queensland, Australia, 131-139

Orpin A, Ridd P (2012) Exposure of inshore corals to suspended sediments due to wave-resuspension and river plumes in the central Great Barrier Reef: A reappraisal. Cont Shelf Res 47:55-67

Orpin A, Ridd P, Stewart L (1999) Assessment of the relative importance of major sediment transport mechanisms in the central Great Barrier Reef lagoon. Aust J Earth Sci 46:883-896

Orpin A, Ridd P, Thomas S, Anthony K, Marshall P, Oliver J (2004) Natural turbidity variability and weather forecasts in risk management of anthropogenic sediment discharge near sensitive environments. Mar Pollut Bull 49:602-612

Patterson D (1994) Oceanographic data collection. In: Benson L, Goldsworthy P, Butler I, Oliver J (eds)Townsville Port Authority Capital Dredging Works 1993: Environmental monitoring program. Townsville Port Authority, Townsville, Queensland Australia, 125-147

Patton JS, Abraham S, Benson AA (1977) Lipogenesis in the intact coral *Pocillopora capitata* and its isolated zooxanthellae: Evidence for a light-driven carbon cycle between symbiont and host. Mar Biol 44:235-247

Perry CT, Larcombe P (2003) Marginal and non-reef-building coral environments. Coral Reefs 22:427-432

Perry CT, Smithers SG, Gulliver P, Browne NK (2012) Evidence of very rapid reef accretion and reef growth under high turbidity and terrigenous sedimentation. Geology 40:719-722

Pineda M-C, Strehlow B, Duckworth A, Doyle J, Jones R, Webster NS (2016a) Effects of light attenuation on the sponge holobiont- implications for dredging management. 6:39038

Pineda M-C, Strehlow B, Kamp J, Duckworth A, Jones R, Webster NS (2017a) Effects of combined dredging-related stressors on sponges: a laboratory approach using realistic scenarios. Sci Rep 7:5155

Pineda M-C, Strehlow B, Sternel M, Duckworth A, Haan Jd, Jones R, Webster NS (2017b) Effects of sediment smothering on the sponge holobiont with implications for dredging management. Sci Rep 7:5156

Pineda M-C, Strehlow B, Sternel M, Duckworth A, Jones R, Webster NS (2017c) Effects of suspended sediments on the sponge holobiont with implications for dredging management. Sci Rep 7:4925

Pineda MC, Duckworth A, Webster N (2015) Appearance matters: sedimentation effects on different sponge morphologies. J Mar Biol Assoc UK:1-12

Pineda MC, Strehlow B, Duckworth A, Doyle J, Jones R, Webster NS (2016b) Effects of light attenuation on the sponge holobiont- implications for dredging management. Sci Rep 6:39038

Prézelin B, Haxo F (1976) Purification and characterization of peridinin-chlorophyll a - proteins from the marine dinoflagellates *Glenodinium* sp. and *Gonyaulax polyedra*. Planta 128:133-141

Prézelin B, Ley AC, Haxo F (1976) Effects of growth irradiance on the photosynthetic action spectra of the marine dinoflagellate, *Glenodinium* sp. Planta 130:251-256

Ralph PJ, Gademann R (2005) Rapid light curves: A powerful tool to assess photosynthetic activity. Aquat Bot 82:222-237

Reine KJ, Dickerson DD, Clarke DG (1998) Environmental windows associated with dredging operations. DTIC Document

Ricardo G, Jones R, Clode P, Negri A (2016a) Mucous Secretion and Cilia Beating Defend Developing 1 Coral Larvae from Suspended Sediments. PLoS ONE 11(9): e0162743.doi:10.1371/journal.pone.0162743

Ricardo GF, Jones RJ, Clode PL, Humanes A, Giofre N, Negri AP (2018) Sediment characteristics influence the fertilisation success of the corals *Acropora tenuis* and *Acropora millepora*. Mar Pollut Bull 135:941-953

Ricardo GF, Jones RJ, Clode PL, Humanes A, Negri AP (2015) Suspended sediments limit coral sperm availability. Sci Rep 5:18084

Ricardo GF, Jones RJ, Negri AP, Stocker R (2016b) That sinking feeling: Suspended sediments can prevent the ascent of coral egg bundles. Sci Rep 6:21567

Ricardo GF, Jones RJ, Nordborg M, Negri AP (2017) Settlement patterns of the coral *Acropora millepora* on sediment-laden surfaces. Sci Total Environ 609:277-288

Ridd P, Day G, Thomas S, Harradence J, Fox D, Bunt J, Renagi O, Jago C (2001) Measurement of Sediment Deposition Rates using an Optical Backscatter Sensor. Estuar Coast Shelf Sci 52:155-163

Risk MJ, Edinger E (2011) Impacts of sediment on coral reefs. In: Hopley D (ed)Encyclopedia of Modern Coral Reefs. Springer Netherlands, 575-586

Rocker MM, Francis DS, Fabricius KE, Willis BL, Bay LK (2017) Variation in the health and biochemical condition of the coral *Acropora tenuis* along two water quality gradients on the Great Barrier Reef, Australia. Mar Pollut Bull 119:106-119

Rodrigues LJ, Grottoli AG, Pease TK (2008) Lipid class composition of bleached and recovering *Porites compressa* Dana, 1846 and *Montipora capitata* Dana, 1846 corals from Hawaii. J Exp Mar Biol Ecol 358:136-143

Rogers CS (1990) Responses of coral reefs and reef organisms to sedimentation. Mar Ecol Prog Ser 62:185-202

Saunders SM, Radford B, Bourke SA, Thiele Z, Bech T, Mardon J (2005) A Rapid Method for Determining Lipid Fraction Ratios of Hard Corals under Varying Sediment and Light Regimes. Environmental Chemistry 2:331

Schlichter D, Fricke H, Weber W (1986) Light harvesting by wavelength transformation in a symbiotic coral of the Red Sea twilight zone. Mar Biol 91:403-407

Schneider CA, Rasband WS, Eliceiri KW (2012) NIH Image to ImageJ: 25 years of image analysis. Nat Methods 9:671-675

Shaffer JM, Beaulieu JJ (2012) Calibration of the Odyssey™ Photosynthetic Irradiance Recorder™ for absolute irradiance measures. J Freshwat Ecol 27:599-605

Sheppard C (1982) Coral populations on reef slopes and their major controls. Mar Ecol Prog Ser 7:83-115

Slattery M, Lesser M, Brazeau D, Stokes M, Leichter J (2011) Connectivity and stability of mesophotic coral reefs. J Exp Mar Biol Ecol 408:32-41

Slivkoff M (2014) Ocean colour remote sensiing of the Great Barrier Reef waters. PhD Thesis School of Science, Department of Imaging & Applied Physics, Perth, Western Australia, Curtin University:321 pp

Song P-S, Koka P, Prezelin BB, Haxo FT (1976) Molecular topology of the photosynthetic light-harvesting pigment complex, peridinin-chlorophyll a-protein, from marine dinoflagellates. Biochemistry 15:4422-4427

Stimson J, Kinzie RA (1991) The temporal pattern and rate of release of zooxanthellae from the reef coral Pocillopora damicornis (Linnaeus) under nitrogen-enrichment and control conditions. J Exp Mar Biol Ecol 153:63-74

Storlazzi C, Norris B, Rosenberger K (2015) The influence of grain size, grain color, and suspended-sediment concentration on light attenuation: Why fine-grained terrestrial sediment is bad for coral reef ecosystems. Coral Reefs:1-9

Storlazzi CD, Field ME, Bothner MH (2011) The use (and misuse) of sediment traps in coral reef environments: theory, observations, and suggested protocols. Coral Reefs 30:23-38

Storlazzi CD, Jaffe BE (2008) The relative contribution of processes driving variability in flow, shear, and turbidity over a fringing coral reef: West Maui, Hawaii. Estuar Coast Shelf Sci 77:549-564

Storlazzi CD, Ogston AS, Bothner MH, Field ME, Presto MK (2004) Wave- and tidally-driven flow and sediment flux across a fringing coral reef: Southern Molokai, Hawaii. Cont Shelf Res 24:1397-1419

Szabó M, Wangpraseurt D, Tamburic B, Larkum AW, Schreiber U, Suggett DJ, Kühl M, Ralph PJ (2014) Effective light absorption and absolute electron transport rates in the coral Pocillopora damicornis. Plant Physiol Biochem 83:159-167

Thomas S, Ridd PV (2004) Review of methods to measure short time scale sediment accumulation. Mar Geol 207:95-114

Thomas S, Ridd PV, Day G (2003) Turbidity regimes over fringing coral reefs near a mining site at Lihir Island, Papua New Guinea. Mar Pollut Bull 46:1006-1014

Titlyanov EA, Titlyanova TV, Yamazato K, van Woesik R (2001) Photo-acclimation dynamics of the coral Stylophora pistillata to low and extremely low light. J Exp Mar Biol Ecol 263:211-225

Veron J (2000) Corals of the World. Volume 3. Australian Institute of Marine Science (AIMS) 463

Verspecht F, Pattiaratchi C (2010) On the significance of wind event frequency for particulate resuspension and light attenuation in coastal waters. Cont Shelf Res 30:1971-1982

Wangpraseurt D, Larkum AW, Ralph PJ, Kühl M (2012) Light gradients and optical microniches in coral tissues. Front Microbiol 3

Wangpraseurt D, Tamburic B, Szabó M, Suggett D, Ralph PJ, Kühl M (2014) Spectral Effects on *Symbiodinium* photobiology studied with a programmable light engine. PLoS ONE 9:e112809

Whinney J, Jones R, Duckworth A, Ridd P (2017) Continuous in situ monitoring of sediment deposition in shallow benthic environments. Coral Reefs 36:521–533

Wilkinson C (1983) Net primary productivity in coral reef sponges. . Science 219: 410–412

Wilkinson C (1987) Interocean differences in size and nutrition of coral reef sponge populations. . Science 236:1654-1657

Wolanski E (1994) Physical oceanographic processes of the Great Barrier Reef. CRC PressI Llc

Wood SN (2006) Generalized Additive Models: an introduction with R, Vol Book 66. CRC Press, Boca Raton, FL,

Wyman K, Dubinsky Z, Porter J, Falkowski P (1987) Light absorption and utilization among hermatypic corals: a study in Jamaica, West Indies. Mar Biol 96:283-292

Yamashiro H, Oku H, Higa H, Chinen I, Sakai K (1999) Composition of lipids, fatty acids and sterols in Okinawan corals. Comparative Biochemistry and Physiology Part B: Biochemistry and Molecular Biology 122:397-407

Yentsch CS, Yentsch CM, Cullen JJ, Lapointe B, Phinney DA, Yentsch SW (2002) Sunlight and water transparency: cornerstones in coral research. J Exp Mar Biol Ecol 268:171-183

Yonge CM, Nicholls A (1931) Studies on the physiology of corals. V The effects of starvation in light and in darkness on the relationship between corals and zooxanthellae. Great Barrier Reef Expedition 1928-29, Scientific Reports British Museum (Natural History) London (UK) 13–57 British Museum 1

Zamoum T, Furla P (2012) *Symbiodinium* isolation by NaOH treatment. The Journal of Experimental Biology 215:3875

Zimmermann NE, Yoccoz NG, Edwards TC, Meier ES, Thuiller W, Guisan A, Schmatz DR, Pearman PB (2009) Climatic extremes improve predictions of spatial patterns of tree species. Proc Natl Acad Sci U S A 106:19723-19728

Reef & Rainforest
RESEARCH CENTRE

www.nesptropical.edu.au